

**The Numerical Modelling of Ecosystem
Response to Nutrients: Application to
the Scheldt Estuary and Plume**

Report to European Commission
Contract No. EVK3-CT-2000-00040
“EUROTROPH”

Institute of Estuarine and Coastal Studies
University of Hull

30 June, 2004

Institute of Estuarine & Coastal
Studies (IECS)
The University of Hull
Cottingham Road
Hull
HU6 7RX
UK

Tel: +44 (0)1482 465667 or 465661
Fax/Tel: +44 (0)1482 465001

E-mail:
iecs@hull.ac.uk

Web site:
<http://www.hull.ac.uk/iecs>

**Author(s): Campuzano-Guillén, F.J., Allen,
J.H and Scott, T.**

Report: ZBB558-F-2004 (Report 2 of 4)



European Commission

The Numerical Modelling of
Ecosystem Response to Nutrients:
Application to the Scheldt Estuary
and Plume

30 June, 2004

Reference No: ZBB558-F-2004 (Report 2 of 4)

For and on behalf of the Institute of Estuarine and Coastal Studies
Approved by: _____
Signed: _____
Position: _____
Date: _____

This report has been prepared by the Institute of Estuarine and Coastal Studies, with all reasonable care, skill and attention to detail as set within the terms of the Contract with the client.

We disclaim any responsibility to the client and others in respect of any matters outside the scope of the above.

This is a confidential report to the client and we accept no responsibility of whatsoever nature to third parties to whom this report, or any part thereof, is made known. Any such parties rely on the report at their own risk.

PREFACE

In recent years, there has been increasing concern about the ecological effects of nutrients in estuaries and nearshore waters. This has been accompanied by an increase in the legislation aimed at controlling nutrient levels and assessing associated biological impacts. However, despite this interest and a large amount of scientific research, many details concerning the impact of nutrients on biological communities remain unclear.

As such, the work undertaken by the Institute of Estuarine & Coastal Studies (IECS), University of Hull (UK), aims to address these issues under Work Package 5 within the framework of a larger European project - *Nutrient Cycling and the Trophic Status of Coastal Ecosystems* 'EUROTROPH' (Contract No. EVK3-CT-2000-00040). This three-year project has been funded by the European Commission under Framework 5, Key Action 3 (Sustainable Marine Ecosystems), the objectives of which were to:

- Determine the trophic status of four European sites using different approaches.
- To breakdown the effects of the various nutrients and organic matter species on the trophic level.
- To develop biochemical and socio-economic models in order to forecast changes and provide management tools.
- To translate the data into information for wider use, and disseminate the results to end-users.
- To provide key information and advice regarding eutrophication to water quality managers and policy makers (monitoring procedures, regulation adapted to trophic status, cost-effective management of nutrients and their disposal), so that they may improve ecosystem health by determining the efficacy of existing and future treatment strategies on a catchment-wide basis.

The EUROTROPH project studied four contrasting European coastal and estuarine ecosystems: the Randers Fjord (Denmark); the Scheldt estuary (Belgium and the Netherlands); the Scheldt plume (Belgium and the Netherlands); and the Bay of Palma (Mallorca, Spain), with the project being divided into the following five Work Packages:

- WORK PACKAGE 1: Compilation of historical data which aimed to compile existing data relevant to the project from the selected study sites.
- WORK PACKAGE 2: Determination of the trophic status using simultaneously different available techniques, and to compare the estimates at several timescales.
- WORK PACKAGE 3: Quantification of the uptake and turnover of dissolved inorganic and organic nitrogen & phosphorus, together with the study of the distribution, composition, and turnover of particulate and dissolved organic matter (labile and refractory).
- WORK PACKAGE 4: Biogeochemical numerical modelling with the integration of data obtained in the previous Work Packages to estimate transfer fluxes and budgets integrated

over various time and space scales, and to forecast the impact of intervention scenarios on the metabolic status.

- WORK PACKAGE 5: Set the regulatory framework for the project and collate the deliverables gained from Work Packages 1-4 in an administrative, legislative, and socio-economic framework.

In order to achieve the aims and objectives of Work Package 5, the following four reports have been produced by the Institute:

1. Hemingway, K.L., Burdon, D., Campuzano-Guillén, F.J., Haythornthwaite, J., Elliott, M. & V.N. de Jonge, 2004. *The Ecological Response to Nutrients in Contrasting Systems and the Role of Conceptual Modelling*. Report 1 of 4. Institute of Estuarine and Coastal Studies (IECS), University of Hull, Hull, UK. Report to the European Commission (Contract No. EVK3-CT-2000-00040).
2. **Campuzano-Guillén, F.J., Allen, J.H. & T. Scott, 2004. *The Numerical Modelling of Ecosystem Response to Nutrients: Application to the Scheldt Estuary and Plume*. Report 2 of 4. Institute of Estuarine and Coastal Studies (IECS), University of Hull, Hull, UK. Report to the European Commission (Contract No. EVK3-CT-2000-00040).**
3. Burdon, D., Atkins, J.P., Mutemererwa, A.M. & J.H. Allen, 2004. *An Economic Evaluation of Water Quality Improvements in European Estuarine and Coastal Ecosystems*. Report 3 of 4. Institute of Estuarine and Coastal Studies (IECS), University of Hull, Hull, UK. Report to the European Commission (Contract No. EVK3-CT-2000-00040).
4. Burdon, D., Elliott, M. & V.N. de Jonge, 2004. *The Administration, Legislation, Monitoring and Management of Nutrients in European Estuarine and Coastal Ecosystems*. Report 4 of 4. Institute of Estuarine and Coastal Studies (IECS), University of Hull, Hull, UK. Report to the European Commission (Contract No. EVK3-CT-2000-00040).

The current volume (Report 2 of 4) details '***The Numerical Modelling of Ecosystem Response to Nutrients: Application to the Scheldt Estuary and Plume***'.

EXECUTIVE SUMMARY (REPORT 2 OF 4)

This particular report aimed to use ecosystem models to clarify some of the processes and interactions defined in previously prepared conceptual models for eutrophication in estuaries and coastal waters. In order to address this issue, two of the EUROTROPH study sites (the Scheldt estuary and plume) were selected to carry out ecosystem modelling. The MOHID model was chosen which operates in the Windows[®] operating system and is developed by the MARETEC (Marine and Environmental Technology Research Center) in association with Hidromod at the Instituto Superior Técnico (IST) which is part of the University of Lisbon (Portugal).

As part of the modelling exercise a hydrodynamic model for the area was initially developed, for which two nested grids were applied to the modelling domain, with the primary model grid at a broader spatial scale (at a resolution of 0.02°) covering the Southern area of the North Sea. The secondary grid covered the Scheldt estuary and Plume in more detail at a resolution of 500m. Boundary conditions for the primary model were obtained from the tidal components derived from the FES95.2 modelling study (carried out by Le Provost *et al.*, 1998) in order to simulate tidal flows through the primary grid. Tidal data from the primary grid was subsequently used to feed the secondary model.

Validation of the hydrodynamic modelling was undertaken with respect to tidal elevation and current velocity/speed at a number of stations both along the estuary, and in the North Sea adjacent to the mouth of the estuary. Tidal elevation predictions were validated using tidal gauge data from Hydro Meteo Centrum Zeeland (HMCZ). In most areas, there was a good agreement between predicted and observed tidal elevation with linear regression models generally with an R^2 of over 0.9. Validation was slightly poorer in the mouth of the estuary due in part to variations in observed elevation as a result of meteorological conditions which could not be taken into account in the model predictions. However, further validation against the XTIDE tidal prediction model (which does not take into account meteorological variation) gave better validation in the outer estuary with R^2 values of over 0.9. Validation of current velocity and direction was similarly undertaken using data from the 2DH-Scalwest model, and in most areas there was a high level of agreement between the two models.

Output from the model in terms of the hydrodynamic regime was broken down into three components - namely instantaneous current velocity, residual current velocity, and calculations of residence time. Results from the model indicated broadly similar ebb and flood tides to those given in the literature with maximum velocities of up to 2.0 m s⁻¹ during flood tides, and velocities of up to 1.8 m s⁻¹ during ebb tides (with the highest velocities generally occurring in the mid to upper estuary). Greater asymmetry in ebb and flood tides is apparent in the mouth of the estuary during spring tides with velocities ranging from 0.7 m s⁻¹ on an ebb tide to 1 m s⁻¹ on a flood tide, whilst on the neap tide differences are less pronounced (ranging from 0.5 m s⁻¹ to 0.6 m s⁻¹). A pronounced tidal stream enters and exits from the mouth of the Scheldt heading south-west on an ebb tide creating the Scheldt plume.

In terms of residual water movement, both residual flux and residual velocities have been calculated. In terms of residual flux, at broader level the residual movement in a northerly direction offshore from the estuary whilst in the immediate area of the estuary mouth, residual fluxes separate to move up and down the coast to the north and south respectively. Within the estuary, the effect of fresh water discharge is apparent in the upper estuary in terms of seaward residual fluxes whilst in the middle estuary some circulation in residual flux is evident within the main channels. In terms of residual velocities, these are relatively insignificant close to the coast around the mouth of the

Scheldt although higher velocities are evident on the northern coast near Westkapelle. Within the estuary, the predominant predicted residual velocity is seaward. In terms of residence time calculations from the model agreed with those given in the literature with residence times of 69 to 74 days for winter and summer respectively.

Once the hydrodynamic model has been set up and tested, salinity, temperature and cohesive sediments were implemented in the model. Two large datasets have been the main databases used to validate the remaining properties of the water quality module: the NIOO-KNAW Scheldt monitoring dataset (EUROTROPH webpage, <http://www.obs-vlfr.fr/eurotroph/index.php>) for the estuarine area, and the IDOD (Integrated and Dynamical Oceanographic Data) from the Belgian Marine Data Centre (BMDC, <http://www.mumm.ac.be/datacentre/>) for the Scheldt plume and coastal area around the estuarine mouth.

Salinity predictions were found very accurate in terms of range, temporal and spatial variation after imposing a constant discharge of 0.5 psu in the riverine boundary and setting initial values for the estuary. Results for temperature were also accurate, describing with great precision the observed values found in the water quality stations set along the estuary and in the plume for all a year period.

Suspended sediments in the water column were imposed at the riverine boundary with a constant value of 106 mg l⁻¹, used successfully by De Smedt *et al.* (1998). It was found that the concentration of sediments in the water column was in agreement with the observed values for the different validation stations. Spatially, two areas could be distinguished, a maximum turbidity zone (MTZ) from Antwerp to Bath where sediment concentrations were high and a less turbid area with more steady concentrations that stretched to the mouth of the estuary where the sediments left the estuary forming the Scheldt plume. The extent and distribution of the modelled Scheldt plume was in agreement in concentration and extension with observed values and aerial pictures.

Once those water properties were tested and validated with observed values, the water quality module was implemented. The water quality model used in the MOHID model is basically an eutrophication model initially developed by EPA (U.S. Environmental Protection Agency) (Bowie *et al.*, 1985). The model simulates inorganic and organic forms of nitrogen and phosphorus as nutrients. It also calculates oxygen, phytoplankton and zooplankton concentrations.

Oxygen concentrations were imposed at both boundaries using cyclic monthly averaged values, and a hourly data series of wind speeds and directions from the Cadzan station corresponding to the year 2000 was also applied to the whole domain (HMCZ webpage, <http://www.hmcz.nl>), to model the aeration from atmosphere. Predicted and observed values for oxygen showed similar patterns; however the model tended to underestimate the oxygen concentration, possibly due to the use of concentrations of organic phosphorus and organic nitrogen from studies dated a decade earlier when higher concentrations of organic matter were input from the river. Three zones could be distinguished according the OSPAR Commission classification of water quality (2003), an acute toxic area coinciding with the extension of the MTZ, an second area which was oxygen deficient and an area with relatively normal oxygen levels covering the outer estuarine area and the nearby coastal zone.

The levels of inorganic nitrogen species predicted by the model showed similar patterns to the observed values, particularly nitrate, whilst the values of nitrite and ammonia were slightly higher than the observed values due to the release of nitrogen as a product of the mineralisation of the organic matter. Total inorganic nitrogen tended to exhibit conservative behaviour in the estuary, or

was removed from the estuary depending on the season. Consequently, it was considered that the estuary was acting as a trap of nitrogen at certain times of the year.

Inorganic phosphorus showed good validation with regard to the observed values both temporally and also spatially along the estuary. Inorganic phosphorus in the Scheldt tended to behave as a conservative nutrient depending on the time of the year or otherwise its concentrations were increased from local inputs from the estuary.

Phytoplankton concentrations was validated using a Carbon:Chlorophyll-*a* conversion factor of 40. The ecological module tended to underestimate the magnitude of the spring bloom outside the estuary however, within the estuary the predictions were of the same order as the observations. In terms of timing, the predicted values were in concordance with the observed values and the descriptions in the literature. In relation to the OSPAR Commission classification (2003) elevated values were predicted at the head of the estuary and at some periods of the year elevated levels extended into the middle of the estuary. Values above these criteria were observed for the majority of the simulation at the head of the estuary.

Zooplankton validation could not be completed due to the lack of adequate temporal data sets for zooplankton biomass in the area, although during some periods of the year an accumulation of zooplankton was predicted in the centre of the estuary.

In conclusion, although the model could be refined to achieve a higher degree of accuracy, the results show that the model is able to reproduce the processes described in the literature and future steps are recommended in order to be able to predict other eutrophication symptoms aside of oxygen levels and chlorophyll *a* concentrations.

This page is intentionally blank.

TABLE OF CONTENTS

PREFACE.....	I
EXECUTIVE SUMMARY (REPORT 2 OF 4)	III
TABLE OF CONTENTS	VII
1. INTRODUCTION	1
1.1 Numerical models	3
1.2 Types of numerical models.....	3
1.3 The MOHID model.....	6
1.4 Management applications	8
1.5 Advantages and Disadvantages of Numerical Modelling.....	8
2. HYDRODYNAMIC MODELLING OF THE SCHELDT ESTUARY	11
2.1 The physical characteristics of the Scheldt Estuary	11
2.1.1 Morphology.....	11
2.1.2 Hydrodynamic Regime.....	12
2.2 Development of the Hydrodynamic Model	16
2.2.1 Model Set-Up.....	16
2.3 Model Results	19
2.3.1 Validation.....	19
2.3.2 Predicted Tidal Currents within the Scheldt Estuary.....	22
2.3.3 Residence Time.....	32
3. WATER QUALITY MODELLING OF THE SCHELDT ESTUARY	35
3.1 Development of the Ecological & Water Quality Model.....	35
3.1.1 Model Set-Up.....	35
3.2 Abiotic and Biotic Modelling Parameters	37
3.2.1 Salinity	37
3.2.2 Temperature	39
3.2.3 Sediments	41
3.2.4 Oxygen	46
3.2.5 Nutrients.....	50
3.2.5.1 Nitrogen.....	50
3.2.5.2 Phosphorus	56
3.2.6 Phytoplankton and Zooplankton	58
4. DISCUSSION	66
4.1 Future Work.....	67
4.2 Acknowledgements	68

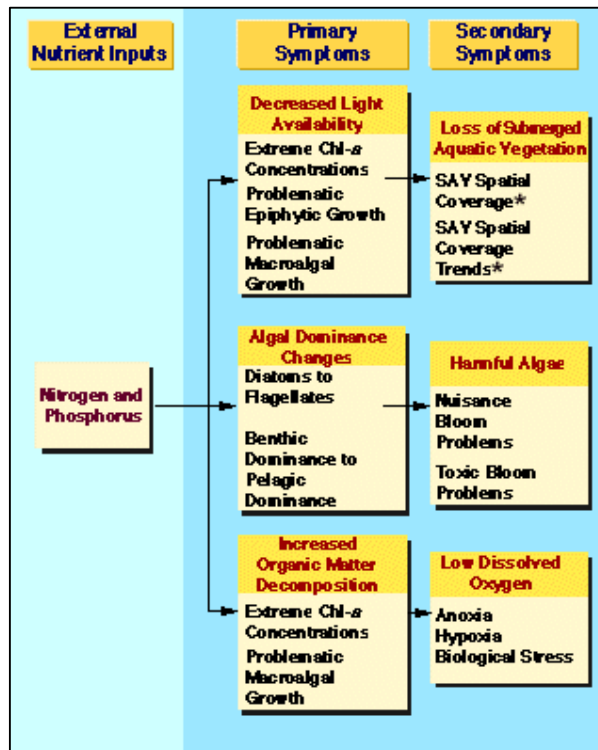
5. REFERENCES.....	69
APPENDIX 1: PREDICTED AND OBSERVED PARAMETERS.....	75
APPENDIX 2: ECOLOGICAL MODEL EQUATIONS	93
APPENDIX 3: PARAMETERS LIST	113

1. INTRODUCTION

Eutrophication is one of the major concerns for the preservation of the coastal areas ecosystems status and a major problem for water quality management (Koelmans *et al*, 2001). The Urban Waste Water Treatment Directive (91/271/EEC) of the European Union defined Eutrophication as

“the enrichment of water by nutrients, especially compounds of nitrogen and/or phosphorus, causing accelerated growth of algae and higher forms of plant life to produce an undesirable disturbance to the balance of organisms present in the water and to the quality of the water concerned”

This enrichment into the coastal waters enhances the growth of phytoplankton and fixed plants, benefiting some food chains at the expense of others. The effects of this enrichment can be summarised into a series of *symptoms* and divided into primary and secondary manifestations of the process (Figure 1). National governments and international organisations (EU, OSPAR.) have established regulatory measures to tackle this issue by identifying waters affected by eutrophication.



* SAV (Submerged Aquatic Vegetation)

Figure 1: The simplified eutrophication model (Bricker *et al.*, 1999)

The Scheldt (Figure 2) is considered to be a turbid, extremely eutrophic estuary which receives large inputs of nutrients from point and non-point sources (Lemaire *et al*, 2002; Kromkamp *et al*, 1995; Heip 1988 in Struyf *et al*, In Press). The river Scheldt is a lowland river originating at St. Quentin (North of France), flowing through Belgium and The Netherlands for 355 km before discharging to the North Sea near Vlissingen (The Netherlands).

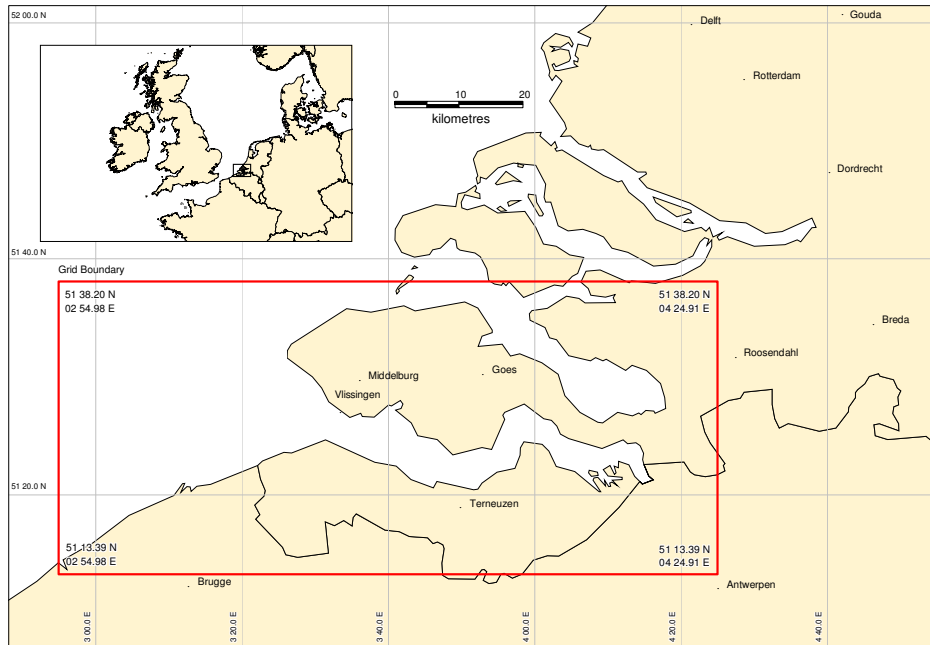


Figure 2: Location of the Scheldt estuary with the *secondary* model domain in red.

Under OSPAR convention (OSPAR commission, 2003) the whole Belgian and Dutch coastal area, including the Scheldt, has been identified as a problem area (highlighted in red in Figure 3) where nutrients inputs are likely to cause pollution. In order to reduce the impact of nutrients in the system water quality improvement measures have been established, including nutrient reduction of the inputs (around 50%) and water quality objectives established for the water body (e.g. O_2 and Chlorophyll *a* concentrations).

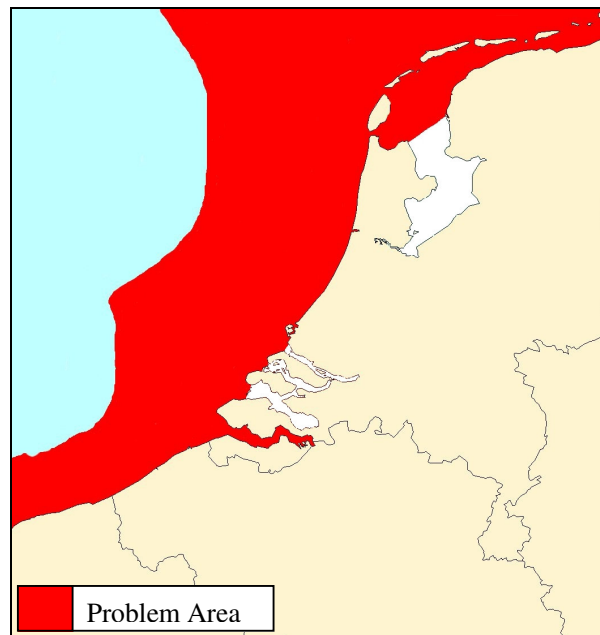


Figure 3: Problem areas on the Belgian and Dutch coast, including the Scheldt (OSPAR Commission, 2003).

1.1 Numerical models

Due to the importance of coastal resources (with respect to both commercial and conservation issues) and the complexity of such habitats numerical models are commonly used to simulate the processes affecting them. Since the late sixties, when the first models based on the *primitive equations* were developed in Princeton a great deal of improvement have been achieved in the field of numerical modelling allowing the simultaneous simulation of a wide range of marine processes at a range of spatial and temporal scales.

One of the advantages of numerical models is that they can provide a continuous and global description of ecological and hydrodynamic processes which can be compared to the observational data (obtained by ships, deployed analytical equipment and satellites telemetry) and consequently used to predict the effect of future change. However, it should be borne in mind that model results should never be used as a substitute for 'real' data. Although they are extremely useful tools, they also present their own intrinsic problems as described below (Steward, online):

Discrete equations are not the same as continuous equations: The use of numerical solutions for the differential equations uses the assumption that the area of study can be summarised as grid points and that the time moves forward in tiny steps.

Practical models must be simpler than the real ocean: Model equations have to be simplified in order to run them on available computers. Due to this reason, many assumptions or simplifications are made with regard to the underlying processes.

Numerical code has errors: Every piece of software has bugs, and whilst the output may appear correct after testing there may be variations in accuracy due to the numerical methods employed which have their own in-built errors which may be compounded by rounding-up errors.

However, it should be recognised that the majority of these errors are relatively small in magnitude and the numerical models currently used provide very detailed results of the hydrodynamical and ecological processes which are of tremendous assistance with regard to the understanding and management of marine systems.

1.2 Types of numerical models

The adequacy of numerical models depends on a number of issues including a good scientific understanding of the main processes, a good conceptual base which underlies that understanding, the ability of the mathematics to reflect that understanding, the availability of data for deriving the model and the availability of data for validating and calibrating the model. In addition a good understanding of the accuracy and precision of the derived data is required and perhaps most importantly that they a fit for purpose, i.e. with regard to the questions being asked or the particular management issues. The latter depends on a sufficiently rigorous set of objectives being set prior to the exercise for which there is a perceived modelling need. The data needs of models vary widely and with empirical models, the more data that are available then the better the mathematical representation (e.g. set of equations) may reflect an observed situation.

Ideally numerical models should be derived from observational data and if the data does not provide sufficient insight with which to develop a model then more/different types of data should be

collected. Models should be used to test scenarios and further the level of understanding gained from the monitoring data, not as a substitute for poor data or lack of data. The model will only be as good as the data it is based on. It is therefore important to use models which are site specific to an area and are calibrated and validated using local hydrological, chemical and biological observational data.

Models allow the simulation of ecosystem changes due to changes in population, land use, or pollution management. Such simulations (scenarios), allow the prediction of positive or negative ecosystem changes due to management actions such as improved sewage treatment, reduced fertiliser application on agricultural land, or controlling urban expansion.

Several groups of model can be distinguished and include:

- *'Simple' one line equation models* - for plotting concentrations of tracers versus salinity and assessing deviations from a conservative mixing line. This approach implicitly uses a transport model. These may be empirical and based on statistical relationships between variables derived by observation and hence they do not necessarily require any understanding of the underlying principles.
- *Population models* - population models are being increasingly used to predict the consequences for populations based on the effects of environmental stress on individuals. Models may be derived for phytoplankton populations e.g. chemostat models (phytoplankton growth versus nutrient input) and macrobenthic or fish population models also either exist or are being developed. Fish population models are classically used in fisheries management by incorporating recruitment, stock, mortality and fishing data.
- *Community models* - these models aim to predict the nature of the community, as described by its species composition (i.e. its taxonomic composition) in relation to physico-chemical variables. These include models such as RIVPACS for freshwater benthic communities (and a similar model - MARINPACS for marine benthic communities). Other models can also be derived for community primary and derived parameters (such as species richness, abundance, biomass and diversity) in relation to environmental variables and are often based on statistical (regression based) techniques e.g. BenOss (Cromeey *et al.*, 1998) and other models as described by Elliott & O'Reilly (1991) and Allen (2004).
- *Hydrodynamical models* - Physical circulation models which predict circulation and transport of tracers and the evolution of temperature, density and salinity fields. They usually treat all material within the system as conservative-substances. Advection and diffusion models include suspended particulate matter (SPM).
- *Water Quality / Eutrophication models* – They describe the cycling of nutrients and the growth of algae, being used to assess water column levels of nutrient and algal biomass and are mainly applied to simulate the effects of control measures to abate eutrophication impacts. These models calculate the growth of phytoplankton in terms of carbon (although the carbon cycle is not completely closed) with carbon production expressed as Chlorophyll *a* production using a conversion factor. Some of these models also include zooplankton. (Koelmans *et al.*, 2001).
- *Biogeochemical models* - Biogeochemical models simulate local processes controlling the cycling of nutrients in estuaries and coastal waters through both the water column and sediments and predict the effects of nutrient loads and transport on water and sediment quality and phytoplankton blooms. They incorporate the scientific understanding of the underlying processes with regard to local sources, sinks and transformations of biogeochemical variables. Biogeochemical models have the advantage of allowing the testing of hypotheses about the importance and nature of key processes against observations in a quantitative sense.

- *Food web models* - Based on the classical Lotka-Volterra model, they try to explain and forecast the feeding relationships among the species in aquatic systems (Koelmans *et al*, 2001). No general theory of food web structure exists (Lawton in Koelmans *et al*, 2001) forcing the models to be site specific.

To fulfil the task assigned in workpackage 5 on modelling issues the current study aims to refine the previously prepared conceptual models followed by the use of ecosystem models to indicate the quantitative nature of the links defined within these models and relate these to the requirements of Annex V of OSPARCOM which aims to maintain habitat integrity. The main intention of the current study is (as with the conceptual modelling) to apply an ecological model to the Eurotroph sites (Bay of Palma - Spain, Randers Fjord – Denmark and the Scheldt Estuary and plume -Belgium/The Netherlands) which reaches as high in the trophic food chain as possible and be able to reproduce the primary and secondary symptoms of eutrophication. Due to limitations with regard to the available data it was decided to focus the modelling effort on the Scheldt Estuary and plume as this area had a wide range of historical data for comparison and model validation.

In order to achieve these objectives an ecosystem based eutrophication model was chosen which would allow the extrapolation of the results into an available food web model (i.e. ECOSIM, AQUATOX). The first model examined was COHERENS (COupled Hydrodynamical Ecological model for REgionNal Shelf seas) (Luiten *et al*, 1999). This model is freely available for scientific and non-commercial purposes and was developed between 1990-1998 by a multinational European group, as part of the MAST projects PROFILE, NOMADS and COHERENS and was funded by the European Union (Marine Science and Technology Programme (MAST-III) MAS3-CT97-0088). However, the software was primarily developed for UNIX workstations (with support for PCs under LINUX/DOS) which proved to be a drawback in terms of the computing facilities available at the time of study (and may also limit the availability of the model for local managers). In addition, user support for COHERENS was limited with an expiration date two years of the release of the software CD-Rom (April 2000). Due to these difficulties, the MOHID model (which is freely available under the same terms and runs in a full windows environment) was chosen to carry out the modelling component of the project.

1.3 The MOHID model

The MOHID model can be considered as an object orientated model, and the ecological module within it has been used to assess eutrophication based on a model initially developed by EPA (Bowie *et al.*, 1985). The core of the model is a fully 3D hydrodynamical model which is coupled to different modules (Figure 4) comprising water quality, atmosphere processes, discharges, oil dispersion, mixing zone model for point source discharges, catchment area (MOHID land, in development), etc. Some of its main features are discussed here.

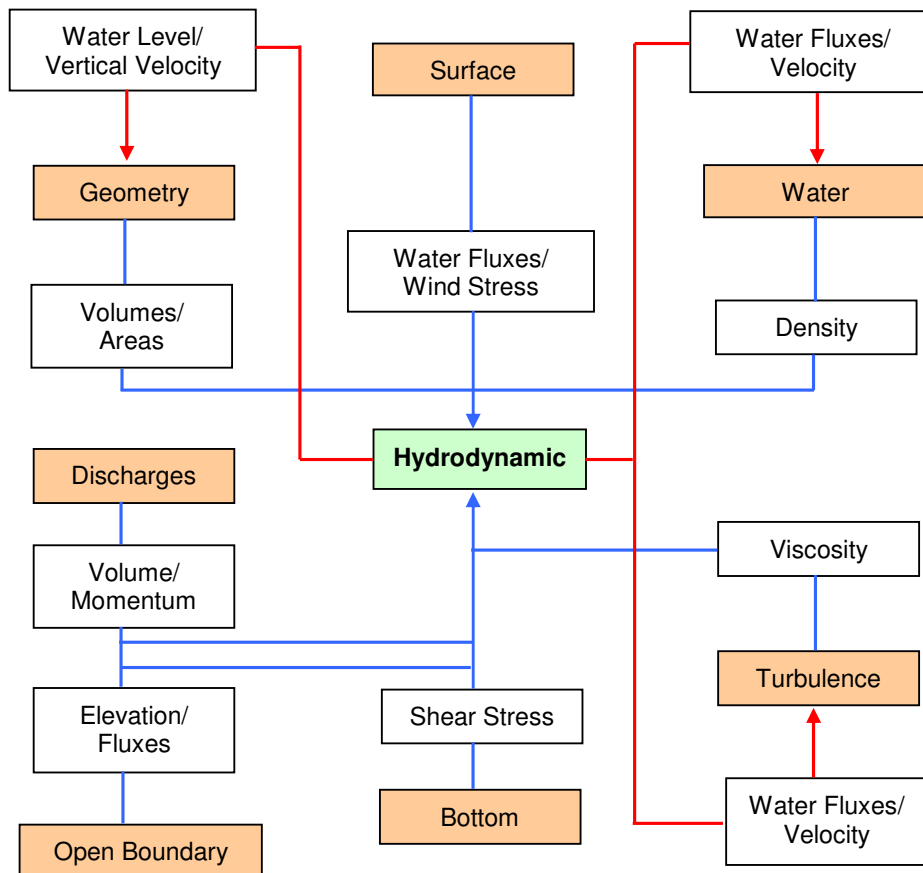


Figure 4: MOHID module oriented structure showing the fluxes of information from and to the central hydrodynamic module (Blue arrows represent inputs and red outputs) (<http://www.mohid.com>).

MOHID is programmed in ANSI FORTRAN 95 using an object orientated philosophy able to simulate eulerian and lagrangian processes and runs on the Windows[®] operating system. The model has been continually developed and improved since 1985 by MARETEC (Marine and Environmental Technology Research Center) in cooperation with Hidromod at the Instituto Superior Técnico (IST) which is part of the University of Lisbon (Portugal). The MOHID model is composed of several modules that can be independently turned on and off. The main modules used during the simulations carried during this project are summarised in Table 1.

Table 1: MOHID main modules description.

Module	Description
Model	Manages the information flux between the hydrodynamic module and the two transport modules and the communication between nested models
Hydrodynamic	Full 3D baroclinic hydrodynamic free surface model. Computes the water level, velocities and water fluxes.
Water Properties	Eulerian transport model. Manages the evolution of the water properties (temperature, salinity, oxygen, etc.) using an eulerian approach
Lagrangian	Lagrangian transport model. Manages the evolution of the same properties as the water properties module using a lagrangian approach. Can also be used to simulate oil dispersion
Water Quality	Zero-dimensional water quality model. Simulates oxygen, nitrogen and phosphorus cycle. Used by the eulerian and lagrangian transport modules. It is based on a model initially developed by EPA (Bowie, <i>et al.</i> ,1985)
Turbulence	One-dimensional turbulence model.
Geometry	Stores and updates the information about the finite volumes
Atmosphere	Responsible of the atmosphere influences to the water body, computing variables as cloud cover, solar radiation, relative humidity, air temperature and wind.
InterfaceWaterAir	Boundary conditions at the top of the water column, regulates the way the Atmosphere module components interact with the water body.
InterfaceWaterSediment	Controls the influence the water dynamics at the bottom of the water column defining its rugosity and including erosion and deposition processes.
Discharges	Rivers or Anthropogenic Water Discharges

The MOHID model has been applied to several coastal and estuarine areas including the main Portuguese estuaries and coastal lagoons. Also it has been used in other European areas (Galician Rías (NW Spain) (Cancino and Neves (1999)), the Scheldt estuary (Belgium-The Netherlands), the Gironde estuary (France), Carlingford (Ireland) and some estuaries in Brazil). One of the most recent applications of the model was a study into the effects of the *Prestige* oil spill off the North West coast of Spain.

Further information on the technical aspects of the model is available at the MOHID website (<http://www.mohid.com>).

1.4 Management applications

Models to be used for management purposes need to be simple, straightforward and require limited specialist knowledge or training so they can be used appropriately by local coastal managers. If the funds and the expertise are available, different modelling procedures may have to be developed for different designated features. It is considered that a hierarchical approach can be taken to modelling and decision making as follows:

- The derivation and adoption of conceptual models
- The production of decision trees giving the likely responses within a given habitat
- The use of numerical models to predict the response in that habitat.

It is emphasised that caution should be exercised in the applications of such models and an adequate assessment made with regard to the degree of confidence which may be attached to the resulting output (due to the inherent variability/uncertainty in the derivation of the model and possible inaccuracies in the underlying data or assumptions on which it is based). In particular, models may be best employed as decision support tools rather than decision-making tools. The choice of approach should be based on the objectives for the site and also the ease (and suitability) with which the model may be applied to the management decision framework. The local manager will still be required to make an expert judgement as to whether a site will be affected by nutrient enrichment based on local knowledge.

1.5 Advantages and Disadvantages of Numerical Modelling

The following features are among the advantages of numerical modelling:

1. The modelling of systems helps to predict the magnitude and spatial extent of possible impacts and to determine the appropriate standards and guidelines required to trigger a management response.
2. Models can be used to scenario test (predictions) but also identify important controlling processes. These should then feedback to monitoring of these processes or parameters that indicate any early changes.
3. Where models simulate natural and anthropogenic changes they will be an effective management tool and may produce an integrated management approach (Neal *et al.* 1998).
4. Sensitivity testing of models may indicate the most important controlling factors/processes in a system. The latter should then target the monitoring approach and also test the understanding of the system.
5. Models are mathematical representations of complex and varying environmental events and conditions and thereby simplify and isolate the most important factors occurring at the study site.

6. Advances in model development tend to increase their complexity but complex models are not necessarily required for all areas or situations. The adequacy of the model reflects the adequacy of the underlying science, e.g. models are good at predicting nutrient concentrations when based on sound hydrodynamic principles and, individually, biogeochemical models are based on good empirical data.
7. They can be used to reduce, but not eliminate uncertainty in environmental decision making and if used properly, are tools that can assist in developing initiatives to reduce nutrient concentrations in the marine environment.

Conversely, some disadvantages can be found in the application of numerical models for management issues.

1. The inadequacy of models in simultaneously considering both bottom-up processes (e.g. nutrient inputs and kinematics) and top-down responses (e.g. the effects on the macrobiology, especially birds and fishes of high nature conservation value and the perceptions by the public etc.). Links between nutrient enrichment, water column effects and benthos/fish/bird response may be poorly understood.
2. The inadequacy of the available quantitative information/data in running those models. There is generally an insufficiency of data for all or many of the components and it is axiomatic that a model is only as good as the data used to produce it.
3. As models become more complex and change from being physically-based to include biological interactions, a greater inherent complexity has to be modelled which produces more uncertainty in prediction.
4. Users should be aware of their capabilities, confidence limits, imperfections and the background or specific purpose for which they were originally built. Models can be used out of context if, for management, the purpose has not been clearly defined, e.g. to predict the effects of improvements within an area, to understand the processes occurring in the environment, or to assess causes, effects and thresholds.
5. With increasing sophistication, the data required to parameterise and validate the model increases.
6. Models generally produce estimates rather than accurate forecasts but their users often overlook such limitations.
7. The potential of integrated models for long term simulations of effects to higher trophic levels is limited because of limitations in the fundamental knowledge of food web processes and modelling (Koelmans *et al*, 2001). Most models do not simulate any higher level ecological effects and the ones available at the higher levels (e.g. ecosystem models) may only be valuable as decision support rather than decision making tools.
8. Modelling of complex processes runs the risk of deriving a good fit with the wrong parameter setting (Scheffer and Beets, 1994 in Koelmans *et al*, 2001).

9. The validation of process formulations against field data may be limited due to the wide range (and inter-correlation) of different explanatory variables i.e. multiple causation (Scheffer and Beets, 1994 in Koelmans *et al*, 2001).
10. Uncertainty with regard to coupling of different levels of the food chain functions occurring at different temporal and spatial scales (Koelmans *et al*, 2001).

Although there are pros and cons for the use of numerical modelling, the need for predictive planktonic ecosystem models is widely recognised (Arhonditsis and Brett, 2004) and recommended as a tool for assessment on eutrophication for many statutory bodies (i.e. OSPAR Commission, 2000 and 2003, Council of the European Communities, 2000).

2. HYDRODYNAMIC MODELLING OF THE SCHELDT ESTUARY

This section gives a brief overview of the physical characteristics of the Scheldt estuary both in terms of its physical structure and its hydrodynamic regime. The modelling domain defined for the Scheldt is then described followed by an overview of the results of the hydrodynamic simulations derived from the MOHID model.

2.1 The physical characteristics of the Scheldt Estuary

2.1.1 MORPHOLOGY

The Scheldt estuary is a later evolution of the Honte, which was a tidal channel which expanded landward from the early Middle-Ages (van der Spek, 1997). This tidal channel connected to the river Scheldt becoming its new mouth to the North Sea, supplanting the original mouth the Oosterschelde. Since then, the estuary has evolved with the tidal channels deepening and many of its intertidal flats and salt marshes disappearing. The estuary acts as a sediment trap, receiving an annual supply of sand from the North Sea in the range of 0.6 to 3.1 million m³ (van der Spek, 1997).

The Scheldt is the only remaining estuary of the Dutch delta (Soetaert and Herman, 1995a) and the influence of the tide extends far upstream into several of its tributaries (Baeyens *et al.*, 1998a). Its shape is comprised of a complex network of ebb and flood channels running through intertidal areas and islands. From head to mouth, there is a single main channel with nearly uniform depth (average of 15 m) which meanders from Antwerp to Bath widening from 500 m to 3.5 km. The estuary between Bath and Hasweert shows an increase of width along the estuary and the splitting of the main channel into a few channels, mostly due to the presence of large intertidal areas in the centre of the estuary. The main channel (15 m depth) runs next to the southern bank next to the Saeftinghe salt marsh, another two shallower channels (2.5 m depth) run through the intertidal areas. From Hasweert, the main channel divides itself into two channels separated by intertidal areas and islands with the southern channel slightly deeper than the one on the northern bank.

These two channels are not isolated from each other as they are connected by shallower channels and eventually the two channels converge between Vlissingen (North) and Breskens (South) into one deep channel that reaches the mouth of the estuary where the estuary narrows to 5 km cross section. Around the mouth of the estuary the natural bathymetry has been modified by some dredging operations for navigation purposes. Outside the estuary, the separation of the northern and southern banks grows rapidly and two channels can be observed one running North parallel to the coast and a southern channel running west from the mouth. Both channels are separated by shallow sand banks. Water depth increases progressively from the mouth of the estuary, reaching 25 m at its maximum depth within the covered area by our model.

The evolution of tidal basins such as the Scheldt greatly depends on the interaction between the tide and basin morphology (van der Spek, 1997). A simplistic model of how they interact can be seen in Figure 2.1. The morphology of the basin and the relative volume and height of the intertidal areas are the main parameters influencing the shape of the tidal wave (Wang *et al.*, 2002). When the tidal wave reaches the sea bed some of its components show an increase in magnitude compared with deeper offshore waters which in turn modifies the shape of the tidal wave. The resulting changes to the tidal regime lead to changes in sediment transport and erosion/accretion cycles which then lead to a corresponding change in the basin morphology.

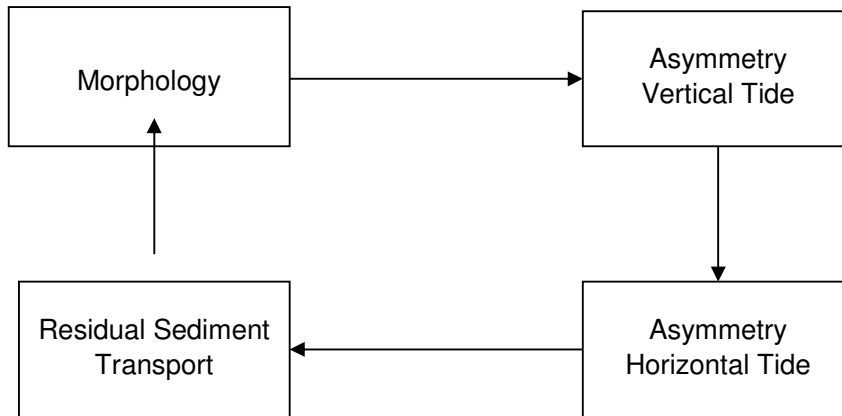


Figure 2.1: Schematic representation of the interaction between morphology and tidal asymmetry (Wang *et al*, 2002).

2.1.2 HYDRODYNAMIC REGIME

The hydrodynamic processes within estuaries are primarily the result of the interaction between river discharges and the tidal wave penetrating from the open sea. The balance between the different external forces then determine some important estuaries characteristics as the residence time, which consequently influence the biological, chemical and transport processes (Regnier *et al*, 1998). For this reason, it is very important to determine accurately the estuaries hydrodynamics before moving to biological and chemical phenomena, because they are strongly coupled.

2.1.2.1 River Forcing

The river Scheldt is a lowland river originates at St. Quentin (North of France) (Figure 2.2) where it is known as the river Escaut. The river flows through Belgium and the Netherlands for 355 km before discharging to the North Sea at its mouth near Vlissingen (The Netherlands). The total catchment area of the Scheldt is 22000 km² (Figure 2.2), primarily in Belgium territory, and the river as well as its main tributaries are fed by rainfall and run-off. Consequently, the exports of the tributaries to the main river changes seasonally, depending on the rain pattern (Baeyens *et al*, 1998a). The quantity of freshwater discharged by the river discharge will influence the fresh water limit within the estuary and the fresh water boundary will advance (with increased discharge) or retreat with decreased discharges. The mean freshwater flow from the river Scheldt is estimated between 100-120 m³s⁻¹ (Portela and Neves, 1994; Baeyens *et al*, 1998; Van Gils *et al*, 1993; Wang *et al*, 2002).

In relative terms, the influence of the river in terms of hydrodynamics is small, since the average water discharged during a tidal period amounts only 0.6- 1% of the tidal prism i.e. 4.8·10⁶ m³ (Van der Spek, 1997; Reigner *et al*, 1998; Wang *et al*, 2002). The mean tidal prism for the Scheldt is estimated between 10⁹ m³ (Cancino and Neves, 1999) and 2·10⁹ m³ (Wang *et al*, 2002). In addition, the low river flow leads to high residence times (Baeyens *et al*, 1998a). However, the river input of water is important in terms of its influence in the residual circulation in the head of the estuary and also as a source of sediments, nutrients and other chemical constituents and biogenic material.

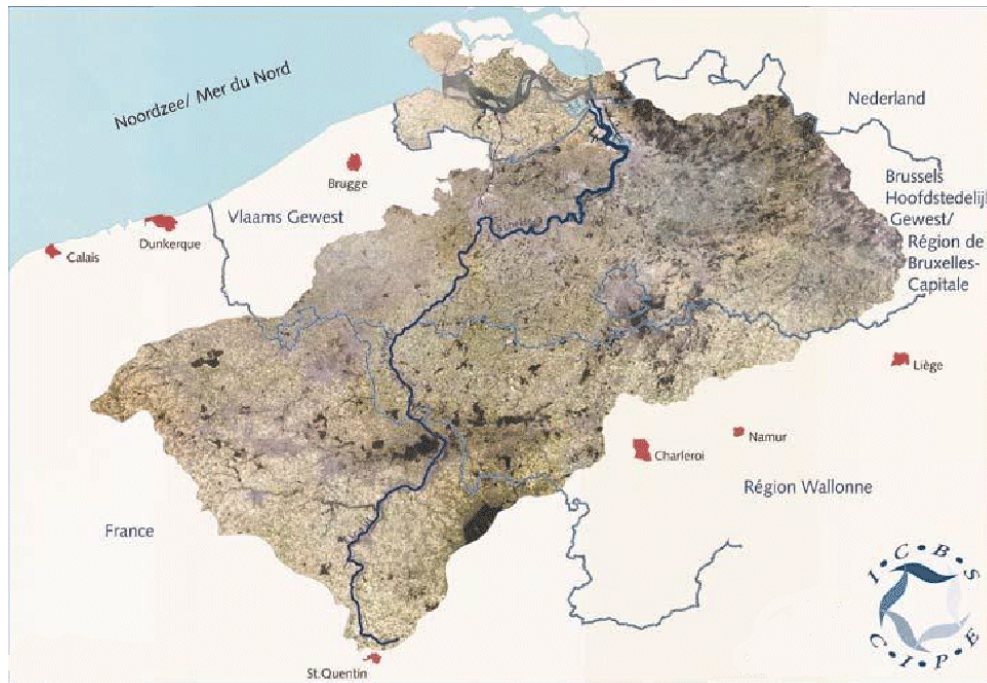


Figure 2.2: Catchment area of the Scheldt estuary (www.icbs-cipe.com).

2.1.2.2 Tidal Forcing

Shallow estuaries with large intertidal areas tend to be flood dominant (flood time is shorter than ebb time) with sediment transport is mainly landward. Conversely, deep tidal basins with small intertidal areas tend to be ebb dominant (ebb time is shorter than flood time) (Wang *et al*, 2002).

Due to advances in computing, the prediction of tides along a coast is a relatively simple task. With data from tidal gauges and the theory of the tidal forcing, the tidal components (or constituents) of the tide in a particular area can be obtained. The tidal wave can be decomposed using *Fourier transform*, which decomposes a periodic signal into sinusoidal or cosinusoidal signals of different frequencies that in combination comprise the original waveform. The frequencies of the tidal principal components correspond to the relative positions of the sun, moon and earth, and can be divided into semidiurnal, diurnal and long period (fortnightly, monthly, semi-annual) constituents.

The tidal wave in the North Sea moves anti-clockwise around its basin, and becomes distorted during its movement in the shallower southern waters due to the direct relationship between speed and depth of waves in shallow water. Consequently, as the wave crest moves through areas of deeper water it becomes increasingly steeper whilst the falling part of the wave becomes steadily flatter (Dronkers, 1986 in Van der Spek, 1997). This can be observed in Figure 2.3, where the tidal wave becomes more asymmetric in its propagation from South to North. This phenomenon causes an asymmetry between maximum flood and ebb tidal currents, known as tidal asymmetry, and is partly responsible for the distribution of residual currents (Van der Spek, 1997).

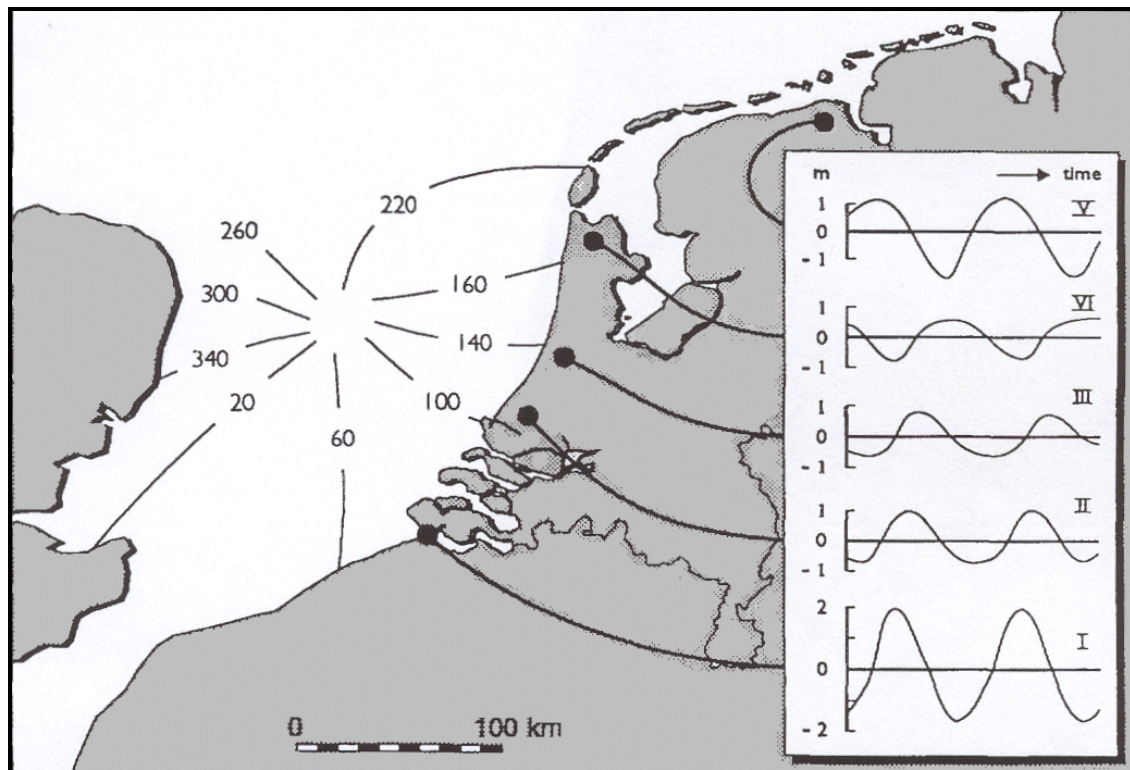


Figure 2.3: Tidal asymmetry in the North Sea (from Van der Spek, 1997).

When the tidal wave penetrates the basin it undergoes changes during its propagation along the estuary in reaction to the morphology of the estuary which, as described above, plays a very important role in the asymmetry of the tide (Van der Spek, 1997). The friction caused by the reduction of depth provokes the retardation of low water through the estuary. This phenomenon in the Scheldt estuary can be observed in Figure 2.4, which shows the same tide for different locations along the Scheldt after high water. The tidal stations are ordered from outside the estuary (Vlakte van de Raan) to the inner part of the model domain (Antwerp).

As Figure 2.4 shows the retarding effect of friction is observed at the Antwerp station where period from high water to low water is 7 hours whilst at the remaining stations it takes only 6.5 hours. The opposite effect is seen for the propagation of high water and as the wave propagates along the estuary the ebb period increases whilst the flood period reduces leading to enhanced flood currents (which are responsible of the inland residual currents). In Figure 2.4 the flooding time reduces from 6 hours outside the estuary to nearly 5 hours at Antwerp. Consequently, the Scheldt can be classified as a flood-dominant estuary.

In addition to the increase in the period of the ebb tide, the tidal range estuary also increase along the tidal range (as can be observed in Figure 2.4) with a mean tidal range at of 3.8m at Vlissingen and 5.2m at Antwerp some 78 km further upstream (Wang *et al*, 2002; Baeyens *et al*, 1998a). The phase difference between the vertical tide and horizontal tide is around 2.5 hours. In terms of tidal range the Scheldt may be considered a predominantly macrotidal estuary (tidal range between 4 and 6 meters) although some authors consider it as either mesotidal (Cancino and Neves, 1999) or both (Van der Spek, 1997).

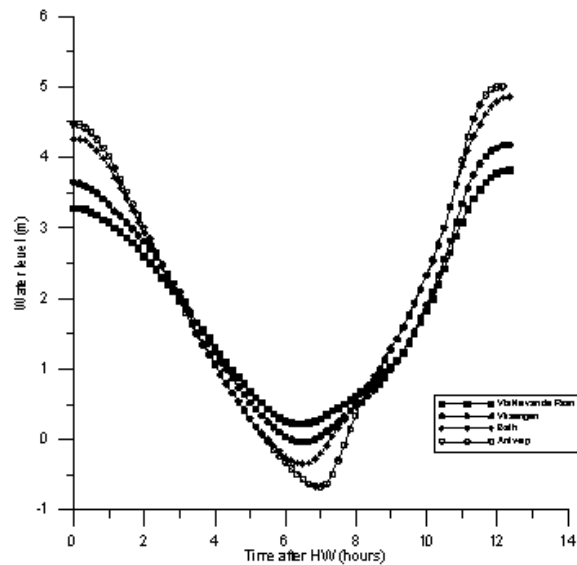


Figure 2.4: Water level at different locations along the Scheldt estuary on the 6th-Jan-2000 (Data source: HMCZ (Hydro Meteo Centrum Zeeland) webpage, <http://www.hmcz.nl/>).

The spatial variation of the vertical tide is primarily due to the increase of the M_2 tidal component (principal lunar semidiurnal tidal component) towards the head of the estuary which is not accompanied by an increase in the M_4 (quarter diurnal shallow water overtide of the M_2 component) tidal component or other tidal components such as the M_6 (sixth diurnal shallow water overtide of the M_2) tidal component (Wang *et al*, 2002).

The amplification in the tidal range along the estuary, according to Savenije (2001), is almost linear, as opposed to non-alluvial estuaries where is exponential. The main reason for this is that there seems to be a negative feedback in tidal propagation due to the river discharges that prevent this exponential behaviour of the tidal range. This theory was tested successfully for different types of estuaries including the Scheldt (Savenije, 2001).

2.2 Development of the Hydrodynamic Model

2.2.1 MODEL SET-UP

In order to simulate the hydrodynamics of Scheldt estuary and plume it was first necessary to define the modelling domain (i.e. area to be modelled) and then superimpose a grid over the domain which divides the area up into a series of cells. These grid cells are then populated with the requisite data to run the model (e.g. water depth) and are used as the basis for calculating water movement within the model domain. In the current study two nested grids were coupled (Figure 2.5) in order to avoid the interference of highly variable hydrodynamic conditions at the outer model boundary conditions with hydrodynamic conditions local to the study area. Consequently, the model comprises a *primary* grid consisting of a regular grid that covers the southern part of the North Sea and the English Channel and a coupled *secondary* grid with a finer and more detailed cell size which covers the Scheldt estuary from Antwerp to the Belgian-Dutch coast adjacent to the mouth of the estuary and influenced ecologically by the Scheldt estuary processes.

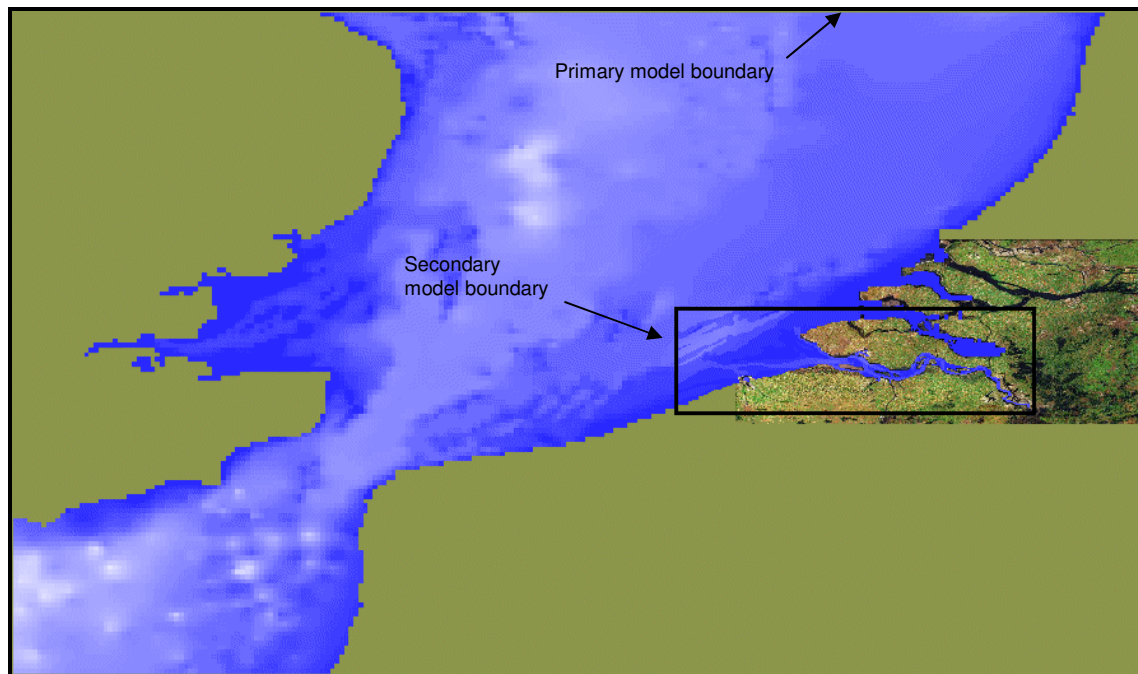


Figure 2.5: Boundaries of the primary and secondary modelling domains.

The *primary* model consists of a regular grid with a cell size of 0.02° populated with the one minute global bathymetric grid data obtained from GEBCO digital atlas (IOC, IHO & BODC, 2003). The larger primary grid was used in order to force the boundaries of the *secondary* model grid with tidal components which were imposed further away from the study area (and subsequently less affected by the variation often found at the boundaries of such models). The limits of the *primary* model are $50^\circ 06' 00''$ N and $52^\circ 54' 00''$ N (from South to North) and $0^\circ 06' 00''$ E and $4^\circ 43' 12''$ E (from West to East) using the World Geodetic System 1984 (WGS84) projection.

The *secondary* model grid covering the Scheldt estuary is based on a regular grid with a cell size of $500\text{m} \times 500\text{m}$. This cell size was chosen in order to obtain as much detail as possible in terms of the area and time series to be simulated (dependant on computational capabilities) without compromising

the model accuracy in terms of estuary morphology and processes. Furthermore, the validation data used was at a level of detail similar to the cell size and so need a smaller grid size was not necessary with regard to this. The secondary model domain (Figure 2.5) and accompanying bathymetric data was been created based on the UK Hydrographic Office Admiralty Charts (numbers 120, 139, 1874).

The *secondary* model grid area is based on the WGS84 projection and covers the estuary from Antwerp (Belgium) to a few kilometres offshore in the North Sea ($4^{\circ} 25' 20.43''$ E to $2^{\circ} 54' 58.63''$ E from east to west) and from Zeebrugge (Belgium) to the Oosterschelde in the Netherlands ($51^{\circ} 13' 23.41''$ N to $51^{\circ} 38' 28.67''$ N from south to north). The secondary model grid is divided into 92 cells from west to east 208 cells from north to south. This design is expected to be able to reproduce the hydrodynamics of the inner estuary in addition to the hydrodynamics of the coastal area (including the Scheldt plume). The MOHID model allows wetting and drying of cells such that the intertidal areas within the estuary and along the coast can be incorporated within the model.

In order to simulate the movement of water within the modelling domain it is first necessary to impose tidal conditions at the boundaries of the model which can then be used to start the simulation. Tides in the MOHID model can be imposed in two different ways as follows:

- Impose a time series of water elevations at the model domain boundaries
- Impose tidal component information at different stations along the model domain boundaries

Using the conditions applied at the model boundaries the model itself calculates by triangulation the water levels within the model domain. The first method is potentially more accurate than the second but requires a regular and good quality temporal dataset and it is not suitable for predicting future events because these water levels need to be measured or modelled separately *a priori*. The second method requires detailed information on the tidal components (e.g. from tidal gauges near to the model boundaries) at points along the entire modelling domain boundary. Such data should ideally have a time series of sufficient length for determining accurately the various tidal components and in particular those with a long return period. The second method has the advantage of allowing calculation of tides for any desired period of time both in the past and in the future. In the current study the second method has been used to characterise tidal boundary conditions.

The tidal boundary conditions (as described in section 2.2.1) utilised in the current study were (<ftp://spike.cst.cnes.fr/pub/techine/tide/>). This study developed a global Finite Element Solution derived by assimilating the empirical Topex/Poseidon CSR2.0 tidal solution into a hydrodynamic model to derive a $0.5^{\circ} \times 0.5^{\circ}$ gridded solution. For the MOHID model tidal gauge stations were positioned along the open water boundaries of the primary model domain (to the north and south-west) using data from the FES95.2 database. The *secondary* model may be considered a sub-model and its boundary tidal conditions are derived from the *primary* model. It should be noted that the FES95.2 database does not include information on the M_4 and M_6 tidal components although this does not appear to have hindered the model simulation in terms of the main hydrodynamic processes and as will be shown below model validation was generally good.

For the purpose of this study the river discharge into the estuary is fixed at Antwerp, which is the inner limit of the estuary in the model domain. The river discharges are modelled using a monthly averaged value with data derived using daily flow data from 1997-2000 (Lenhart & Paetsch, 2001; database online at <ftp://ftp.ifm.uni-hamburg.de/pub/data/riverload/>). Fresh water discharges into the Scheldt as described in Figure 2.6 show a maximum discharge of over $250\text{m}^3\text{s}^{-1}$ in December which

decreases to $70\text{m}^3 \text{ s}^{-1}$ in August and then increases rapidly once more towards winter. Due to the availability of physical, biological and geochemical data required to impose boundary conditions and for validation purposes the model was set to run hydrodynamic simulations for a period of one year starting from the 1st of January 2000.

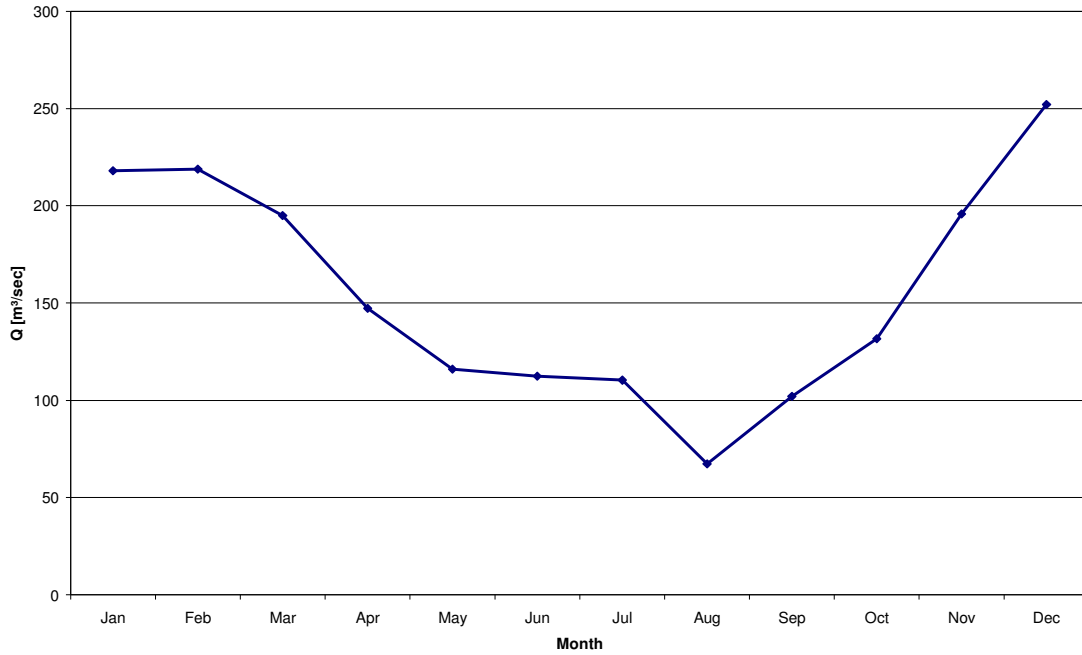


Figure 2.6: Scheldt estuary monthly averaged river discharges for the period 1997-2000.

2.3 Model Results

2.3.1 VALIDATION

To validate the predicted tidal elevation derived from the MOHID model the results have been compared with observed tidal elevation data derived from tidal gauge records provided by the Hydro Meteo Centrum Zeeland (HMCZ). Validation has been carried out for 16 stations along the estuary and the North Sea (Figure 2.7, Table 2.1). The location and name of the stations shown in Figure 2.7 with station names and acronyms and locations summarised in Table 2.1. The tidal gauge records describe the water level every ten minutes and are provided online by the Hydro Meteo Centrum Zeeland (HMCZ, <http://www.hmcz.nl/>).

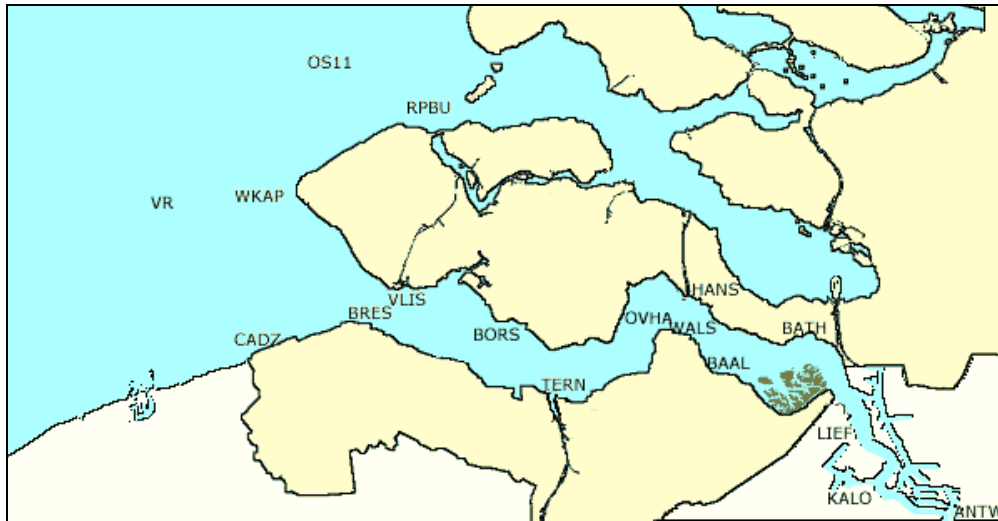


Figure 2.7: Location of the Tidal Stations (Source: Hydro Meteo Centrum Zeeland (HMCZ), <http://www.hmcz.nl/>).

Table 2.1: Name, acronym and location of the tidal gauge stations in the Scheldt.

Station Name	Acronym	Latitude	Longitude
Antwerp	ANTW	51° 13' 50'' N	4° 24' 00'' E
Baalhoek	BAAL	51° 22' 30'' N	4° 04' 50'' E
Bath	BATH	51° 24' 00'' N	4° 13' 00'' E
Borssele	BORS	51° 25' 20'' N	3° 42' 20'' E
Breskens	BRES	51° 24' 50'' N	3° 34' 00'' E
Cadzan	CADZ	51° 23' 00'' N	3° 23' 00'' E
Kallo	KALO	51° 15' 00'' N	4° 19' 30'' E
Liefkenshoek	LIEF	51° 18' 00'' N	4° 17' 30'' E
Oosterschelde 11	OS11	51° 38' 00'' N	3° 29' 00'' E
Overloop van Hansweert	OVHA	51° 25' 05'' N	3° 55' 10'' E
Roompot Buiten	RPBU	51° 37' 00'' N	3° 40' 00'' E
Terneuzen	TERN	51° 20' 00'' N	3° 50' 00'' E
Vlakte van de Raan	VR	51° 30' 00'' N	3° 10' 00'' E
Vlissingen	VLIS	51° 27' 00'' N	3° 36' 00'' E
Walsoorden	WALS	51° 24' 00'' N	4° 01' 50'' E
Westkapelle	WKAP	51° 31' 00'' N	3° 26' 00'' E

Results obtained with the model MOHID, show an acceptable level of accuracy in predicting the different periodicities occurring in the Scheldt tides. As an example of this, Figure 2.8 shows observed and predicted values for water elevation in Antwerp during the year 2000. Only astronomical tides can be predicted with this method and other variation in water levels e.g. due to meteorological phenomena (such as storm events) can explain some of the observed variability especially in the open coast around the mouth of the Scheldt.

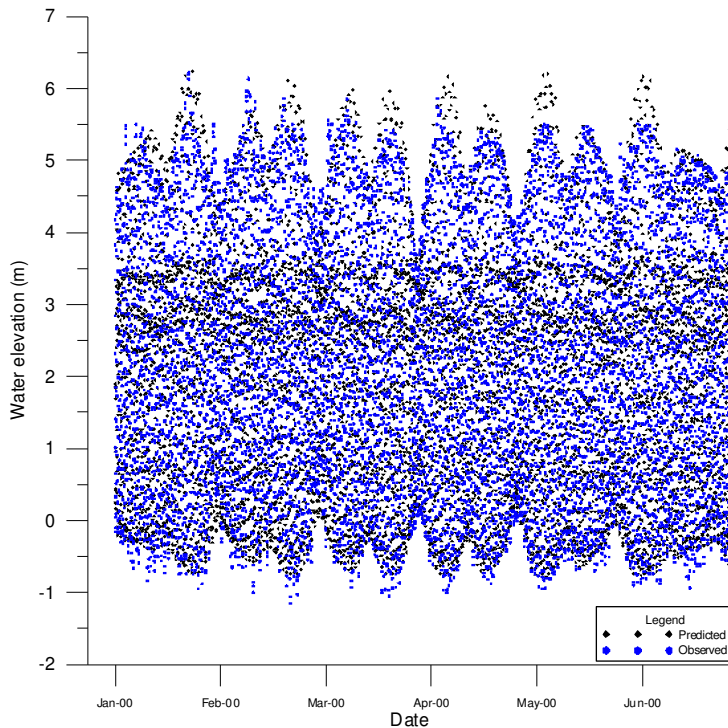


Figure 2.8: Water level predicted and observed during the first six months of the year 2000 at Antwerp (Data source Hydro Meteo Centrum Zeeland (HMCZ), <http://www.hmcz.nl/>).

In order to validate the MOHID model with regard to tidal elevation the predicted values of water level at each station for the year 2000 were compared with observed data for the 16 stations provided by HMCZ and linear regression models subsequently derived.

Theoretically, if a model fits perfectly a set of observed values, the representation of the predicted versus the observed values would be forming a line with 45° from both axes (Figure 2.9). If the linear regression is calculated for the set of data, it will show a coefficient of determination (R square) equal to one, which means that the relationship is able to explain the 100 % of the variability in the data. The R square describes the proportion of the total variation in Y explained by X in a scale from 0 to 1. The equation of a linear regression line is $y = a \cdot x + y_0$, where a = the slope of the line and y_0 = the point where the line intersects the y-axis. In the case of a perfect fit, the slope would be equal to unity (i.e. 1) and the y axis intersection would be at 0 i.e. the equation would be $y = x$.

The results of linear regression analysis for the validation of at the stations in the Scheldt estuary are summarised in Table 2.2 which shows regression coefficients together with the coefficient of determination (R^2). It is apparent that in the outer reaches of the estuary the model validation is less successful (although still within acceptable limits) due in part to the influence of meteorological variation as described above. To validate astronomical tidal predictions from MOHID (whilst

removing the variability due to atmospheric interference) the predicted values from the model were also compared with the astronomical tidal data derived from the XTIDE tidal prediction model (<http://tbone.biol.sc.edu/tide/index.html>, last accessed 19/05/04). Results of this validation show a greater degree of accuracy for the coastal areas of the model (R^2 values between 0.93-0.95).

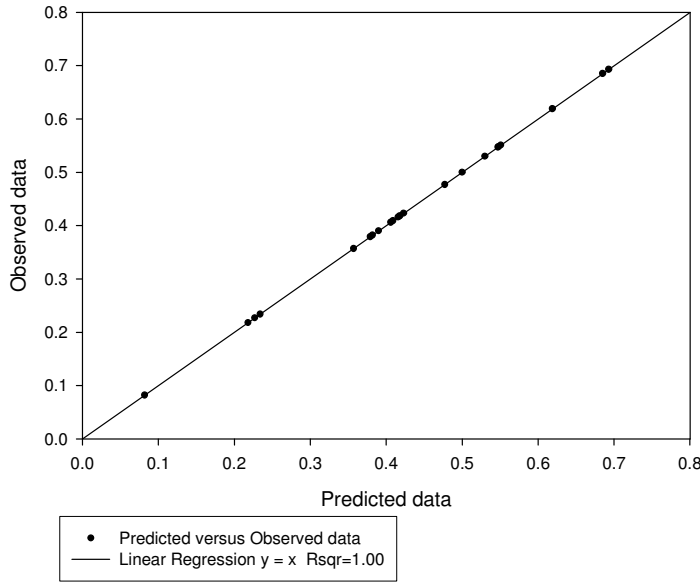


Figure 2.9: Example of a perfect fit between observed and predicted values.

Table 2.2: Linear regression analysis results for the different stations in the Scheldt estuary.

Station Name	Slope (a)	Y-Intercept (y_0)	R square
Antwerp	1.019	0.078	0.9317
Baalhoek	1.160	- 0.181	0.9612
Bath	1.099	- 0.101	0.9493
Borssele	1.006	0.034	0.8410
Breskens	1.006	0.034	0.8410
Cadzan	0.950	0.082	0.8223
Kallo	1.025	0.095	0.9264
Liefkenshoek	1.049	0.050	0.9329
Oosterschelde 11	0.856	0.238	0.7211
Overloop van Hansweert	1.136	- 0.179	0.9383
Roompot Buiten	0.842	0.239	0.6974
Terneuzen	1.009	0.057	0.8424
Vlakte van de Raan	0.851	0.286	0.7588
Vlissingen	1.005	0.006	0.8601
Walsoorden	1.154	- 0.250	0.9602
Westkapelle	0.896	0.248	0.7786

In order to further validate the hydrodynamic results from MOHID with regard to current velocity and direction the data derived from the 2DH-Scalwest model provided by Leen Dekker (Directie Zeeland, Directoraat-Generaal Rijkswaterstaat, Ministerie van Verkeer en Waterstaat) has been used. This data set gives predicted current speeds and directions at 23 stations for the date 05-05-1996 along the Scheldt estuary. However, as the location of the stations from the 2DH model were only

available on a map it proved difficult to match data spatially from the 2DH model and the MOHID model which may explain some of the observed variability between the results of the two modelling approaches. However, there was generally a good agreement between the models as shown in the polar plots given in Figure 2.10 where both the order magnitude and direction of the currents show a high degree of concordance.

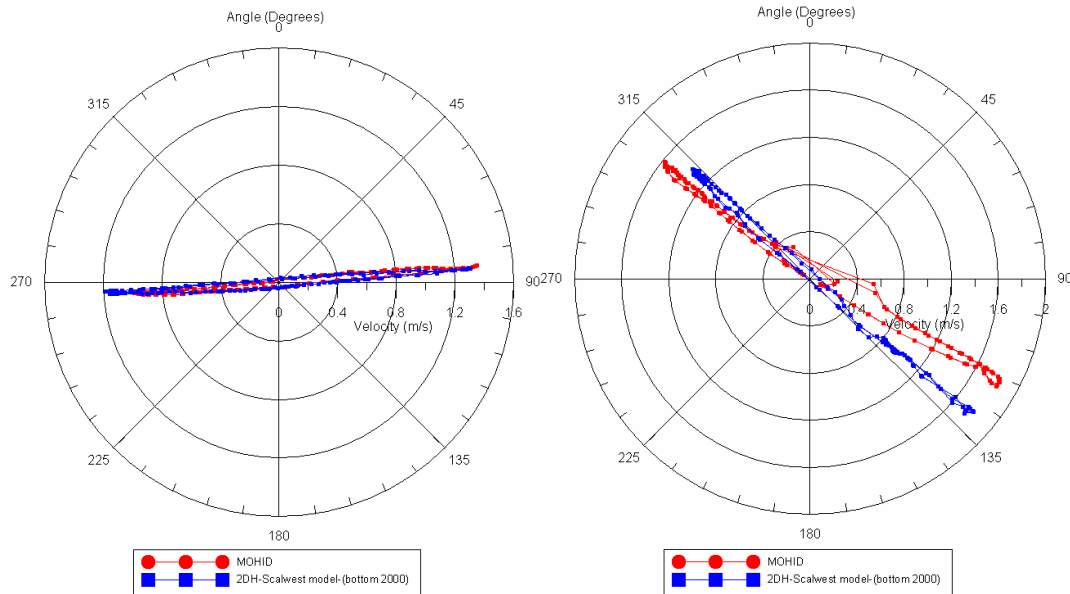


Figure 2.10: Polar plots of water velocity (radial axis) and direction (angle axis) for Wielingen (left, near Cadzan) and O.v.Hansweert 42-49 (right, near Walsoorden).

2.3.2 PREDICTED TIDAL CURRENTS WITHIN THE SCHELDT ESTUARY

The water currents predicted by MOHID can be separated into instantaneous and residual currents. Instantaneous currents are given for a single point in space at a single time whilst residual currents are the net long term currents which are obtained after subtracting currents in opposite directions. Residual currents can be considered to be the result of the tidal asymmetry of currents in flow and ebb directions. Freshwater flow into the estuary (river discharge) is relatively small in comparison to water movement due to tidal currents. However, freshwater input into the Scheldt is an important factor in terms of residual currents, particularly with regard to seaward residual flow, although tidal asymmetry is generally the major factor determining residual currents.

2.3.2.1 Instantaneous currents

Tidal currents at the mouth of the estuary are the result of the cumulative processes of the outer general circulation and the distortion produced by the estuary hydrodynamics (Van der Spek, 1997). Flood velocities are generally larger than the ebb velocities outside the estuary (Figures 2.11 and 2.12) due to the direct relationship between velocity and depth. However, within the estuary once the estuary starts to flood and water begins to cover the large intertidal areas the volume available for flooding is increased leading to somewhat lower than expected current speeds. The reverse occurs on the ebb tide within the estuary with slightly higher than expected maximum ebb velocities. Due to this phenomenon broadly similar velocities are observed for the flood and ebb within the estuary.

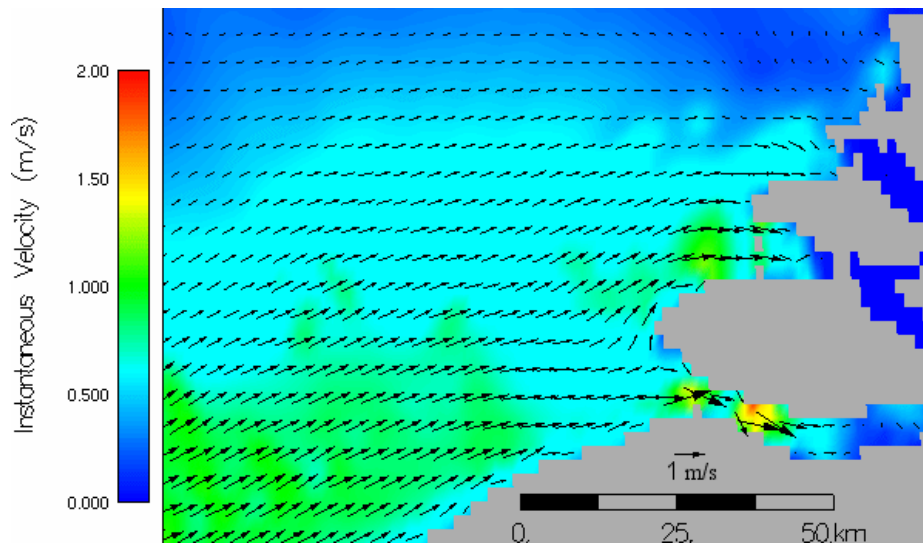


Figure 2.11: Instantaneous velocity for the *primary* model while flooding during a spring tide (12:00 22/01/00).

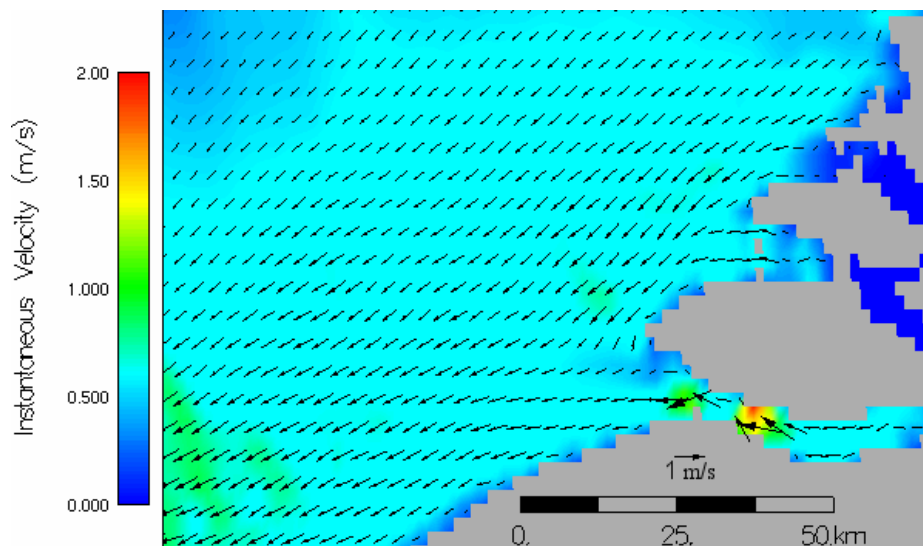


Figure 2.12: Instantaneous velocity for the *primary* model while ebbing during a spring tide (19:00 22/01/00).

According to Franken *et al* (2004) maximum instantaneous velocities occur in the upper part of the estuary with a maximum value of 1.3 ms^{-1} and 1.7 ms^{-1} during ebb tides for an averaged neap and spring tide respectively. These figures increase to values around 1.6 ms^{-1} and 2.0 ms^{-1} during flood tides. Similar flow rates are predicted from the MOHID model and Figures 2.13 and 2.14 show the velocities during the flood and ebb tide within the estuary during a spring tide while Figures 2.15 and 2.16 show the velocities predicted for a flood and ebb tide during a neap tide (note the difference of scales).

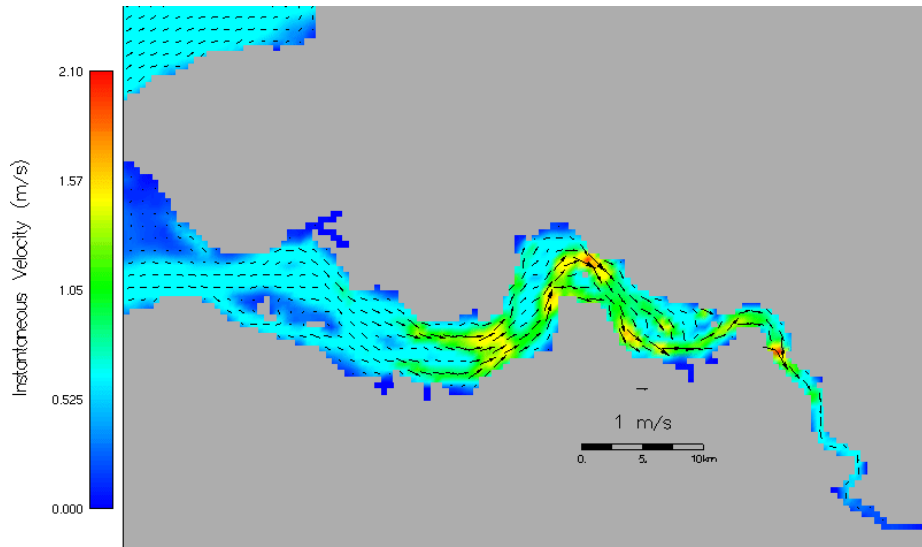


Figure 2.13: Instantaneous velocity for the *secondary* model while flooding during spring tide (14:00 22/01/00).

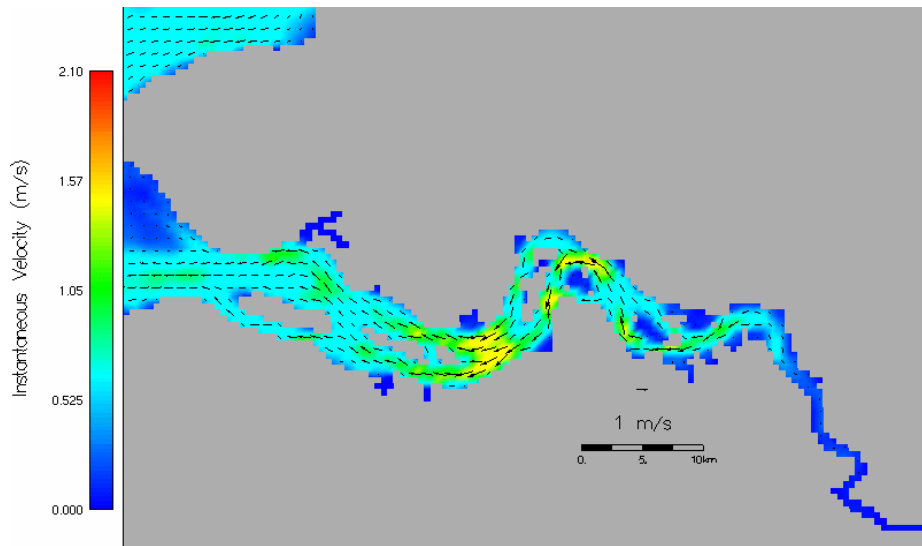


Figure 2.14: Instantaneous velocity for the *secondary* model while ebbing during a spring tide (20:00 22/01/00).

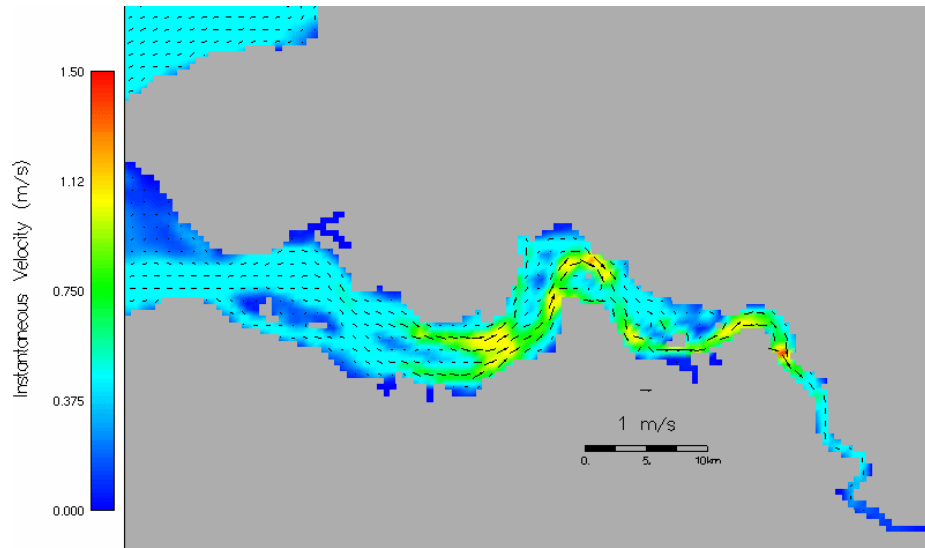


Figure 2.15: Instantaneous velocity for the *secondary* model while flooding during a neap tide (07:00 29/01/00).

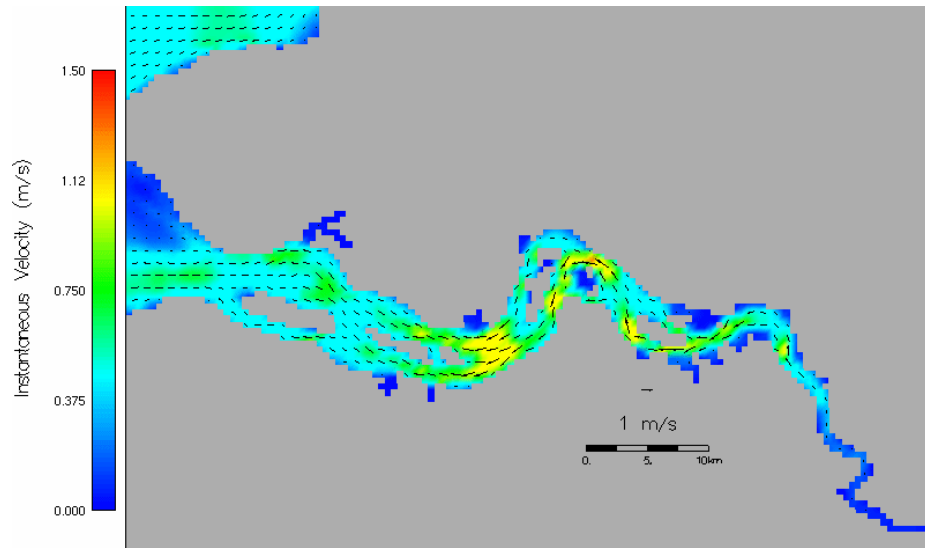


Figure 2.16: Instantaneous velocity for the *secondary* model while ebbing during a neap tide (13:00 29/01/00).

Some authors have described the existence of flood and ebb channels in the estuary although the model results do not appear to confirm this. The scale of the estuary is not large enough to be affected by the coriolis force and only small increases in velocity in some of the channels can be observed. Due to presence of large intertidal areas and the reduction in channel volume on an ebb tide a proportion of the water discharged is forced to flow through the shallower channels and these shallow channels subsequently show slightly higher velocities during an ebb tide compared with a flood tide.

In the estuary mouth, due to its larger area and the absence of large tidal flats, the instantaneous velocities observed during flow and ebb tides differ in their intensity. The reason for these

differences is due to the tidal asymmetry present in the shallow waters with the flood period shorter than the ebb period which leads to the movement of the same amount of water in a shorter time and thus with higher velocities. These differences are more apparent close to the shoreline and in particular during spring tides. To illustrate this phenomenon, the tides at the station of Cadzan (51°23'N, 3°23'E) have been described in Figure 2.17 which shows the water level and current velocities simulated for this station during a spring tide. Figures 2.18 and 2.19 illustrate the general distribution of velocities during the same time period for the outer area of the estuary. Maximum observed velocities are around 1 m/s which is in general agreement with those described by Baeyens *et al* (1998a).

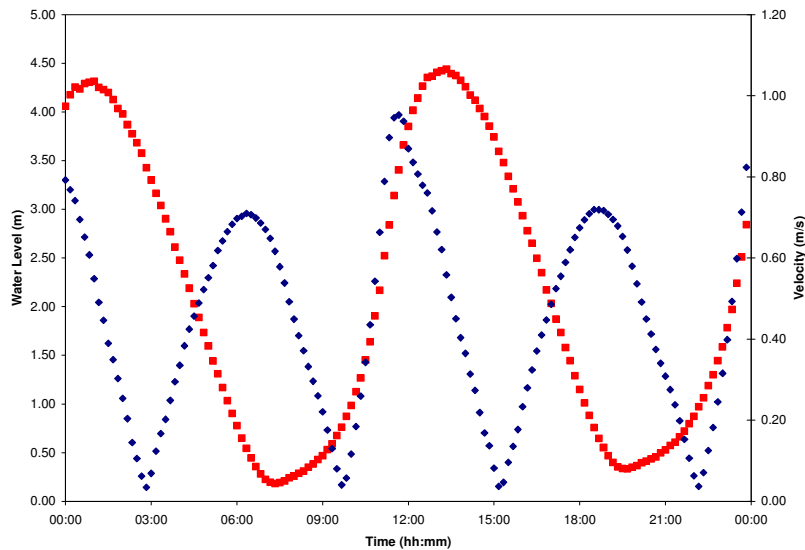


Figure 2.17: Ten minute interval water level and speed for Cadzan during a spring tide (22/01/00).

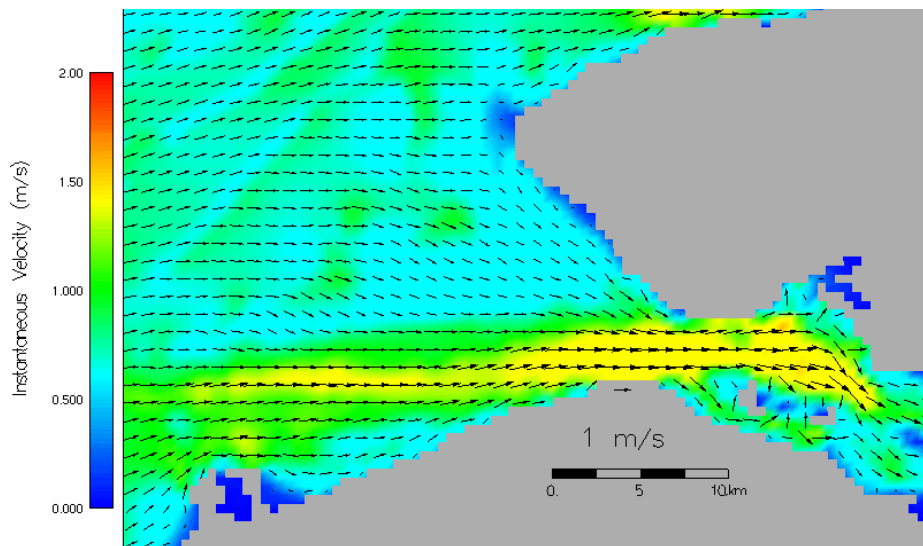


Figure 2.18: Instantaneous velocity for the *secondary* model while flooding during spring tide (22:00 22/01/00).

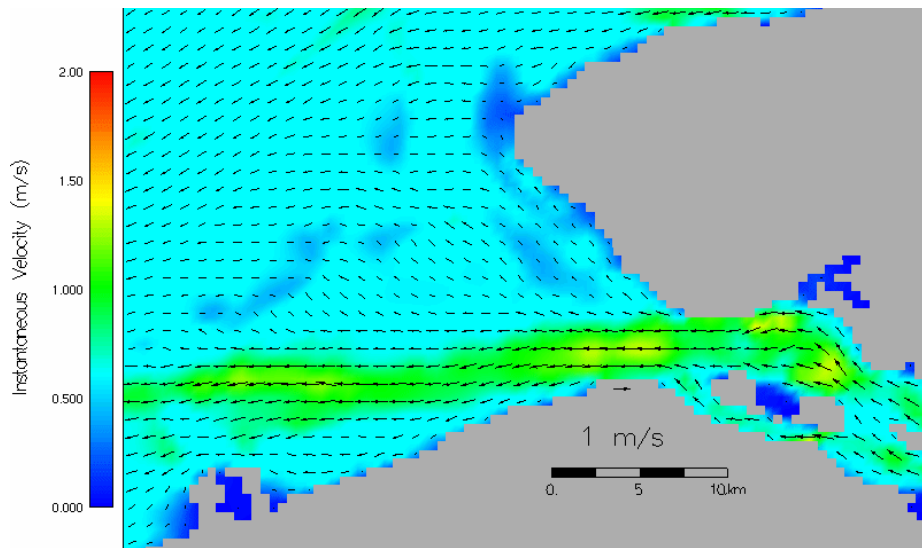


Figure 2.19: Instantaneous velocity for the *secondary* model while ebbing during spring tide (19:00 22/01/00).

During a neap tide the differences in tidal asymmetry are less pronounced due to reduced water volumes moving in and out the estuary. This can be seen in Figure 2.20 for Cadzan and in Figures 2.21 and 2.22 for the estuarine mouth (note the difference in scale with respect to the spring tide). Maximum values predicted on a neap tide are around 0.60 m/s.

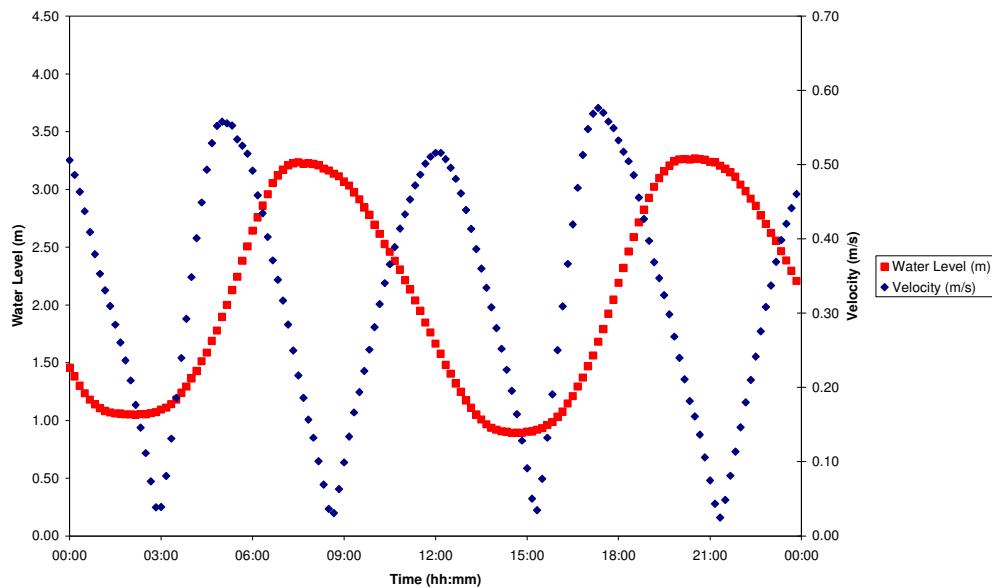


Figure 2.20: Ten minute interval water level and speed for Cadzan during a spring tide (29/01/00).

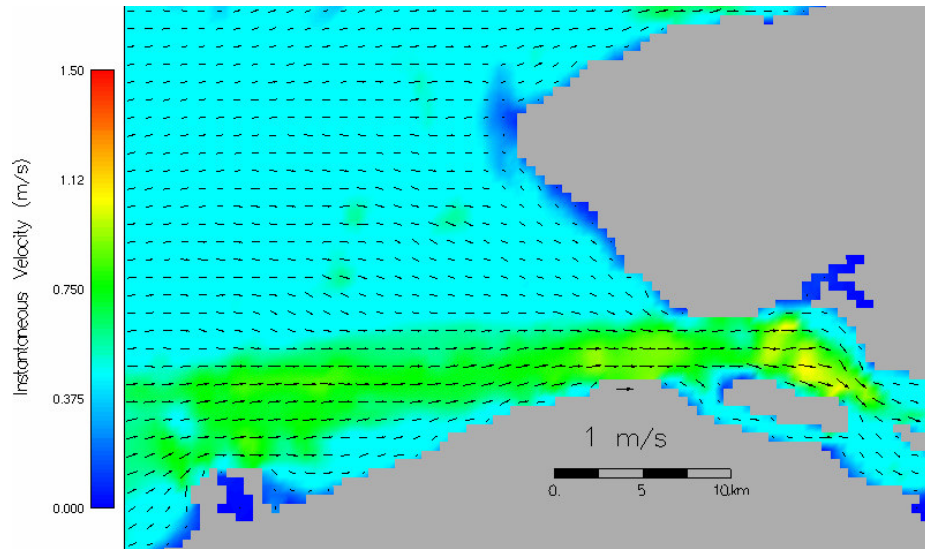


Figure 2.21: Instantaneous velocity for the estuarine mouth while flooding during a neap tide (05:00 29/01/00).

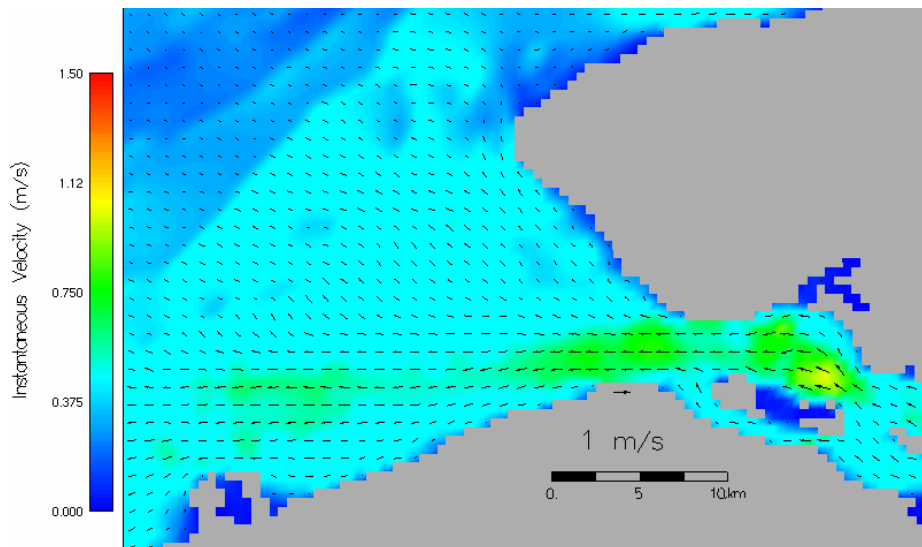


Figure 2.22: Instantaneous velocity for the estuarine mouth while ebbing during a neap tide (11:00 29/01/00).

The mouth of the Scheldt which is practically perpendicular to the coastal zone is relatively narrow in cross-section which constricts the flow in and out of the estuary. This is evident in the increased currents in this region and there is a noticeably increased outgoing and incoming tidal stream in this area moving from the mouth of the estuary and on an ebb tide this heads in a south west direction toward the coast creating the Scheldt plume. A weaker tidal stream separates to move in a northerly direction along the coast mainly due to the Coriolis Effect. In addition, the local influence of the port of Zeebrugge is also evident in the weaker inshore currents to the north of the port where it is sheltered from stronger tidal streams on the flood tides.

2.3.2.2 Residual currents

An important factor with regard to the import and export of nutrients and other chemical constituents of the estuarine system are residual currents. The residual currents represent the net transport of each of the model cells in the study site. Two different residuals are important in terms of describing the hydrodynamic properties of the estuary namely residual flux velocity and residual velocity. Residual flux velocity may be defined as the depth integrated residual water flux and is important in terms of the transport of dissolved properties in the water column (i.e. nutrients). Residual velocity is more important for the net transport of particulate matter (i.e. sediments).

Residual Flux velocities

This hydrodynamic feature is calculated as the integration over depth of the specific residual water fluxes occurring during a defined period and is expressed in ms^{-1} . In this study, this feature has been averaged for a month period in January and in an estuary can present a null cross-sectional average.

In the primary grid the residual flux velocities show residual movement parallel to the coast heading North with maximum values around $1\text{-}1.5 \text{ ms}^{-1}$ (Figure 2.23). Such residual flows would be an important factor with regard to the area of influence of the Scheldt plume. These velocities reduce near of the coast probably due to the influence of the Scheldt plume jet to values near 0.5 ms^{-1} . According to the modelling results the Scheldt plume would be influencing the northern Dutch coast and also estuaries such as the Oosterschelde in terms of water quality.

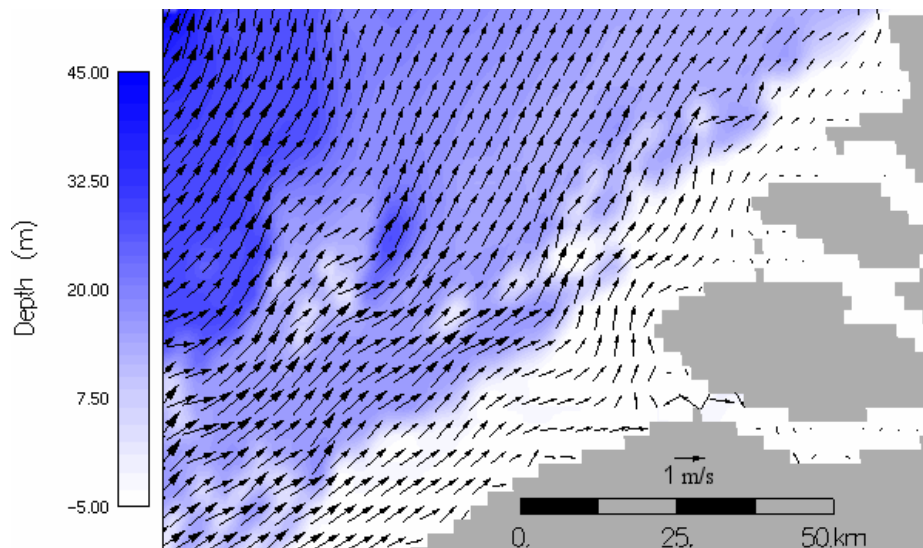


Figure 2.23: Residual flux velocities in the primary Scheldt model.

A more detailed examination of residual flux velocities around the mouth of the estuary (Figure 2.24) shows that the net movement in this region is seaward in the northern area and landward in the southern area, following the pattern in bathymetry. Part of the seaward flux is directed to the west forming the estuarine plume whilst the remainder follows the northern coast near Westkapelle due in part to the coriolis force in conjunction with broader circulation patterns. In addition, the local effects of the Zeebrugge port can be observed with increases in the intensity of the northerly residual flux in the vicinity of the port.

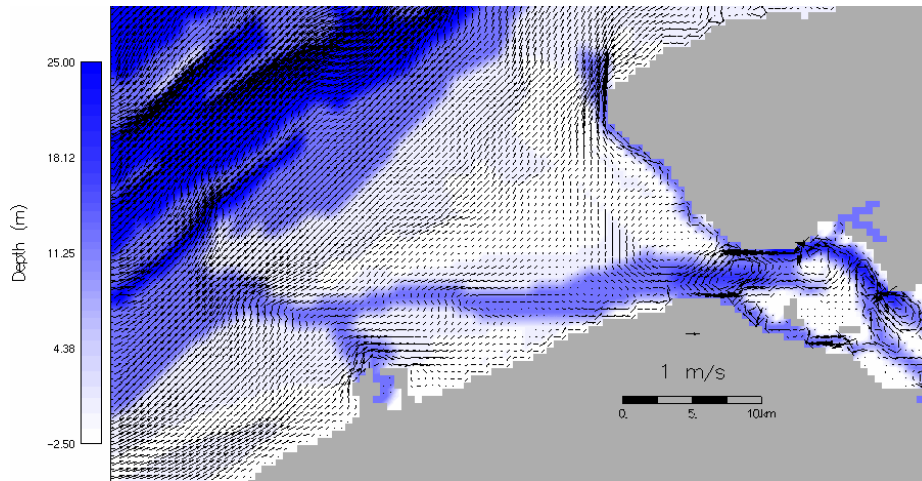


Figure 2.24: Residual flux velocities in the outer part of the Scheldt estuary.

Within the estuary, the effects of the river discharge can be seen near to the initial discharge point heading seaward; however its influence is limited to a small area due to the dominance of tidal forcing (Figure 2.25). The large intertidal areas located between the channels in the middle estuary play an important role in terms of water flux circulation with net transport almost absent in these areas whilst fluxes increase in the deeper channels which show some circular pattern. Averaged across the estuary however, the residual flux velocities in this region may be negligible.

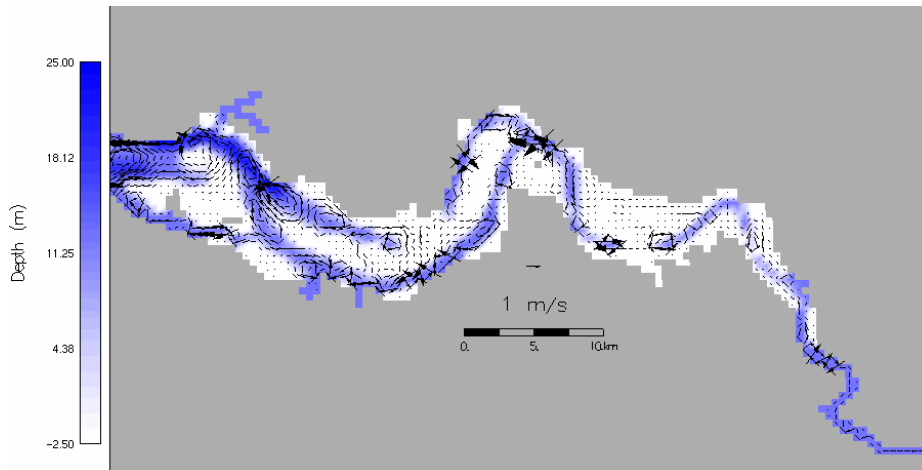


Figure 2.25: Residual flux velocities in the inner part of the Scheldt estuary.

Residual Velocity

The residual velocities are the net velocities obtained after balancing currents in different directions and they are of particular importance with regard to transport of particulate matter such as sediment transport. The primary Scheldt model shows that the residual velocities are not particularly important close to the coast around in the vicinity of the Scheldt with velocities of $0.01-0.02 \text{ m}^{-1}$ (Figure 2.26), although residual velocities are higher near the to the estuary mouth at Westkapelle.

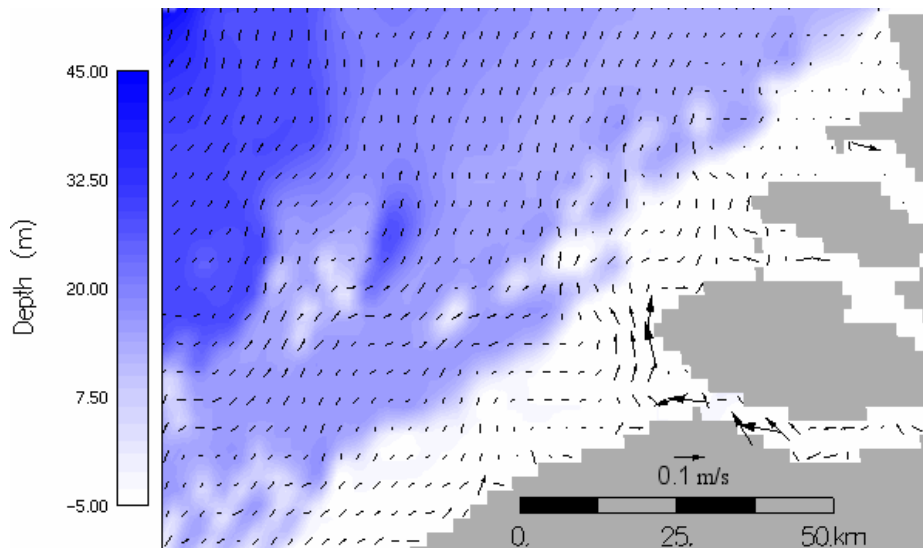


Figure 2.26: Residual velocities in the primary Scheldt model.

Results of the modelling using the secondary model grid shows greater seaward net velocities compared with landward residuals in the mouth of the Scheldt estuary (Figures 2.27 and 2.28) and this has implications with regard to the movement of suspended sediments area. Outside the estuary the residual currents split into two directions driven by the inertia of the currents at the mouth with the residual currents moving to northwest eventually moving inshore and joining the general residual flow and reaching high intensities near Westkapelle compared to the surrounding areas.

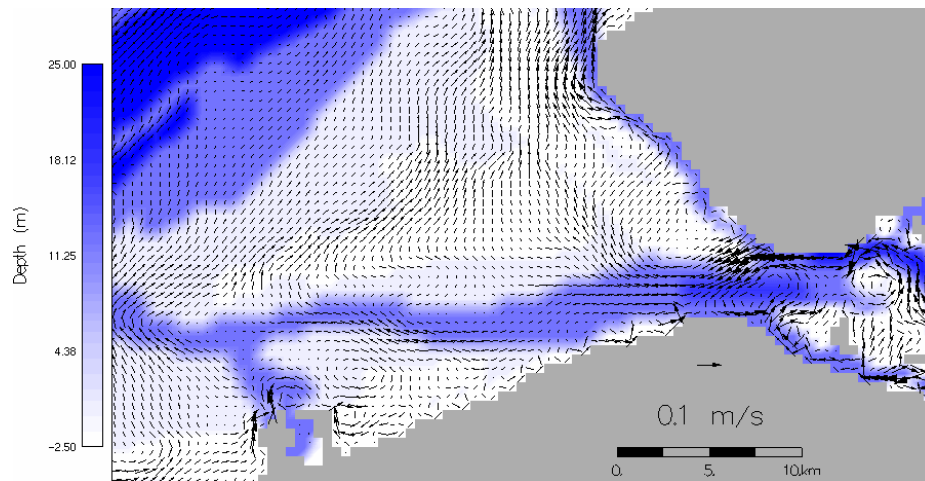


Figure 2.27: Residual velocities in the outer Scheldt area.

In the inner part of the scheldt the main circulation pattern for net residual currents is seaward which is in agreement with the observed sediment transport of the area as evident in the transport of cohesive sediments out of the estuary.

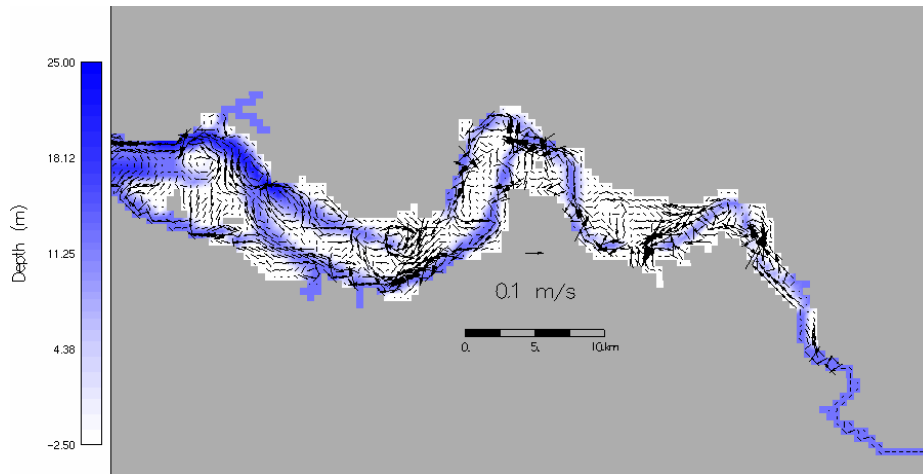


Figure 2.28: Residual velocities in the inner Scheldt area.

2.3.3 RESIDENCE TIME

An important parameter in terms of the hydrodynamic regime and subsequently for water quality is the residence time i.e. the length of time required to evacuate water from the estuary and replace it by new water. This property plays an important role with regard to the water quality of the water reaching the sea, because it dictates the length of time that the compounds carried by the sea water are subject to the ecological processes within the estuary.

In addition, residence time determines the quantity of compounds such as nutrients reaching the estuary mouth (Wollast, 1993 in Soetaert and Herman, 1995a) and is a major factor in terms of primary production (Braunschweig *et al*, 2003). To estimate the residence time in the Scheldt, a methodology proposed by Braunschweig *et al* (2003) has been followed. The methodology applied to the Scheldt estuary consists of in defining a box covering the whole estuary from Antwerp to the estuarine mouth (Figure 2.29) and then calculating the average residence time for a set of tracers with a volume equal to the entire water body. The water fraction (f) inside the box at each time step is calculated by the following expression:

$$f(t) = \frac{V(t)}{V_0}$$

With $V(t)$ being the volume of tracers contained in the box at a time t , and V_0 the original volume contained by the box, which sums the total volume of the estuary. When $V(t)$ equals to zero implies that all the original volume of water has been replaced by new water and then t would be the residence time of that mass of water.

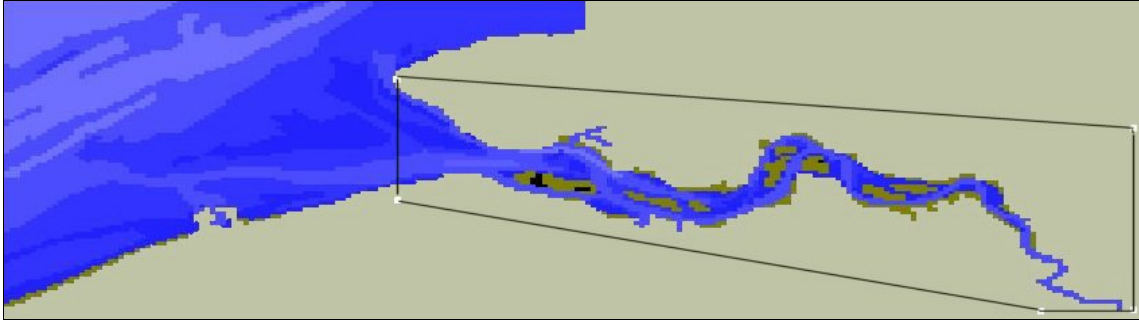


Figure 2.29: Defined box for calculating residence time in the Scheldt estuary.

Tracers with a volume of $5 \cdot 10^6 \text{ m}^3$ were defined to occupy the whole estuarine basin and the volume of these tracers were set as constant so their evolution in time within the estuary could be calculated. Figures 2.30 and 2.31 depict the original situation of these tracers and a snapshot of their location after 19 days (19-Jan-2000), where it can be observed how the particles are able to travel through the intertidal channels and along the estuary.

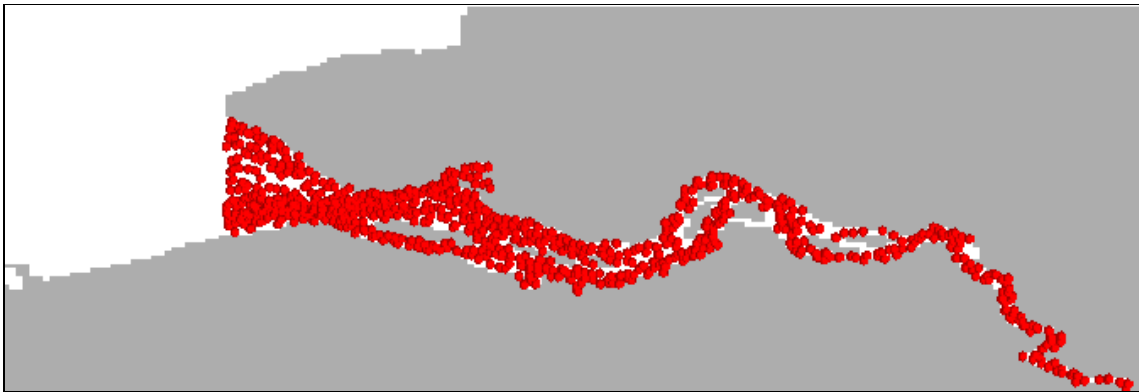


Figure 2.30: Original position of the tracers within the Scheldt estuary.

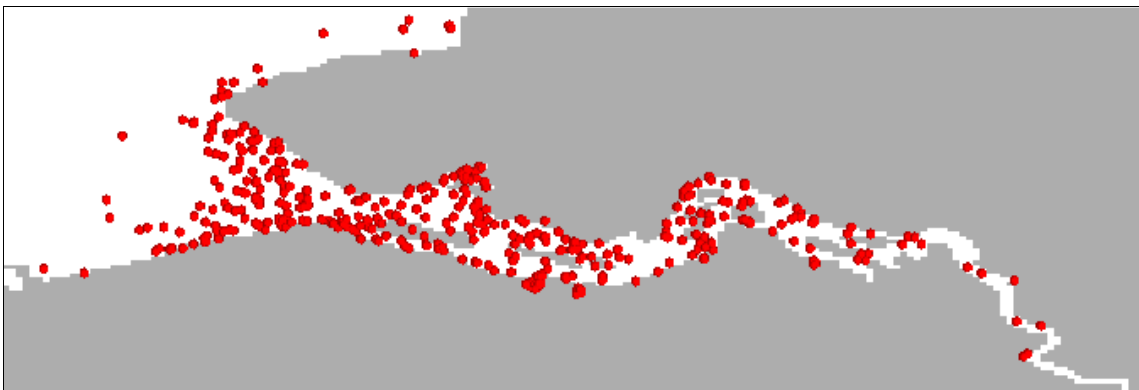


Figure 2.31: Position of the tracers nineteen days after their release in the Scheldt estuary (19-Jan-2000).

Two different scenarios were used to determine the residence time, one related to winter conditions with the particles released on the 1st of January 2000 and a second one during summer with particles released in the 1st of August 2000 where the river discharges applied were 2-3 times smaller. Eventually during the modelling process the volume of particles within the estuary becomes static with a small fraction of the tracers confined within the box for a prolonged period of time and this leads to the derivation of a misleadingly high residence time. Due to this behaviour, the residence time has been defined as the time needed to evacuate 95 % of the original volume of particles. The remaining volume (of tracer particles) within the estuary generally tends to show an exponential relationship to time (until particle movement in the estuary becomes static) and subsequently the remaining volume of particles has been plotted on a log₁₀ scale to transform the relationship from an exponential relationship to a linear one (Figure 2.30). Linear regressions of (log transformed) remaining volume against time in winter and summer over the first 170 days subsequently show a very good fit (Table 2.3).

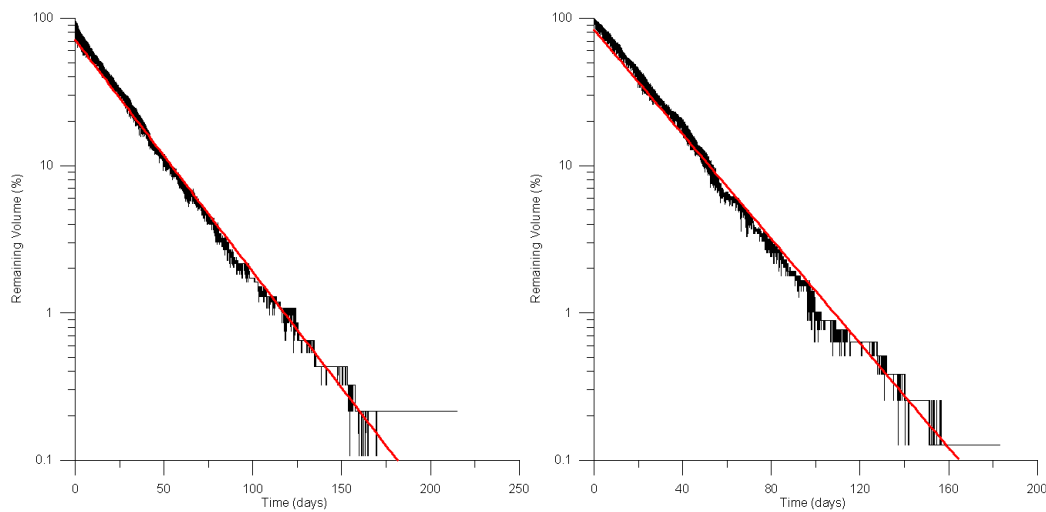


Figure 2.32: Relative remaining volume within the estuarine box (with exponential fit lines in red) during winter conditions (left) and summer conditions (right).

Table 2.3: Linear regression analysis results for the different stations in the Scheldt estuary.

Release Time	Exponential Fit Equation	R square
01-January-2000	$\ln(Y) = -0.04083079445 * X + 4.425949528$	0.990584
01-June-2000	$\ln(Y) = -0.03624407692 * X + 4.265497178$	0.992123

Assuming that the estuary volume would be completely renewed when the 95% of the original volume has moved from the estuarine basin, and applying the formulas above, residence times for winter and summer are 69.38 days and 73.68 days respectively. These values are in concordance with the values for residence times described in the literature e.g. 60 days (Gerringa *et al*, 1998), 1-3 months (Wollast, 1986 in Cancino and Neves (1998)), 50-70 days (Soetaert and Herman, 1995a) and 75 days (Van Spaendonk *et al*, 1993, Kromkamp *et al*, 1995).

3. WATER QUALITY MODELLING OF THE SCHELDT ESTUARY

Following the simulation and validation of the hydrodynamic regime the next aim of the current study was to use MOHID to run the ecological and water quality modules in order to assess fluxes of nutrients through the estuary, the resulting impact on phytoplankton and zooplankton populations and the implications for eutrophication in the Scheldt system. On the basis of available data for model set-up and validation, modelling in the Scheldt was carried out for the year 2000 and the simulation was carried out for a period of one year (from January 1st 2000).

3.1 Development of the Ecological & Water Quality Model

3.1.1 MODEL SET-UP

Once the hydrodynamic model has been tested and validated with regard to the observed empirical measurements, the next step is to utilise the ecological and water quality modules of MOHID. Initial water quality conditions and boundary conditions were set up using recently measured observed data. The primary data sources for this was the NIOO-KNAW Scheldt monitoring dataset (EUROTROPH webpage, <http://www.obs-vlfr.fr/eurotroph/index.php>) and the IDOD database (Integrated and Dynamical Oceanographic Data) from the Belgian Marine Data Centre (BMDC, <http://www.mumm.ac.be/datacentre/>). The NIOO-KNAW Scheldt monitoring dataset is comprised of observed data for 63 oceanographic variables from 16 fixed stations along the Scheldt estuary, from Vlissingen to the fresh water reaches of the estuary, measured for the period comprising 1995-2003. Data from these stations have been used to provide the initial conditions and the river boundary concentrations and for validation purposes along the estuary. The stations used to model the Scheldt estuary are represented in Figure 3.1.

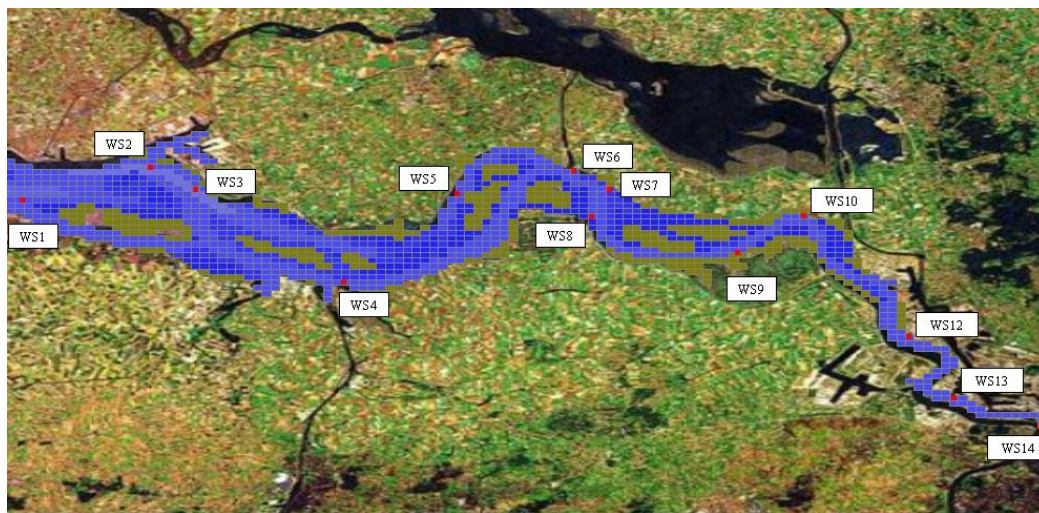


Figure 3.1: NIOO-KNAW water quality stations along the Scheldt estuary used for modelling.

The IDOD database contains parameters and variables for the Belgian coastal area and the Scheldt estuary. As the NIOO-KNAW dataset was more complete for the Scheldt estuary, the IDOD database has been used for the Belgian coast. From the large number of stations within IDOD, two stations for which the most data was available have been used, namely stations 330_a and 710_a (Figure 3.2). Data from these stations have been used to provide the boundary conditions for the surrounding North Sea area and to validate the model results in the Scheldt plume, respectively. Hereafter, the

stations 330_a and 710_a will be referred as WSMARINE and WSPLUME respectively. These two datasets have complement each other, covering the completely the Scheldt plume and estuary till the fresh water area. Parameters and variables from other datasets and sources have been used punctually during the process of modelling, and will be referred in the text when appropriate.

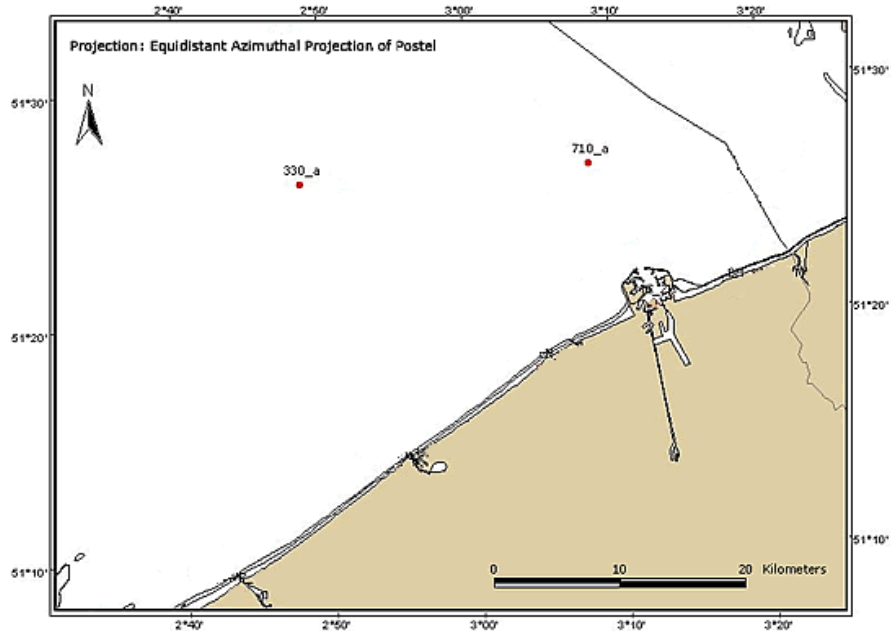


Figure 3.2: Location of the IDOD database stations used during the modelling experiments (source: modified from the original in BMDC webpage).

3.1.1.1 Initial conditions

In order to simulate as accurately as possible the initial conditions in the estuary, a series of boxes comprising the whole estuary were defined covering completely the *secondary* model domain (Figure 3.3). These boxes allow are used to give an initial concentration to all the model cells comprised within the box for every water property and are also used to measure fluxes between the different areas of the estuary.

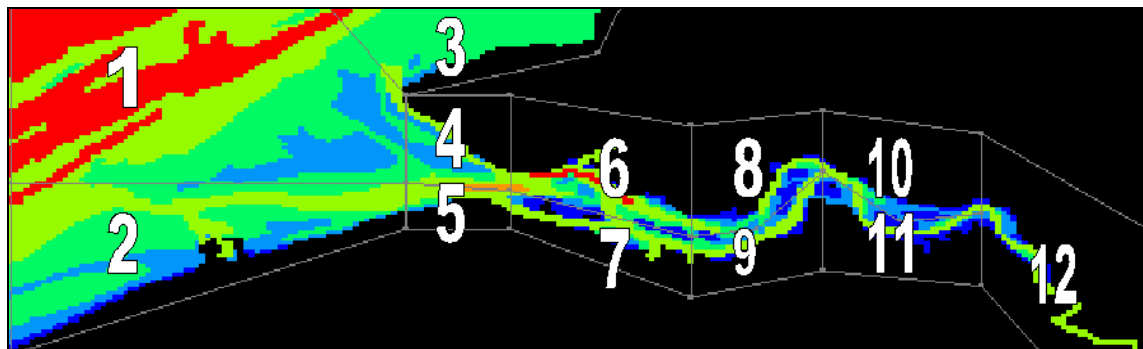


Figure 3.3: Defined boxes for calculating water properties in the Scheldt estuary.

To recreate the initial values of the estuary for each water property, a synthetic year was created using the average value of the water quality stations contained in each box from the previously

mentioned datasets. As the model runs start on January averaged values from 1995-2003 for that month have been used as the initial value when data for the modelled variable was available. The IDOD database provided data for the three external boxes; whilst the NIOO-KNAW database has been used to provide values for the nine estuarine boxes. However, for variables not present on these databases a constant (default) value has been applied.

3.1.1.2 Boundary conditions

Two different sets of boundary conditions have been applied when modelling the Scheldt estuary, one for the fresh water discharge and a second one for the North Sea boundary. At each boundary a set of monthly averaged values from the year 1995 have been calculated in order to reproduce the variations in discharges concentrations occurring over a year period. In the case of the marine boundary, when data from a particular month for a particular variable (e.g. temperature, oxygen concentration) was absent a sixth order polynomial regression was calculated to complete the series.

3.2 Abiotic and Biotic Modelling Parameters

Abiotic variables are those which are considered to be largely independent from the influence of the biological processes occurring in the area. In this study this includes salinity, temperature and sediments.

3.2.1 SALINITY

The Scheldt estuary has a wide range of salinity values along its basin going from freshwater values at the head to fully marine values near its mouth. Salinity in the upper reaches of the Scheldt estuary is a relatively constant varying between 1 and 5 PSU, whilst further downstream the estuary large fluctuations in salinity occur throughout the year (± 8 PSU) until salinity begins to stabilise again near the mouth of the estuary (Kromkamp *et al*, 1995).

Salinity in the model is influenced mainly by the freshwater discharge and to a lesser extent by the evaporation processes occurring at the water surface. Constant values have been applied at both the fresh water and the marine boundary, as salinity has been considered relatively constant at these areas throughout the year. The values applied are 0.5 and 33.7 PSU for the upstream and downstream boundaries of the estuary respectively. The initial values imposed in the model boxes (Figure 3.3) are represented in Table 3.1.

Table 3.1: Initial values for salinity applied to the model boxes.

Box Number	1	2	3	4	5	6	7	8	9	10	11	12
Salinity (PSU)	33.4	33.4	33.4	25.0	25.0	22.0	22.0	18.0	18.0	15.0	15.0	4.0

The modelled salinity results generally show a good agreement with the dynamics of the area and with the observed values along the Scheldt estuary. In Figure 3.4, the averaged salinity distribution corresponding to March 2000 is shown. The salinity continuum along the estuary can be observed addition to the salinity front at estuary mouth, which is the response in terms of salinity of the residual hydrodynamical front, as described by Baeyens *et al* (1998b).

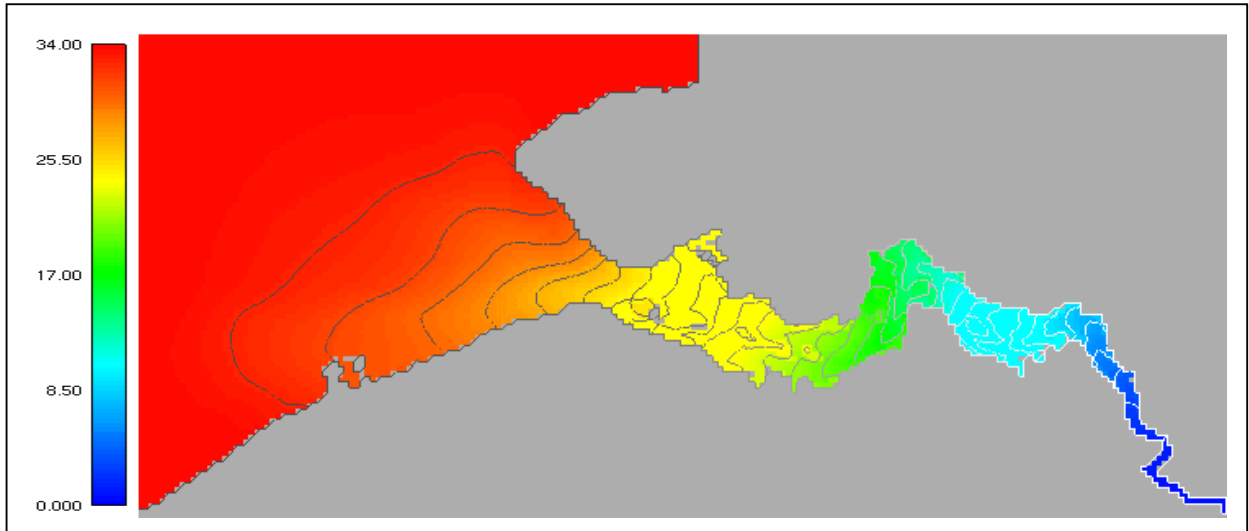


Figure 3.4: Salinity continuum along the Scheldt estuary and coastal area, average values March 2000 (isolines every 1 PSU).

As was discussed, the main factor controlling salinity in the estuary is river discharge. When the river discharge reduces intrusion of saltier water occurs in the freshwater reaches. This phenomenon can be observed in WS14 (Figure 3.5), as our imposed value is constant from the freshwater area (0.5 PSU), it increases when the discharge values decrease. The values on this area show a great concordance with the observed values (red squares). The increase of salinity in this area occurs simultaneously in our model results and in the observed values.

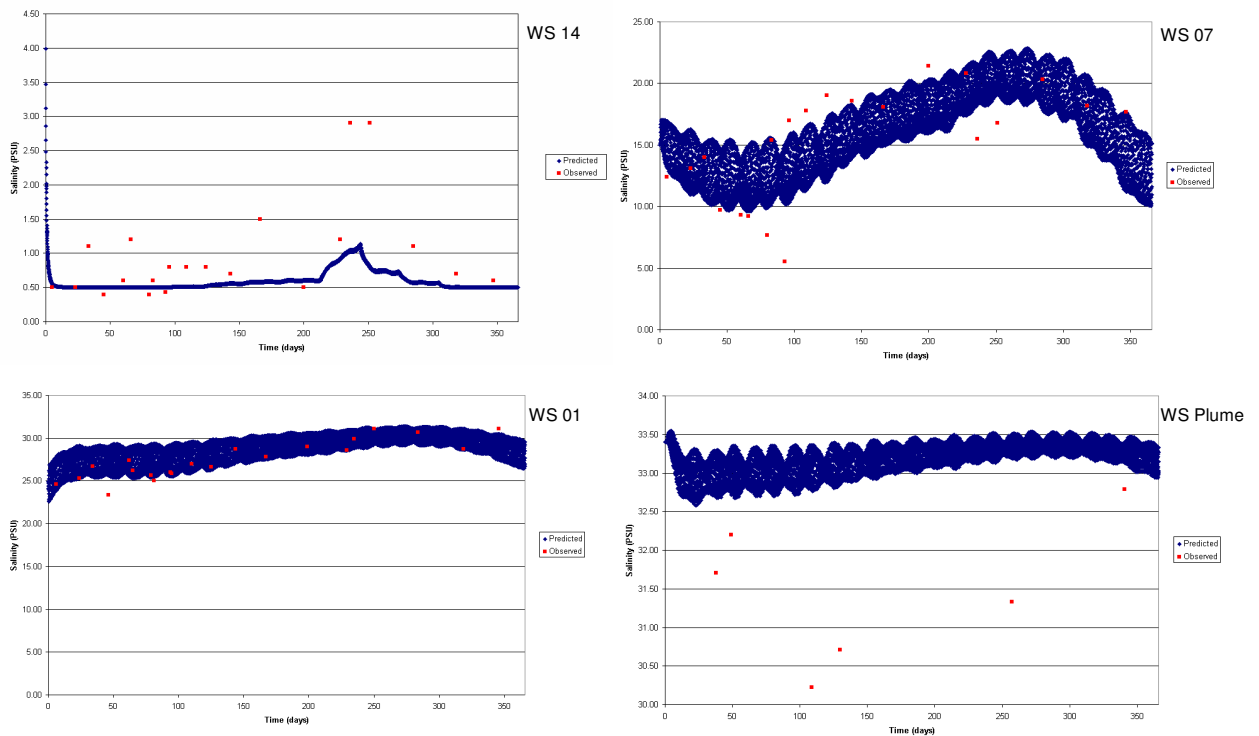


Figure 3.5. Predicted and observed salinity at different stations along the Scheldt estuary.

The variability of salinity ranges as described by Kromkamp *et al* (1995) can be observed in Figure 3.5. It is evident that variability in salinity is highest in the centre of the estuary meanwhile at the head and mouth the temporal variation along the year is relatively small. With respect to the plume, the values predicted are slightly higher than the observed values although there was relatively little observed data for the year 2000 and this lack of agreement could be due in part to the use of a constant value for this boundary. However, in general it is considered that the modelling of the salinity field was completed satisfactory for the Scheldt estuary and the surrounding area. Figures for the remaining water quality stations in terms of salinity are included in Appendix I.

3.2.2 TEMPERATURE

Temperatures observed in the Scheldt estuary are highly variable ranging from around 5°C in winter to more than 20°C during summer. The observed values in the estuary are highly dependant on the temperature of riverine inputs (which also have a broad range of values throughout the year) in addition to meteorological conditions such as air temperature, solar radiation, cloud coverage etc. The adjacent North Sea water also shows a range of temperatures during the year due in part to the fact that the coastal waters here are relatively shallow. The initial values imposed to the model boxes are based on averaged values for the month of January during 1995-2003 (Table 3.2).

Table 3.2: Initial values for temperature applied to the model boxes.

Box Number	1	2	3	4	5	6	7	8	9	10	11	12
Temperature (°C)	5.92	5.92	5.92	5.76	5.76	5.80	5.83	5.80	5.86	5.92	6.15	6.35

In order to simulate the range of temperatures occurring during throughout the year, monthly temperature values have been set for the freshwater and marine boundaries in addition to the air temperature (Table 3.3). The model also computes the intensities of solar radiation based on latitude of the survey area in conjunction with the level of cloud coverage present in the area. For this reason, a monthly value of cloud coverage factor has also been applied (values ranging from 0-1 with a value 1 indicating total cloud cover). In addition, a monthly value for relative humidity (ranging from 0-1 with a value of 1 indicating 100% relative humidity) has been used to represent latent heat flux. More technical details with regard about the atmosphere module are given in the MOHID manual (<http://www.mohid.com>).

The data for calculating the monthly values of these parameters were derived from the Royal Netherlands Meteorological Institute (KNMI, webpage: <http://www.knmi.nl>). Daily time series of weather data for the weather station at Vlissingen were averaged for the period 1991-2000 to obtain cloud coverage and atmospheric temperature. Relative humidity was obtained from the KNMI averaged values for the Vlissingen station. A summary of this data are be found in Table 3.3.

Table 3.3: Monthly values applied at the river, marine and atmosphere boundaries.

Month	1	2	3	4	5	6	7	8	9	10	11	12
Temperature river (°C)	5.06	6.68	8.36	10.77	15.42	19.35	20.75	22.41	19.29	14.96	10.38	7.26
Temperature marine (°C)	5.81	6.26	7.29	8.99	11.37	14.13	16.64	18.06	17.61	15.04	11.29	9.22
Temperature air (°C)	4.15	4.40	6.99	9.26	13.07	15.45	18.02	18.53	15.74	11.70	7.72	4.92
Cloud coverage (0-1)	0.70	0.70	0.68	0.64	0.61	0.64	0.60	0.57	0.66	0.67	0.73	0.73
Relative Humidity (0-1)	0.87	0.85	0.84	0.79	0.78	0.79	0.79	0.78	0.81	0.83	0.83	0.87

Observed maximum temperatures in the estuary, the North Sea and in the atmosphere are reached during August, whilst minimum values occurred in January (Table 3.3). This pattern was also replicated with the modelling results and in general a good simulation of water temperatures over time was obtained (Figure 3.5). Spatially the maximum temperatures are observed in the river discharge, decreasing towards the mouth of the estuary, whilst the minimum temperatures tended to occur within the estuary with values below 5°C.

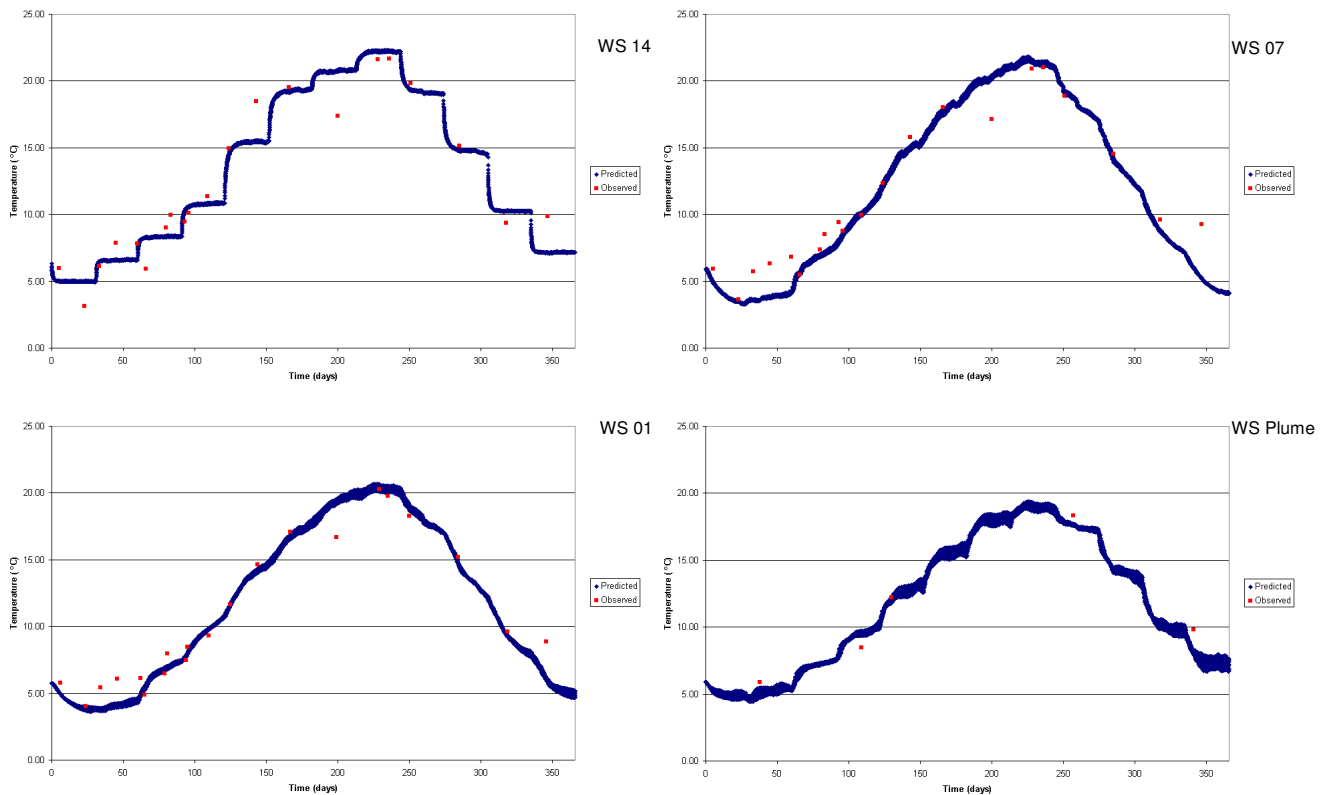


Figure 3.5: T Predicted and observed temperature at different stations along the Scheldt Estuary.

3.2.3 SEDIMENTS

The sediments within the Scheldt are influenced mainly by the transport of sand from the North Sea and coastal areas adjacent to the estuary as the sand fluxes from the river are practically nonexistent. Sediment transport into the Scheldt is a major factor influencing the variation in morphology of the Scheldt system (Van der Spek, 1997). As the intensity of currents during flood tides are greater than during ebb sand is transported into the estuary and this is not compensated for by the seaward transport on the ebb tide. Thus results in a net upstream transport of sands in contrast to other many other European estuaries which are primarily sediment exporters (Cancino and Neves, 1999). The Scheldt bottom consists mainly of sand, either fine sand (Van Eck (1997) or coarse, medium-coarse and medium-fine sand (Baeyens *et al*, 1998a). The proportion of mud is highly variable spatially, with very low values (<0.02%) in the channels (Mulder and Uddink, 1991) which mainly consist of erosion-resistant bottoms with gravel and shell fragments (Franken *et al*, 2004). In the current study, as the scope of the modelling exercise is related to water quality, the sediments studied are primarily cohesive sediments (mud) and in particular those which are transported in the water column (suspended sediment). Subsequently, the following discussions on sediment transport relate only to cohesive sediments.

In the Scheldt estuary, turbidity variations due to cohesive sediments in suspension is relatively small compared to the upper freshwater reaches, as the processes of sedimentation and erosion are less intense in the estuary due to the composition of the bottom sediments (Baeyens *et al*, 1998a). In the long term, meteorological conditions and river discharge are the main processes affecting the quantity of sediments reaching the estuary.

Along the estuary, sediment concentration shows a decrease by a factor of 4 to 5 between the upper and downstream estuarine areas (Baeyens *et al*, 1998a), with the annual averages varying from more than 80 mg/l at the freshwater boundary to less than 30 mg/l at the seaward boundary (Kromkamp and Peene, 1995). The maximum turbidity area is located in the upper parts of the estuary near the port of Antwerp (Portela and Neves, 1994) although the exact location varies depending on the river discharges and the neap-spring cycle in the estuary (Fettweis *et al*, 1998). Suspended sediment concentration is greater during winter than during summer (Fettweis *et al*, 1998).

Suspended sediments (and other particles) which make up the total suspended particulate matter (SPM) in the Scheldt is a factor of great importance because of the limitation that it imposes on the level of photosynthesis activity due to shading from solar radiation. Due to the high variability on the value of suspended matter in the Scheldt upper reaches and in the North Sea boundary, a temporal pattern could not be found to impose at the boundaries. A constant SPM concentration has been applied to both boundaries with values of 106 mg/l applied at the head of the estuary (as used by De Smedt *et al*, 1998) and 8.39 mg/l applied at the North Sea boundary (derived from the average of the observed values at the WSMARINE station). An average value from 1995-2003 (from the NIOO-KNAW database) has been applied to the model boxes (Table 3.4).

Table 3.4: Initial values for suspended particulate matter (SPM) applied to the model boxes.

Box Number	1	2	3	4	5	6	7	8	9	10	11	12
SPM (mg/l)	25.0	25.0	25.0	33.52	33.52	29.12	29.12	35.10	42.61	30.89	37.83	54.70

In terms of cohesive sediments on the sea bed an initial value of 1.00 kg m^{-2} over the estuary as a whole is used to start the simulation of erosion and deposition processes. The equations used by the model to modify these original values relate to the erosion algorithm derived by Partheniades (1965):

$$\frac{dM_E}{dt} = E \left(\frac{\tau}{\tau_E} - 1 \right) \quad \text{for } \tau > \tau_E$$

$$\frac{dM_E}{dt} = 0 \quad \text{for } \tau < \tau_E$$

where τ is the bed shear stress, τ_E is a critical shear stress for erosion and E is the erosion constant ($\text{kgm}^{-2}\text{s}^{-1}$). The model simulates erosion processes when the shear stress goes above than the critical shear stress needed for erosion and stops when the shear stress falls below this critical value.

For sediment deposition the equations described by Krone (1962) are used which define the probability of deposition as:

$$p = \left(1 - \frac{\tau_b}{\tau_{cd}} \right)$$

where τ_b and τ_{cd} are the bottom shear stress and a critical shear stress for deposition respectively.

Assuming that the deposition flux can be defined as:

$$F_p = \frac{dm}{dt} = -pW_sC$$

where p is the probability of sediment deposition, W_s the settling velocity and C the near-bed cohesive sediment concentration. Substituting the probability defined by Krone (1962), the resulting equations are:

$$\frac{dM_D}{dt} = (CW_s)_B \left(1 - \frac{\tau}{\tau_D} \right) \quad \text{for } \tau < \tau_D$$

$$\frac{dM_D}{dt} = 0 \quad \text{for } \tau > \tau_D$$

As with the erosion process, when the stress applied over the sediments in the bottom is lower than a critical value matter is deposited onto the seabed, whilst if the stress value is higher than the critical value deposition does not occur.

The values assigned to the erosion parameters have been taken from those proposed by Mulder and Udink (1991) to model the cohesive sediment transport in the Scheldt estuary (Table 3.5) and the critical shear deposition parameter are those described by Winterwerp *et al* (1991) during laboratory experiments with Scheldt estuary mud.

Table 3.5: Parameters used to model the erosion and deposition of cohesive sediments.

Parameter	Symbol	Value	Source
Critical shear erosion	τ_E	0.4 Nm ⁻²	Mulder and Udink (1991)
Erosion rate	E	5·10 ⁻⁵ kgm ⁻² s ⁻¹	Mulder and Udink (1991)
Critical shear deposition	τ_{cd}	0.2 Nm ⁻²	Winterwerp <i>et al</i> (1991)

The model results show a decrease in suspended sediments (SPM) from the head to mouth of the estuary, and a plume of suspended sediments is evident at the mouth of the estuary in the vicinity of the hydrodynamic front. Figure 3.6 shows a snapshot of the distribution of sediments during an ebb tide on the 16th March 2000 and distribution and extent of the Scheldt plume is clearly visible. The extent of the plume reaches as far as the port of Zeebrugge port and the modelled distribution shows a high degree of correlation observed suspended sediments (Figure 3.7).

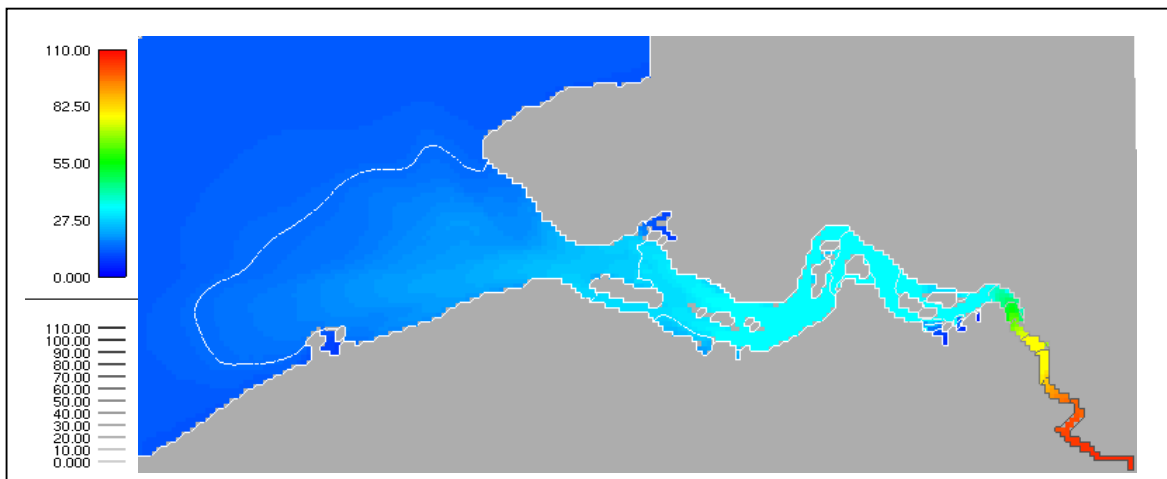


Figure 3.6: Distribution of predicted suspended sediments on an ebb tide (16th March 2000).



Figure 3.7: Aerial view of the Scheldt estuary and plume (source: Eurotroph webpage).

As the prediction of salinity derived from the model was highly correlated to the observed values it is useful to plot values of SPM against salinity in order to describe the variation in levels suspended sediment along the estuary after 100 days of model simulation (March). Two different areas in the estuary can be distinguished with an area of high suspended sediment at the maximum turbidity zone (MTZ) below 5 PSU (where deposition takes place) and a second area covering the remainder of the estuary where the sediment slope is less acute and concentrations gradually decrease downstream (Figure 3.8). Linear regressions of SPM against salinity for these two areas are highly significant with high R^2 values (>0.99). Similarly strong relationships were also found after 200 days (July) and 300 days (October) of simulation (not shown).

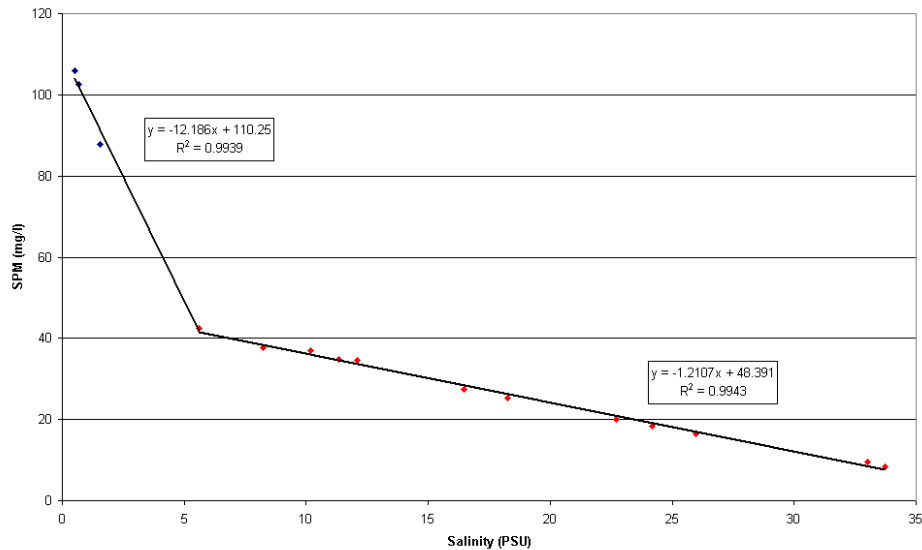


Figure 3.8: SPM plotted against salinity after 100 days.

The pattern of cohesive sediment distribution on the seabed changes markedly from the original default values (1kgm^{-2} over the whole bed) following one year of simulation due to changes in sediment erosion and deposition predicted by the model and entry of the suspended sediments from the river discharges. The final distribution after one year's simulation shows an upper estuarine area where sediments have been deposited with cohesive sediment largely absent from the remainder of the estuary with the exception of areas such as ports, salt-marshes and other areas with low current velocities (Figure 3.9).

Temporal variations in suspended sediment concentrations at the water quality stations show a similar pattern with high levels during the winter months which then decreasing rapidly to lower and more stable values (Figure 3.10). Model results are generally in concordance with the observed values along the estuary and in the plume. At the upper estuary water quality station the intrusion of brackish downstream water during low river discharge is evident, although the SPM concentration at the river discharge area does not appear to show a clear seasonal pattern.

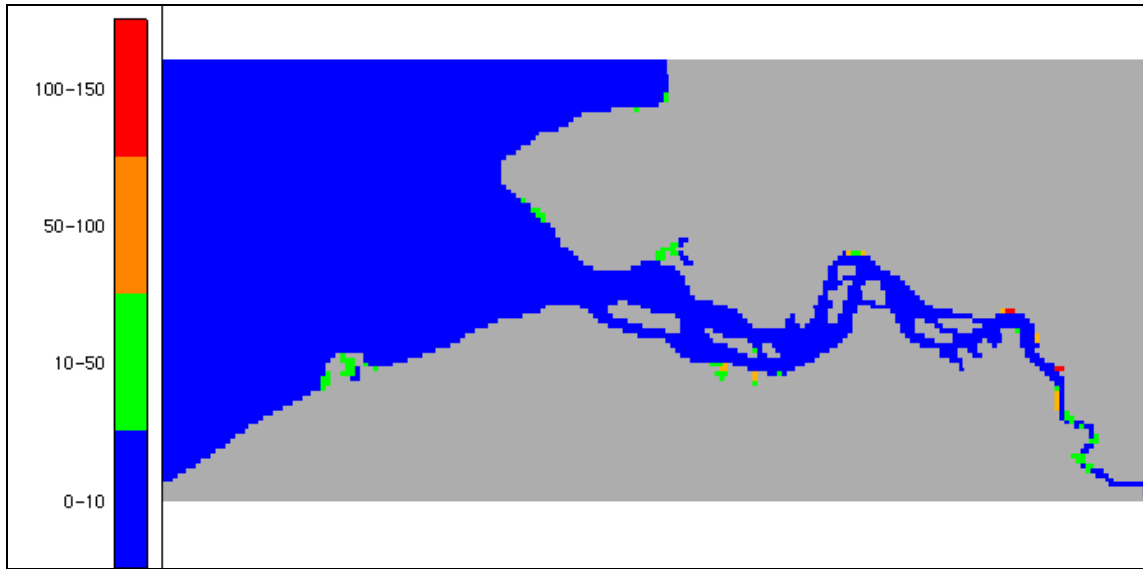


Figure 3.9: Seabed cohesive sediment distribution after one year of simulation (in kgm^{-2}).

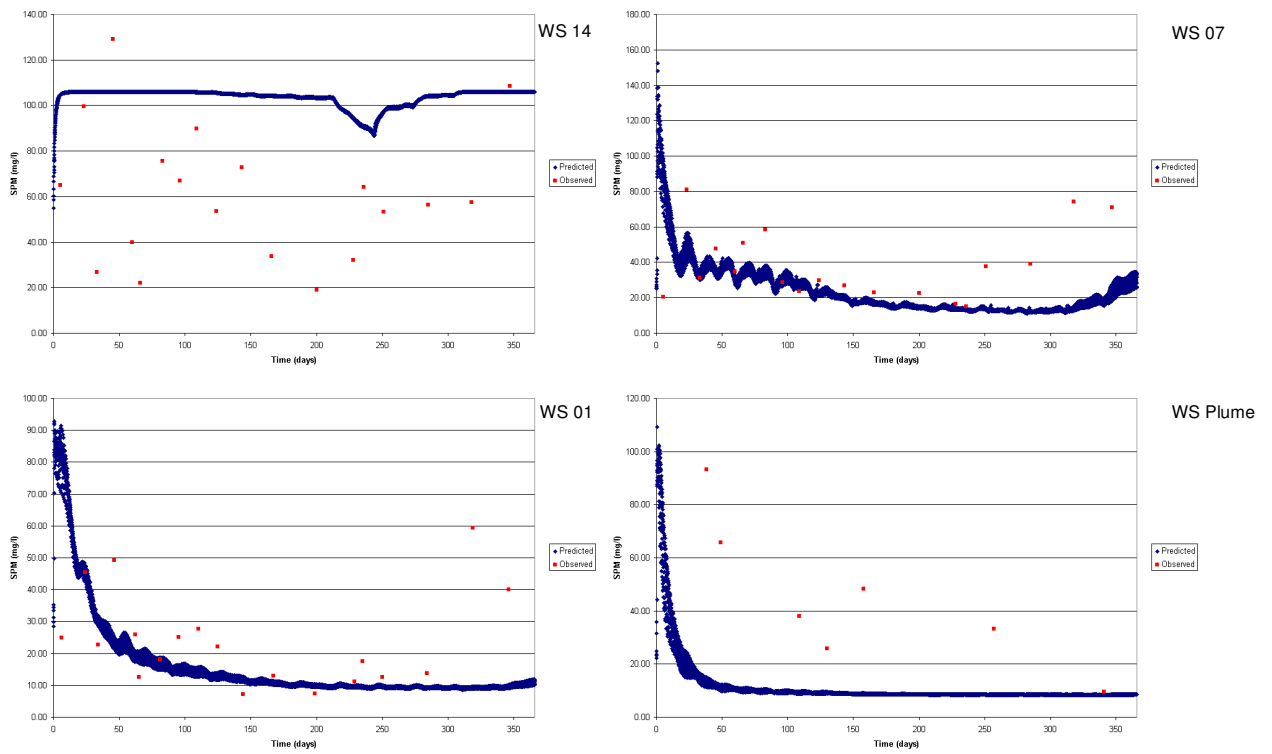


Figure 3.10: Predicted and observed SPM at different stations along the Scheldt estuary.

3.2.4 OXYGEN

Oxygen levels in the Scheldt estuary show a great deal of variation from anoxic or nearly anoxic values during some periods of the year in the upper reaches of the estuary (Van Spaendonk *et al.*, 1993; Kromkamp and Peene, 1995) to oxygen saturated waters a few kilometres downstream.

The processes that act as a source of oxygen within the system and are implicitly modelled in the MOHID model comprise photosynthesis by phytoplankton, denitrification and nitrate uptake by phytoplankton (Figure 3.11). In addition, atmospheric aeration also increases the oxygen concentration in the water column. Conversely, aerobic respiration by phytoplankton and zooplankton and the mineralisation of the dissolved organic matter (DOM) and particulate organic matter (POM) remove oxygen from the system and these are also modelled by MOHID. A more detailed formulation of the processes involving oxygen contents can be found in Appendix II and in the model manual (MOHID webpage: <http://www.mohid.com>).

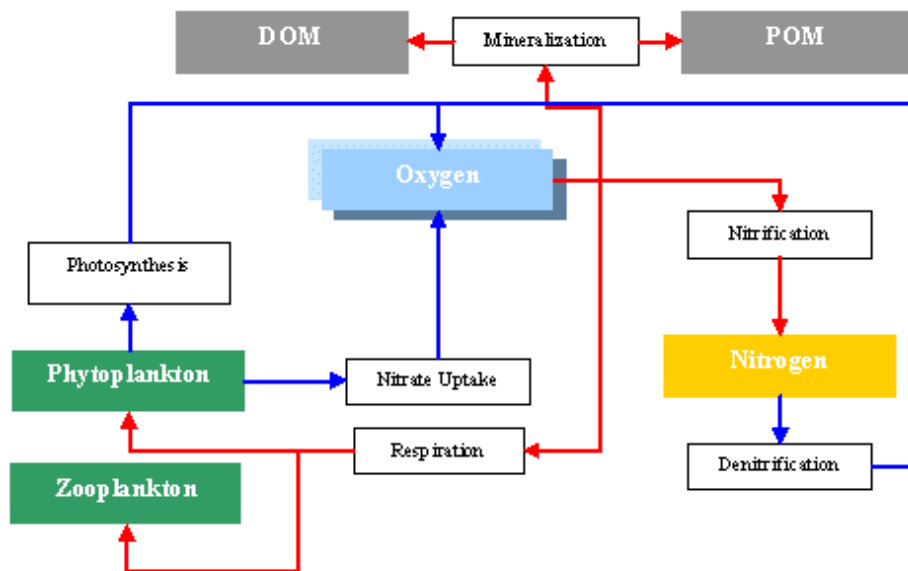


Figure 3.11: Internal fluxes of inorganic oxygen (blue arrows indicate sources and red arrows indicate sinks) from the MOHID description manual <http://www.mohid.com>.

As for the other water quality parameters a monthly averaged value has been imposed on both boundaries (marine and freshwater) (Table 3.6), and averaged January values have been defined as the initial values for the estuary boxes (Table 3.7) in order to start the simulation.

Table 3.6: Monthly oxygen values applied at the freshwater and marine boundaries.

Month	1	2	3	4	5	6	7	8	9	10	11	12
O ₂ river (mg/l)	6.257	5.520	4.478	2.324	1.041	0.983	1.525	2.239	1.294	1.620	1.965	4.187
O ₂ marine (mg/l)	10.169	9.985	10.997	11.155	10.245	8.888	7.811	7.419	7.635	8.045	8.315	8.901

Table 3.7. Initial values for inorganic oxygen concentrations applied to the model boxes.

Box Number	1	2	3	4	5	6	7	8	9	10	11	12
Oxygen (mg/l)	10.169	10.169	10.169	10.448	10.448	10.678	10.678	11.02	10.683	10.705	9.987	6.556

The difference between the marine and freshwater boundaries of the estuary are apparent from Table 3.6 with the open sea saturated in oxygen and the river boundary almost depleted in oxygen during most of the year, particularly in the summer period. From Table 3.7 it is evident that in January moving downstream from the freshwater boundary a substantial increase in oxygen levels takes place almost immediately. This phenomenon is presumably due to atmospheric aeration, as the biological processes taking place during January are not of great magnitude.

In order to reproduce this effect, wind has been imposed onto the model for the water quality module (although wind stress was not been used for the hydrodynamic calculations). An hourly series of wind strength and direction from the Cadzan station corresponding to the year 2000 has been applied to the whole domain (HMCZ webpage, <http://www.hmcz.nl>). The prevailing wind in the area is from the North-East and can reach speed of over 20 m/s (Figure 3.12)

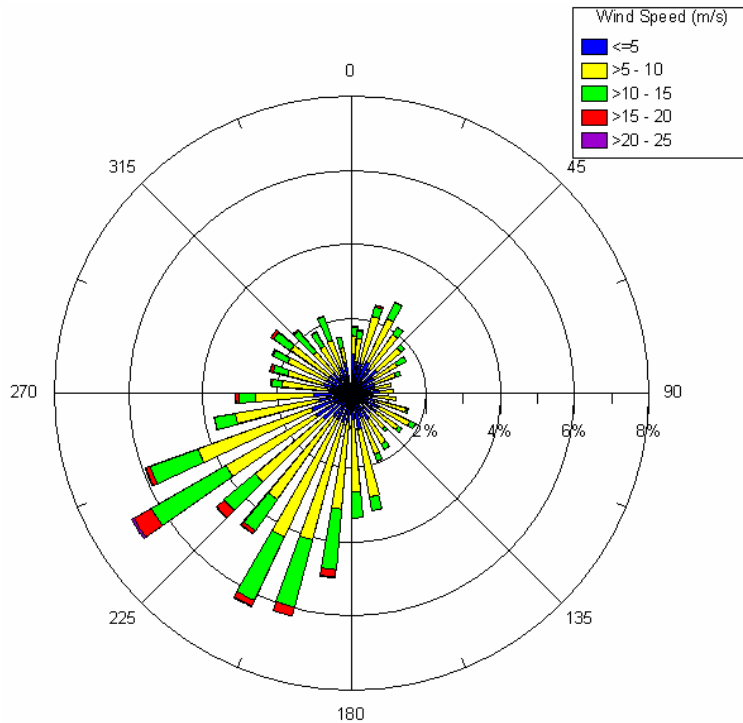


Figure 3.12: Wind distribution at Cadzan station for the year 2000.

Model predictions of oxygen concentration generally show a similar pattern and range to observed values (Figure 3.13). High oxygen concentrations are found during winter and then decrease during the summer months due to the lower capacity of dissolved gas at higher temperatures. The values obtained show a strong relationship to the observed values at the upper estuary and in the open sea. In the middle of the estuary due, to the high amount of organic nutrients that have been imposed onto the model, the water quality module consumes a large proportion of the oxygen available in mineralisation processes, giving lower oxygen concentrations than expected.

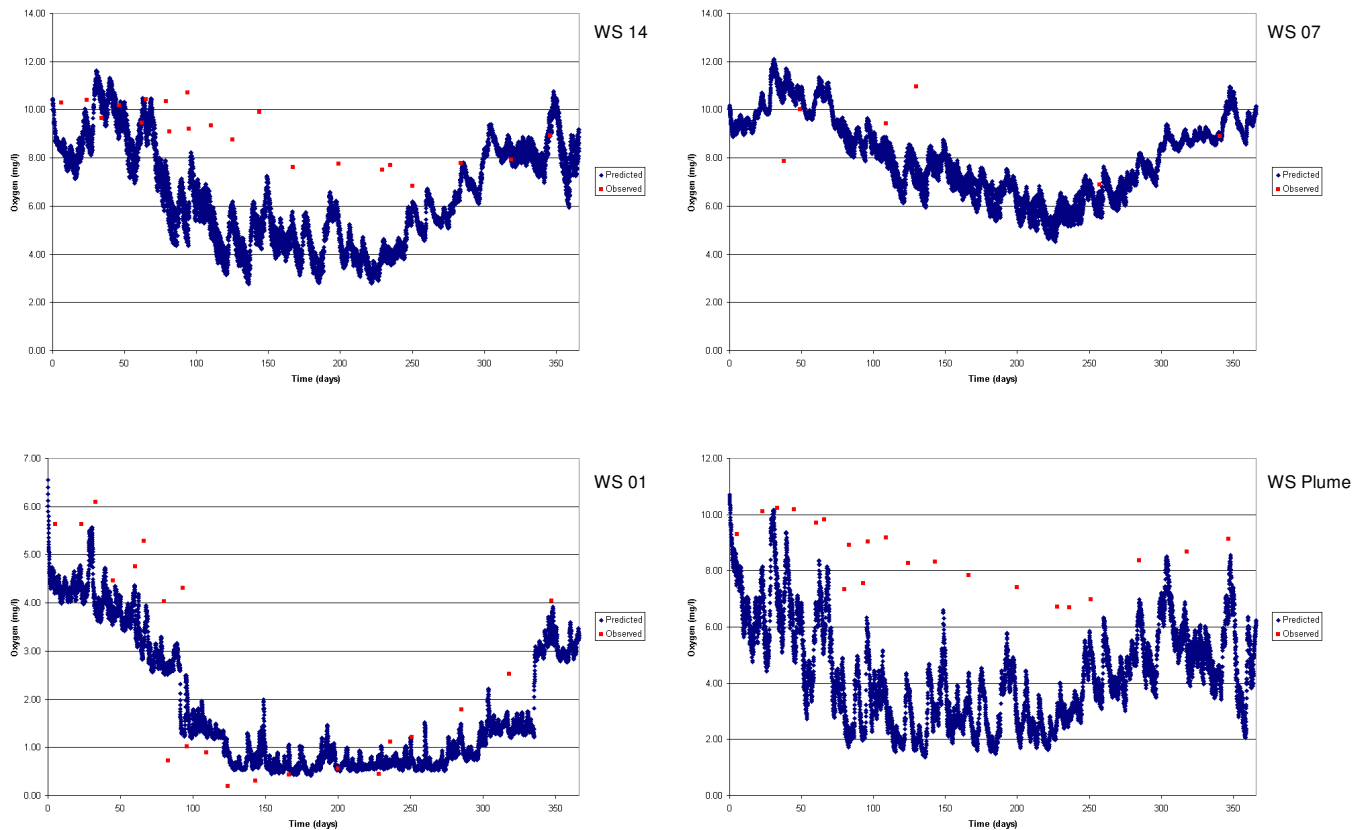


Figure 3.13: Predicted and observed oxygen levels at different stations along the Scheldt estuary..

Along the estuary a gradient of oxygen concentrations can be observed (Figure 3.13) with very low values in the upper reaches (with minimum values of approximately 0.5 mg/l over much of the year) and extremely saturated oxygen concentrations (with values greater than 10 mg/l, particularly during the winter period) a few kilometres downstream. According to the OSPAR Commission (2003) oxygen levels under 2 mg/l are considered acutely toxic whilst concentrations under 6 mg/l are considered oxygen deficient. The modelling results were used to assess which the areas of the Scheldt may potentially fail these criteria by using the 90th percentile to define which category a section of the estuary belonged to (i.e. if an area of the estuary had oxygen concentrations below 0.2mg/l for 90% of the time then it would be classed category 1 (acutely toxic) as shown in Table 3.8. The results of this approach for the Scheldt estuary during the first 100 days simulation, where the results were more accurate, can be observed in Figure 3.14.

Table 3.8: Categories for oxygen levels.

Category	Oxygen levels ranges (mg/l)
1	0-2
2	2-6
3	6-10

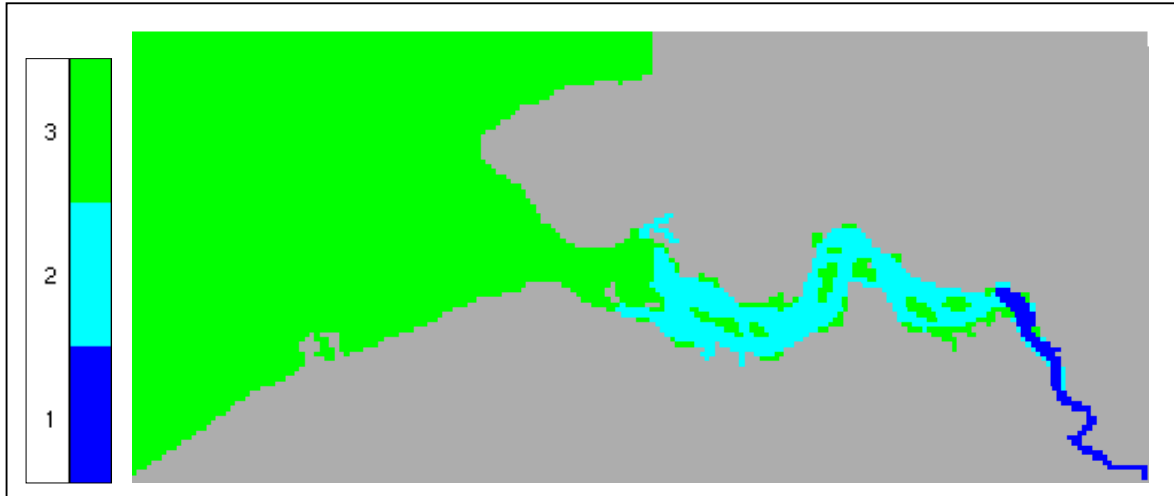


Figure 3.14: Oxygen levels in the Scheldt estuary according to the defined categories (Table 3.8) for the first 100 days of the year 2000.

From the results of the modelling three different areas can be distinguished according to their oxygen levels namely the head of the Scheldt estuary where oxygen levels would be acute toxic, the main estuary which is oxygen deficient, except for shallower areas and intertidal zones, and the mouth and outer estuary where oxygen levels are satisfactory. Whilst it should be emphasised that that the model tends to underestimate somewhat the oxygen levels in the estuary, using the precautionary approach the results are quite useful in highlighting which areas are potentially very poor quality in terms of oxygenation. As may be anticipated, oxygen along the estuary does not appear to show conservative behaviour and depending on the time of the year the estuary acts as either a sink or a source of oxygen (Figure 3.15). After 200 days simulation (July) the entire estuary is acting as an oxygen sink whilst 100 days later (in October/November) the estuary is produces more oxygen than has been consumed.

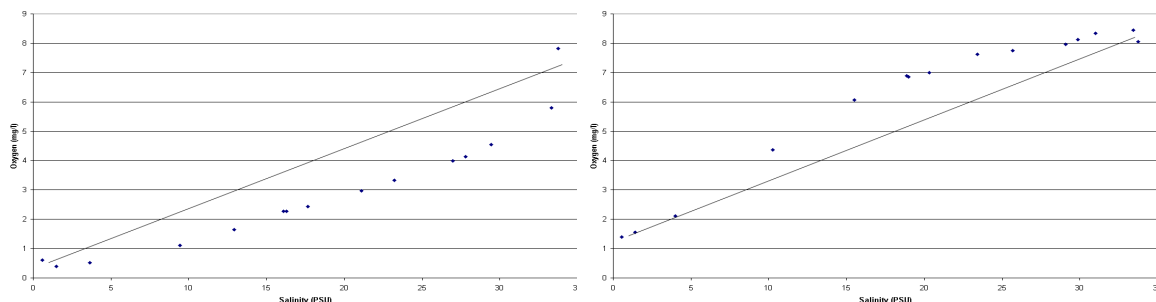


Figure 3.15: Oxygen levels vs salinity with the theoretical mixing line after 200 days (left) and 300 days (right).

3.2.5 NUTRIENTS

Due to the large scale and intense biological and physico-chemical processes occurring in estuarine environments they are often able to remove a significant proportion of the amount of nutrients entering the system. Nixon *et al* (1996 in Tappin, 2002), estimated the reduction of total nitrogen and phosphorus as 30-60 % and 10-55 %, respectively. The Scheldt estuary shows a clear nutrient enrichment in terms of inorganic (NO_3 , NH_4 and PO_4) (Cabeçadas *et al*, 1999) and organic nutrients (Soetaert and Herman, 1995b) when is compared with other European estuaries (i.e. Elbe, Gironde)(Goosen *et al*,1999).

3.2.5.1 NITROGEN

Nitrogen is the most important factor limiting primary production in the Belgian coastal zone in particular (Pichot, 1980 in Billen *et al*, 1980), and in the North Sea, in general (Regnier and Steefel, 1999). Due to this limitation and the impact that high concentrations of nitrogen reaching the coastal area would have in terms of large-scale phytoplankton growth and changes in species composition (especially in coastal areas where the light conditions are more favourable for phytoplankton growth) the management of this nutrient is particularly important.

The MOHID water quality module distinguishes between organic and inorganic nitrogen. The inorganic nitrogen is divided into ammonia (NH_4), nitrite (NO_2) and nitrate (NO_3).The organic nitrogen is divided into particulate organic nitrogen (PON), dissolved organic nitrogen (DON). The latter is divided into dissolved non refractory organic nitrogen (DONnr) and dissolved refractory organic nitrogen (DONre). DONnr includes small molecular substrates, assumed to be degraded in the day of production and DONre with a longer turn over.

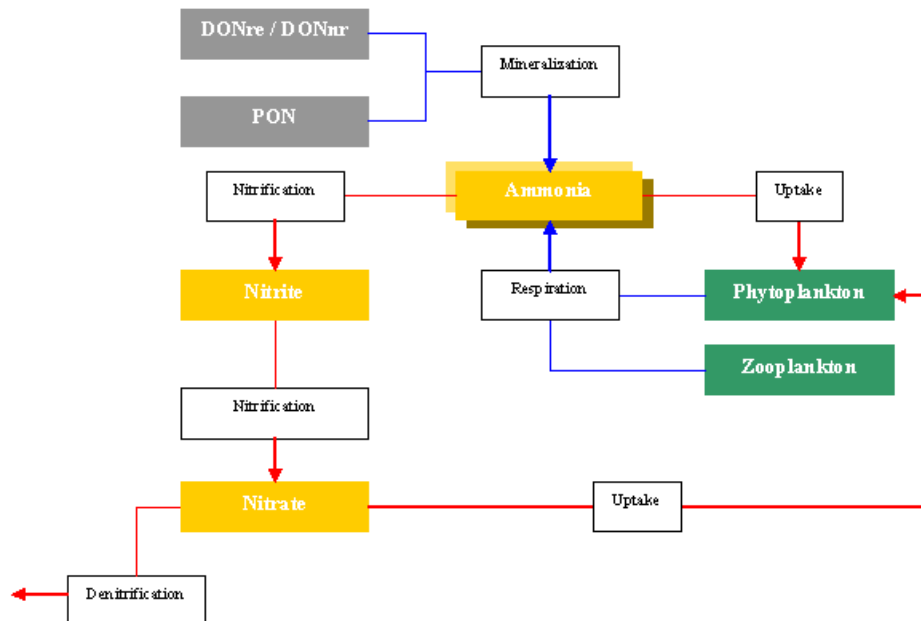


Figure 3.16: Internal flux of inorganic nitrogen.

The processes affecting inorganic nitrogen comprise a closed cycle (Figure 3.16), except for denitrification where nitrogen is lost to the atmosphere. Ammonia and nitrate are taken by the phytoplankton, which having preference for ammonia as it is less costly metabolically than the uptake of nitrate. Inorganic nitrogen sources include mineralisation from organic, dissolved and particulate, nitrogen and respiration from phytoplankton and zooplankton. Inorganic nitrogen compounds are inter-related through the nitrification process where ammonia is converted into nitrite and after this process, nitrite could suffer a second nitrification process being converted into nitrate.

Phytoplankton and zooplankton increase the organic nitrogen pool through excretion, producing non refractory dissolved organic nitrogen (DON_{nr}) and particulate organic nitrogen (PON) that can in addition be mineralised into refractory dissolved organic nitrogen (DON_{re}). An extra source for DON_{nr} is from the mortality of phytoplankton and zooplankton. Supplementary information about the formulation and processes of nitrogen in the MOHID water quality module can be found in Annex II and in the MOHID manuals (<http://www.mohid.com>).

According to Billen (1975), in terms of nitrogen concentrations, two different areas can be distinguished in the Scheldt estuary. An area covering the upper reaches where ammonium is the dominant form of nitrogen, while nitrite and nitrate have concentrations below 0.13 mg/l and a downstream area where nitrogen is mostly presented in its oxidised forms.

Along the estuary the most important process in reducing the nitrogen load reaching the Belgian coast is probably denitrification (Billen *et al.*, 1985, Cabçadas *et al.*, 1999). This process tends to be more important in the sediments than in the water column, except in highly eutrophic estuaries as the Scheldt (Tappin, 2002), where the nitrification rates found are among the highest reported (De Bie *et al.*, 2002).

In order to simulate the behaviour of inorganic nitrogen concentrations of the various types were imposed at the marine and riverine boundaries as shown in Table 3.9 and averaged values used as initial concentrations for each estuary box as shown in Table 3.10. As no clear pattern was found for ammonia at the outer WSMARINE station, an average value was imposed for this variable at the marine boundary (0.06 mg/l).

In terms of organic nitrogen, fluxes in particulate organic nitrogen have been simulated by the model. Whilst the percentage of nitrogen in suspended particulate matter as shown in the NIOO-KNAW database was quite variable and it was assumed for the purposes of this study that all the nitrogen found in the SPM is of organic origin although De Bie *et al.* (2002) found that around 57-86 % of the nitrifying biomass is attached to particles. The initial data values applied to the model boxes can be seen in Table 3.10 while constant values were imposed to the boundaries using 0.37 mg/l at the river boundary (data obtained from zooplankton database provided by Soetaert, K. (unpublished data) for the years 1989-1990, unpublished data) which is broadly similar to the concentrations given by (Zwolsman, 1994) and 0.05 mg/l at the marine boundary.

For the dissolved organic nitrogen, accurate baseline was not during this study and constant values along the estuary were used (0.001 mg/l and 0.01mg/l for refractory and non-refractory respectively). Values at the riverine and marine boundaries were assumed to be 0.02 mg/l and 0.002 mg/l for DON_{nr} and 0.01 mg/l at both boundaries for DON_{re} .

Table 3.9: Monthly nitrate (NO₃), nitrite (NO₂) and ammonia (NH₄) values applied at the river and marine boundaries.

Month	1	2	3	4	5	6	7	8	9	10	11	12
NO ₃ river (mg/l)	21.112	21.055	22.295	21.252	18.661	16.539	15.939	17.687	16.538	16.726	16.981	21.226
NO ₂ river (mg/l)	0.3131	0.3284	0.3594	0.7952	0.8288	1.0028	0.9369	0.5698	0.7986	0.7681	0.6573	0.4174
NH ₄ river (mg/l)	3.5135	2.8235	2.8125	2.692	3.0241	1.9688	0.8862	0.1981	0.6075	1.4909	3.187	2.1115
NO ₃ marine (mg/l)	1.8986	1.3473	1.7596	0.4267	0.6547	0.1329	0.1940	0.0911	0.4521	0.4860	0.9720	0.6176
NO ₂ marine (mg/l)	0.0272	0.0214	0.0166	0.0105	0.0117	0.0120	0.0231	0.0175	0.0341	0.0218	0.0319	0.0293

Table 3.10: Initial values of nitrate (NO₃), nitrite (NO₂), ammonia (NH₄) and particulate organic nitrogen (PON) concentrations applied to the model boxes.

Box Number	1	2	3	4	5	6	7	8	9	10	11	12
NO ₃ (mg/l)	0.950	0.950	0.950	4.186	4.186	5.606	5.606	9.952	8.319	12.843	14.906	19.485
NO ₂ (mg/l)	0.030	0.030	0.030	0.086	0.086	0.109	0.109	0.150	0.157	0.168	0.199	0.469
NH ₄ (mg/l)	0.050	0.050	0.012	0.123	0.123	0.119	0.119	0.150	0.167	0.221	0.291	1.460
PON (mg/l)	0.15	0.15	0.15	0.20	0.20	0.20	0.20	0.20	0.20	0.20	0.20	0.35

River discharge of inorganic nitrogen species shows a marked seasonal behaviour as shown in Figures 3.17, 3.18 and 3.19. Ammonia changes from high concentrations in winter (up to 3.5 mg/l) to much lower concentrations during summer (and especially in August with less than 0.5 mg/l). Nitrate is by far the most abundant of the inorganic nitrogen species with concentrations over 20 mg/l during winter, although its concentrations reduce during summer they are still elevated (over 15 mg/l). Nitrite shows the opposite behaviour with higher concentrations during summer (around 1 mg/l) than during winter (less than 0.5 mg/l) probably due to nitrification from ammonia.

The seasonal behaviour of the nitrite in the upper estuary can be extrapolated to the rest of the estuary although though the concentrations and the range of variation are smaller in scale. The model is able to reproduce this behaviour but the concentrations are slightly overestimated in the landward part of the estuary due to the excess of nitrogen of resulting from the mineralisation process.

Although, the ammonia yearly pattern is well represented, its values are slightly overestimated compared with observed values near the head of the estuary where the organic nitrogen is being discharged. A sharp decline in concentrations can be observed in August along the entire estuary. The ammonia concentrations suggest consumption in the inner estuary (Van Spaendonk *et al*, 1993) as it is only found at low levels in the inner estuary during the growing season. However, the model results also show a clear annual pattern in the centre of the estuary, though this pattern is less noticeable toward the outer estuary.

Nitrate concentrations appear to be realistically represented by the model along the estuary continuum in comparison to observed data and its concentration decreases simultaneously with the other inorganic species, although its decline is not as sharp. These findings are in agreement with descriptions from the literature, e.g. Van Spaendonk *et al* (1993) who described a decrease of nitrate concentrations during the period May-August in addition to a decrease as for the total amount of NO_3+NH_4 .

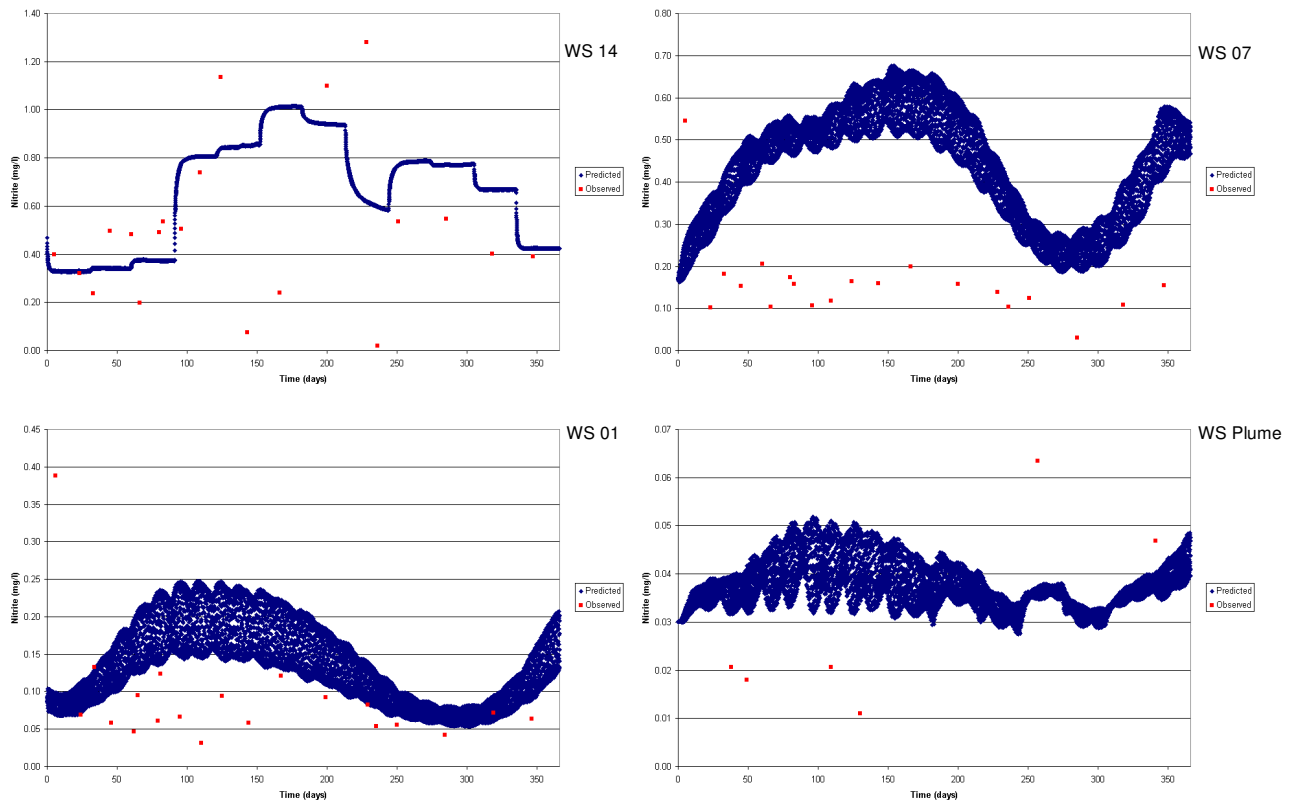


Figure 3.17: Predicted and observed nitrite levels at different stations along the Scheldt Estuary.

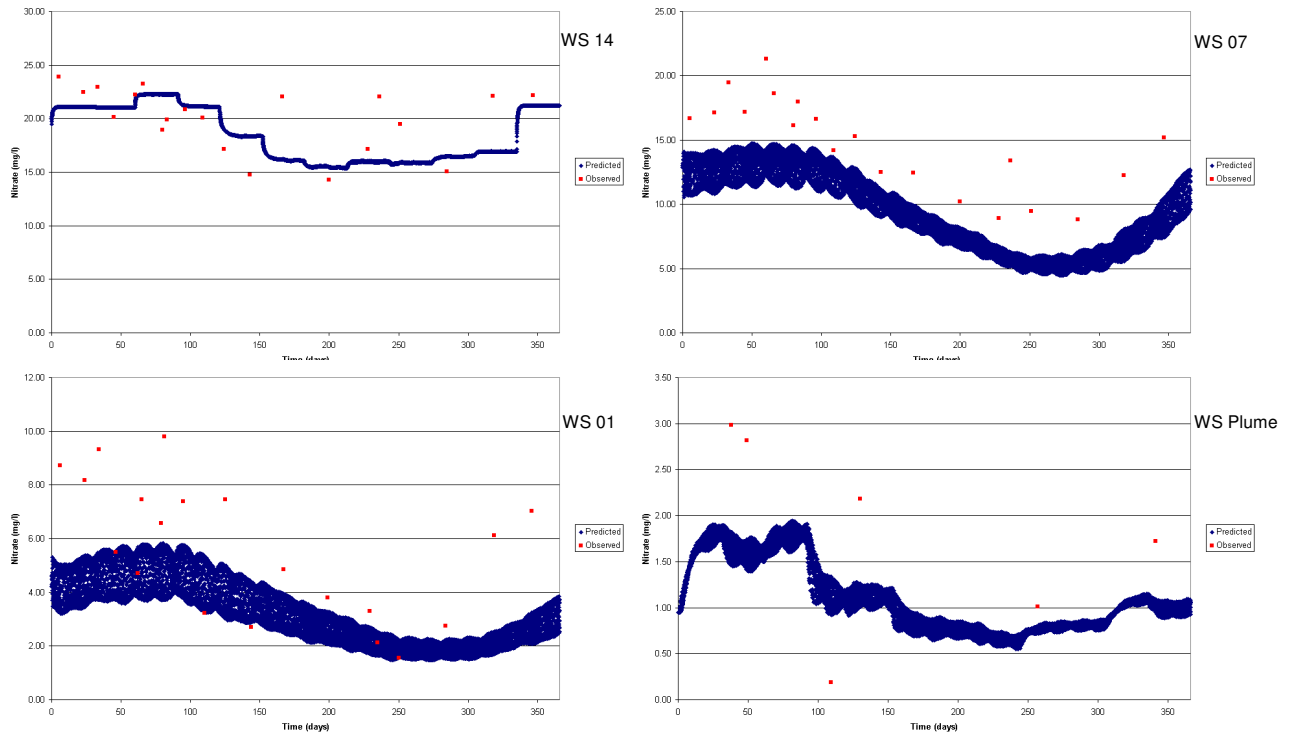


Figure 3.18: Predicted and observed nitrate levels at different stations along the Scheldt Estuary.

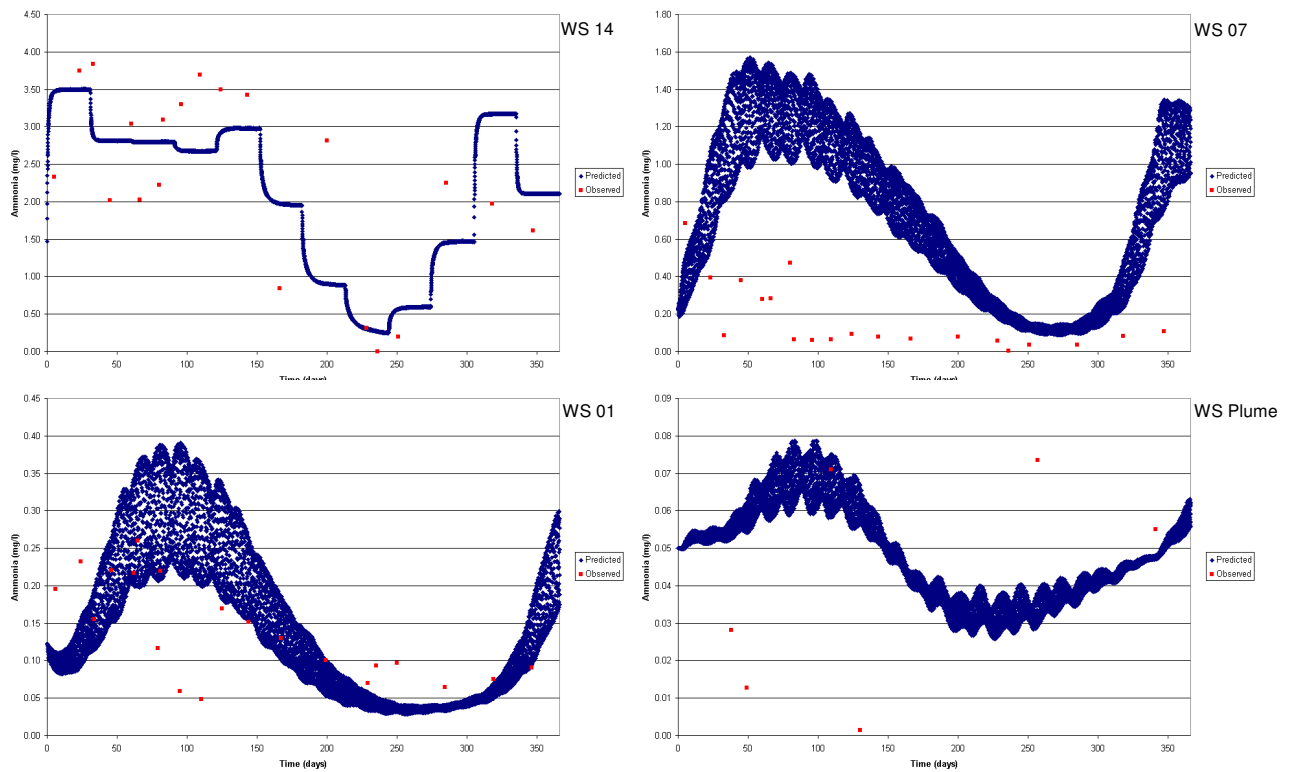


Figure 3.19: Predicted and observed ammonia levels at different stations along the Scheldt Estuary.

Inorganic nitrogen compounds appear to show conservative behaviour in the Scheldt estuary, according with Van Spaendonk *et al.*(1993). However, Kromkamp *et al* (1995) found different behaviour of the dissolved nitrogen compounds at different times of the year with these differences particularly noticeable in the upper estuary compared with the outer estuary. The model predictions shown in Figure 3.20 shows that both statements may be the correct and during certain times of the year the estuary can act as a sink for total inorganic nitrogen e.g. in march (100 days) and October (300 days) whilst in the summer (200 days) conservative properties for total nitrogen can be observed.

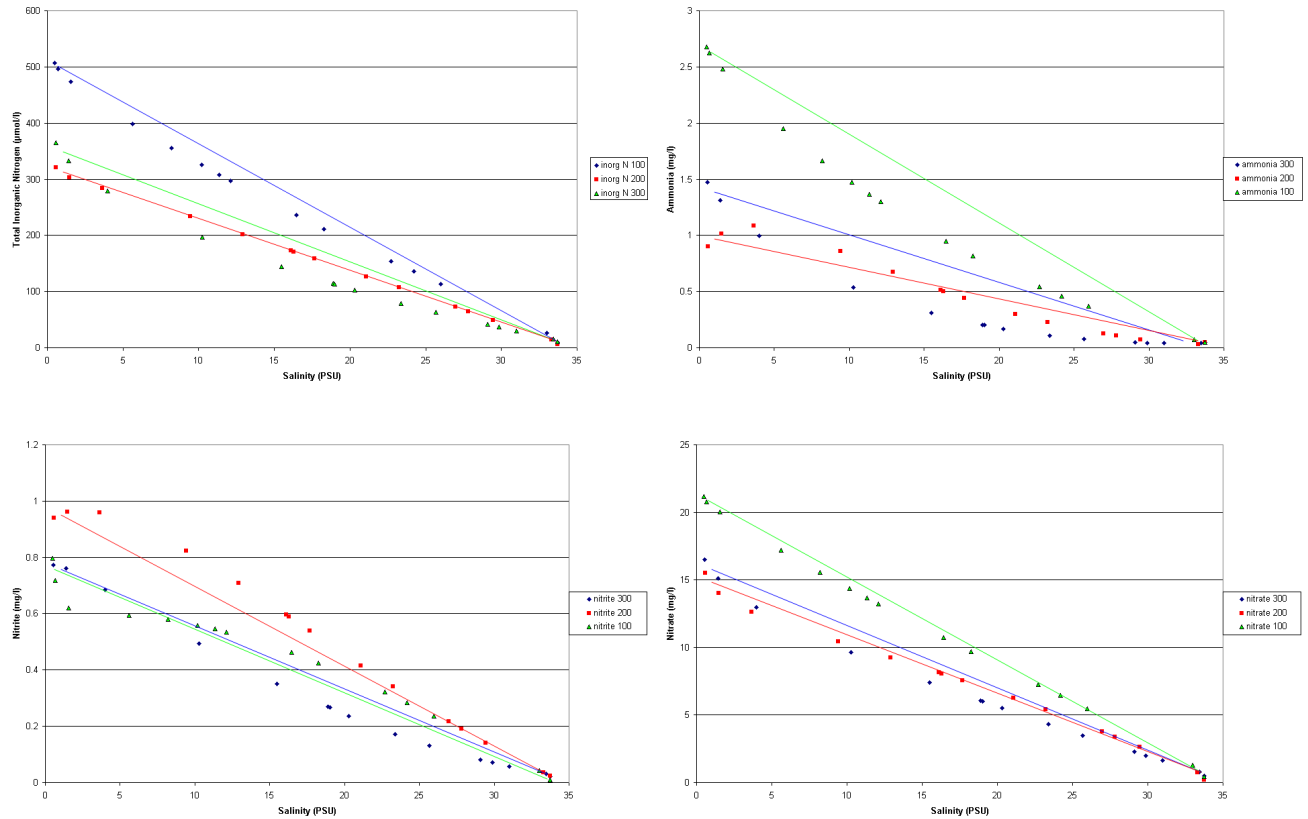


Figure 3.20: Total inorganic nitrogen, ammonia, nitrite and nitrate vs. salinity at different times of the year (From left to right and from up to down).

As shown for the total inorganic nitrogen concentrations, the spatial variation of each inorganic species varies with the time. The modelling results suggest that the estuary acts as a sink of ammonia for in spring (100 days) and autumn (300 days) whilst in the summer (200 days) the estuary appears to be a source low salinities and a sink downstream. The estuary seems to add nitrite in the summer (200 days) whilst removing it in autumn (300 day) and the spring results (100 days) display a mixed curve. The nitrate-salinity diagram shows that the estuary acts eventually as a sink, especially in the brackish area, while the predicted points are close to the mixing line. For all the species and its sum, it can be seen that the differences in behaviour decrease seawards.

3.2.5.2 PHOSPHORUS

The general background levels of phosphate in the Scheldt estuary typically range between 0.018-0.18 mg/l (Froelich, 1988 and Fox, 1991 in Zwolsman, 1994). However, the observed average maximum discharged concentrations can reach values of around 0.85 mg/l (Table 3.11), which reflects the anthropogenic influence on nutrient loadings in the estuary. The MOHID water quality module distinguishes between organic and inorganic phosphorus. Organic phosphorus is divided into particulate organic phosphorus (POP) and dissolved organic phosphorus (DOP), which itself is divided into dissolved refractory and non refractory organic phosphorus (DOP_{re} and DOP_{nr}).

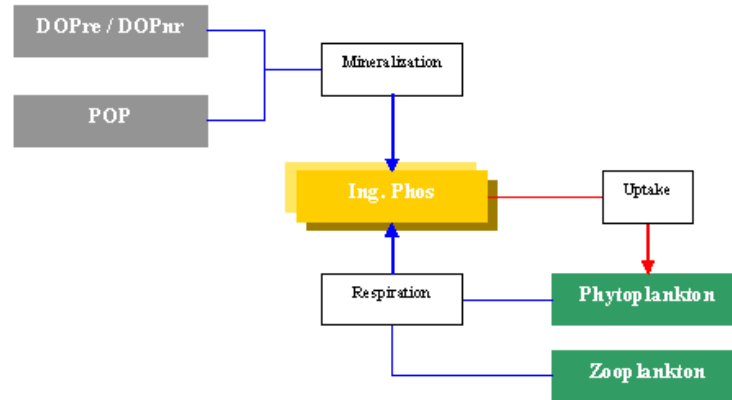


Figure 3.21: Internal flux of inorganic phosphorus.

The Inorganic phosphorus pool in the estuary is increased by respiration processes from the phytoplankton and zooplankton and by mineralisation from dissolved and particulate organic phosphorus. Processes affecting organic phosphorus species are similar to those modelled for the nitrogen. Supplementary information about the formulation and processes of phosphorus in the MOHID water quality module can be found in Annex II and in the MOHID manuals (<http://www.mohid.com>)

Phosphorus concentrations imposed at the marine and riverine boundaries for the model are shown in Table 3.11 and the averaged values used as initial concentrations for the model boxes are given in Table 3.12. In terms of organic phosphorus the initial values for the model boxes of particulate phosphorus have been calculated using the percentage of phosphorus in suspended particulate matter according to the salinity concentration (Zwolsman, 1994) and assuming that all the phosphorus found in the SPM is of organic origin. In the riverine area of estuary a value of 0.795 mg/l has been imposed for POP based on estimates that the organic content in SPM is 0.75 % (Zwolsman, 1994). For the North Sea boundary a constant value of 0.02 mg/l has been applied.

Table 3.11: Monthly phosphate (PO₄) concentrations applied at the river and marine boundaries.

Month	1	2	3	4	5	6	7	8	9	10	11	12
PO ₄ river (mg/l)	0.4879	0.4751	0.4564	0.5119	0.6367	0.6968	0.7882	0.7521	0.8078	0.8582	0.8333	0.6301
PO ₄ marine (mg/l)	0.1152	0.0859	0.0723	0.0417	0.0441	0.0443	0.0304	0.0625	0.0790	0.0872	0.0832	0.0764

Table 3.12: Initial values for phosphate (PO₄) and particulate organic phosphorus (POP) concentrations applied to the model boxes.

Box Number	1	2	3	4	5	6	7	8	9	10	11	12
PO ₄ (mg/l)	0.950	0.950	0.950	4.186	4.186	5.606	5.606	9.952	8.319	12.843	14.906	19.485
POP (mg/l)	0.0645	0.0645	0.0645	0.0918	0.0918	0.0675	0.0675	0.0793	0.0962	0.0698	0.0854	0.2850

Different behaviour can be observed during the first half of the year at the two boundaries of the model. While the phosphate concentration at the river discharge tends to increase, at the outer boundary phosphate tends to decrease in concentration. During the second half of the year, both areas tend to increase from their discharge values although the upstream area of the estuary tends to increase at a greater rate. Van Spaendonk *et al*, 1993 described average phosphate values in the estuary as fluctuating between 0.28-0.57 mg/l with minimum values occurring during May (0.09 mg/l). The range of values predicted with the ecological model in Figure 3.22 (and from the observed data tended) to be higher than these estimates and others described in the literature which could be due to an increase in discharged phosphates in the estuary. Temporarily, within the main estuary the concentration of phosphorus decrease slightly till August (in contradiction with the cited literature) after which concentrations tend to increase reaching the maximum values (around 70 mg/l) at the end of the year. The observed and predicted values show a high level of agreement both within the estuary and in the outer area.

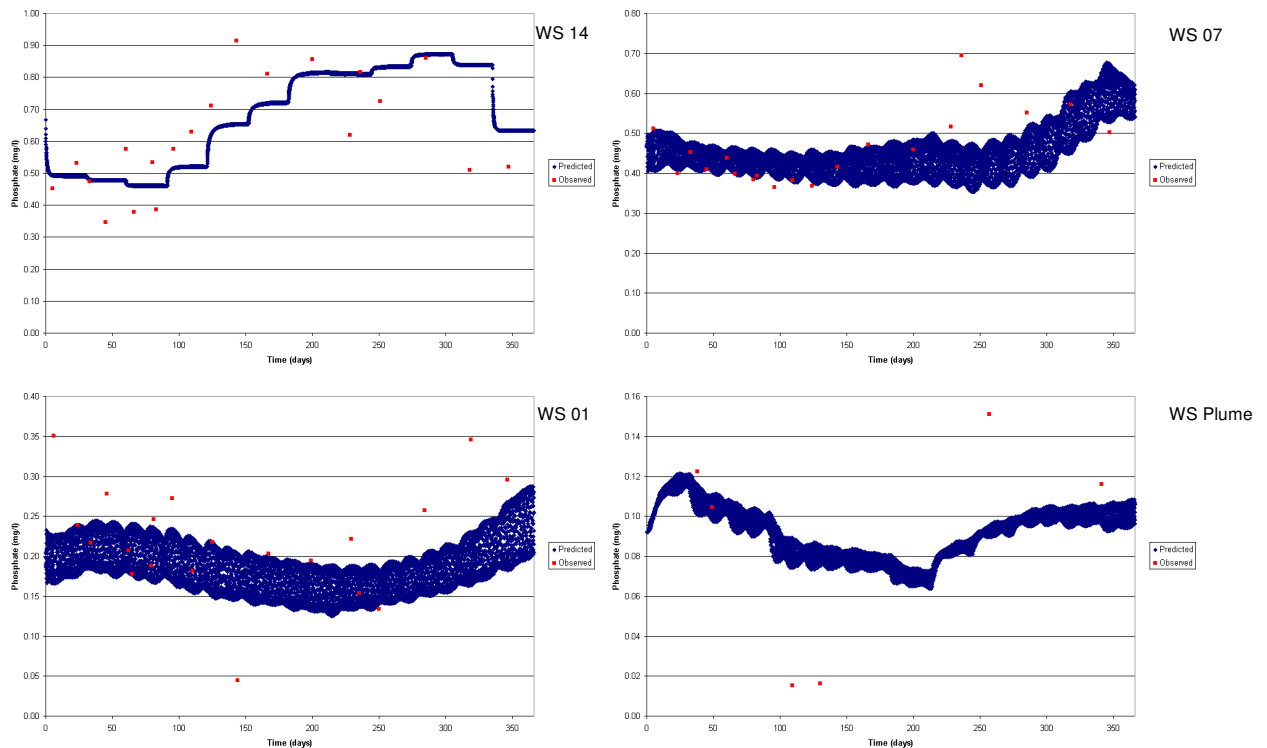


Figure 3.22: Predicted and observed phosphate levels at different stations along the Scheldt Estuary.

The results from the model suggest that slight phosphate enrichment may occur in the estuary as shown by the positive deviation from the theoretical mixing line in Figure 3.23, though during some periods e.g. summer phosphate can exhibit conservative properties (Zwolsman, 1994). The data obtained during the modelling exercise shown here also describe this situation with inorganic phosphorus concentrations along the salinity continuum showing either an addition of phosphorus within the estuary or nearly conservative behaviour.

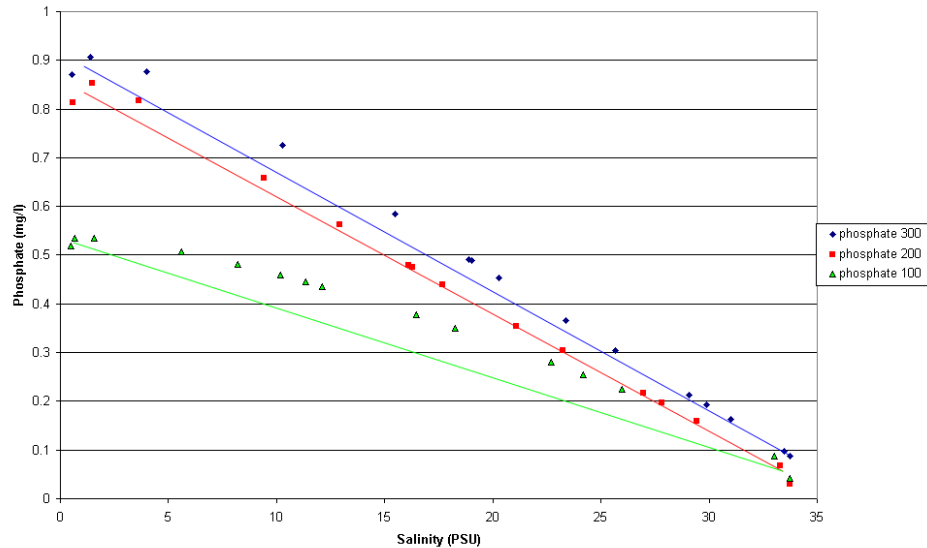


Figure 3.23: Phosphate concentrations versus salinity with theoretical mixing line after 100 and 200 days (left and right respectively).

3.2.6 PHYTOPLANKTON AND ZOOPLANKTON

Riverine phytoplankton blooms commence in spring (when levels of solar irradiance increase and the river discharges decrease) whilst estuarine phytoplankton populations develop with the rise in temperatures during summer (Muylaert *et al*, 2000). Whilst it is often assumed that net phytoplankton production is not possible in turbid estuaries it has been shown that net phytoplankton production does place in the Scheldt estuary due to physiological adaptation to the turbid environment (Van Spaendonk *et al*, 1993; Kromkamp *et al*, 1995).

The MOHID water quality model considers a single class of phytoplankton and its population growth is limited by several factors including light, temperature, nutrient availability and zooplankton grazing. The internal fluxes relating to phytoplankton production in MOHID are shown in Figure 3.24. Light is limited by the level of solar radiation reaching both the water surface and within the water column (by autoshading and by the sediments in suspension). In order to develop, phytoplankton populations need adequate supplies of nutrients which in the MOHID model are nitrogen and phosphorus. Ammonia is the preferred source of nitrogen by phytoplankton, although if levels are not optimal for the growth demands then nitrate can also be consumed. To simulate the temperature limitation of phytoplankton growth within MOHID two ranges are defined. These are the range of tolerable temperatures and the range of temperatures where growth is optimal. Zooplankton grazing of phytoplankton also limits phytoplankton growth and the level of natural

mortality also needs to be determined. The values imposed to model the phytoplankton variables can be found in appendix III.

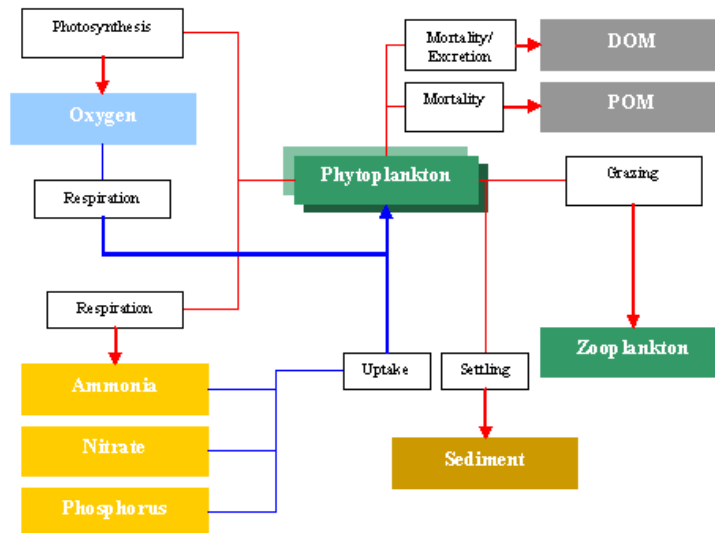


Figure 3.24: Internal fluxes related to phytoplankton in the MOHID model.

Zooplankton populations rely primarily on the availability of phytoplankton in order to develop and consequently they also regulate the phytoplankton populations on which they feed as described by the classic Lotka-Volterra predator-prey model. The levels of zooplankton are regulated by phytoplankton levels, temperature, grazing by higher trophic levels and by natural mortality. A minimum concentration of phytoplankton for zooplankton growth is imposed in the model for in order to define the temporal separation between the peaks of phytoplankton and zooplankton and in the current study a value of 0.0045 mg C/l of phytoplankton has been used. The fluxes used to model zooplankton are shown in Figure 3.25 and also in appendix II and III.

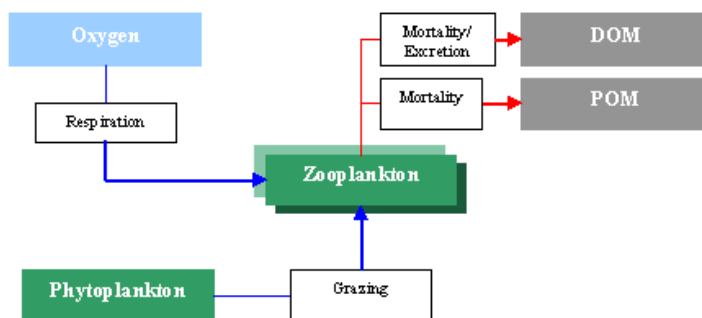


Figure 3.25: Internal fluxes related to zooplankton in the MOHID model.

Measuring phytoplankton biomass in terms of levels of carbon in the water column is problematic as it is difficult to separate carbon related to phytoplankton from other from other components of the particulate organic carbon (POC). Consequently, it is common practice to use Chlorophyll *a* (Chl *a*) as a surrogate for phytoplankton levels and then apply a correction based on the assumption of a constant ratio of phytoplankton carbon:chlorophyll *a* (Wienke and Cloern, 1987). However, the appropriate correction is often difficult to determine, especially in turbid estuaries such as the Scheldt

estuary where the composition of POC includes a high level of dead organic matter relative to live algal cells (Wienke and Cloern, 1987, Kromkamp, J., pers. comm.).

Furthermore the C:Chl *a* ratio is dependent on growth conditions as nitrogen or phosphorus limited plankton cells have higher C:Chl *a* ratio than light limited plankton cells although it is likely that in the Scheldt the phytoplankton populations are primarily light limited (Kromkamp, J, pers. comm.). Data from during the year 2003 showed that values for this ratio ranging from 27 to 935 (Kromkamp, J., pers. comm.). As a general rule, the conversion factors calculated in the Oosterschelde estuary have been commonly used for the Scheldt estuary with values ranging from 30 (Kromkamp and Peene, 1995) to 40 (De Jong and de Jonge, 1995). As the value of 30 is somewhat low compared with the values frequently found in the literature (Kromkamp J. pers. comm.) the value of 40 has been in the current study.

Assuming a conversion C: Chl *a* of 40, phytoplankton values were imposed at the river boundary (Table 3.13) whilst constant values were assumed for the marine boundary (0.03 mg C/l). A constant value was also used as the initial condition for the whole water body (0.03 mg C/l). Zooplankton levels were assumed as being one order of magnitude lower than the phytoplankton (0.003 mg C/l) over the estuary as a whole and a default value of 0.01 mg C/l was assumed as the default value at the river boundary throughout the year as low zooplankton abundances can be found in the water column in the oligohaline and freshwater tidal reaches (Kromkamp and Peene, 1995; Muylaert and Sabbe, 1999). These initial concentrations were utilised as the simulations started from January when chlorophyll *a* concentration and total phytoplankton biomass tends to be relatively low (Muylaert *et al*, 2000). A factor defining the limitation by nutrients is also implemented within MOHID ranging from 0 to 1 and Table 3.14 gives these factors averaged for the whole year for each box. Limitation by nutrients in the inner estuary is close to zero whilst outside the estuary, box 1 is most limited as this box encloses a large area with no influence from the estuarine plume and discharge.

Table 3.13: Monthly phytoplankton (mg C/l) concentrations applied at the river boundary.

Month	1	2	3	4	5	6	7	8	9	10	11	12
Phytoplankton river (mg C/l)	0.157	0.165	0.316	0.272	0.984	1.729	1.724	1.523	0.898	1.386	0.456	0.166

Table 3.14: Average nutrient limitation factor for each box.

Box	1	2	3	4	5	6	7	8	9	10	11	12
Nutrient limitation Factor	0.94	0.33	0.11	0.05	0.03	0.07	0.03	0.02	0.03	0.01	0.02	0.03

Muylaert *et al* (2000) found in their study of the phytoplankton communities in the upper reaches of the estuary that the highest concentrations of Chl *a* (2.80 mg C/l using the C:Chl *a* ratio of 40) in the fresh water area were found in spring (March-May) whilst spatially averaged phytoplankton biomass peaked in summer (Jun-Aug) with maximum values of 1.88 mg C/l, being found in the lower reaches of the freshwater tidal estuary and in the oligohaline area. Muylaert *et al* (2000) also showed that, during autumn phytoplankton biomass declined rapidly.

In the central area of the estuary, phytoplankton increases in May and reaches its maximum in early June with a secondary maximum in August. Following the secondary maximum production decreases and only recovers slightly during September (Van Spaendonk *et al*, 1993). Temporal trends in basin production near the mouth of the estuary is somewhat variable and Van Spaendonk *et*

al (1993) found that production normally starts to increase in March reaching the maximum in July after a marginal maximum in April, whilst Kromkamp *et al* (1995) found at Vlissingen a spring bloom followed by a summer minimum. Results of the MOHID model are given in Figure 3.26 and generally tend to agree with previous studies in terms of the magnitude and the temporal distribution of the blooms along the estuary. However, whilst the timing of the first peak of phytoplankton predicted by the model for the outer estuary and coastal areas agrees with the observed data the intensity of the bloom is underestimated, which indicates that further refinement in the phytoplankton parameterisation may be required (Appendix III). When the phytoplankton populations reach a certain level a reduction in population occurs indicating top-down control of the population and similar trends were described by Muylaert *et al* (2000).

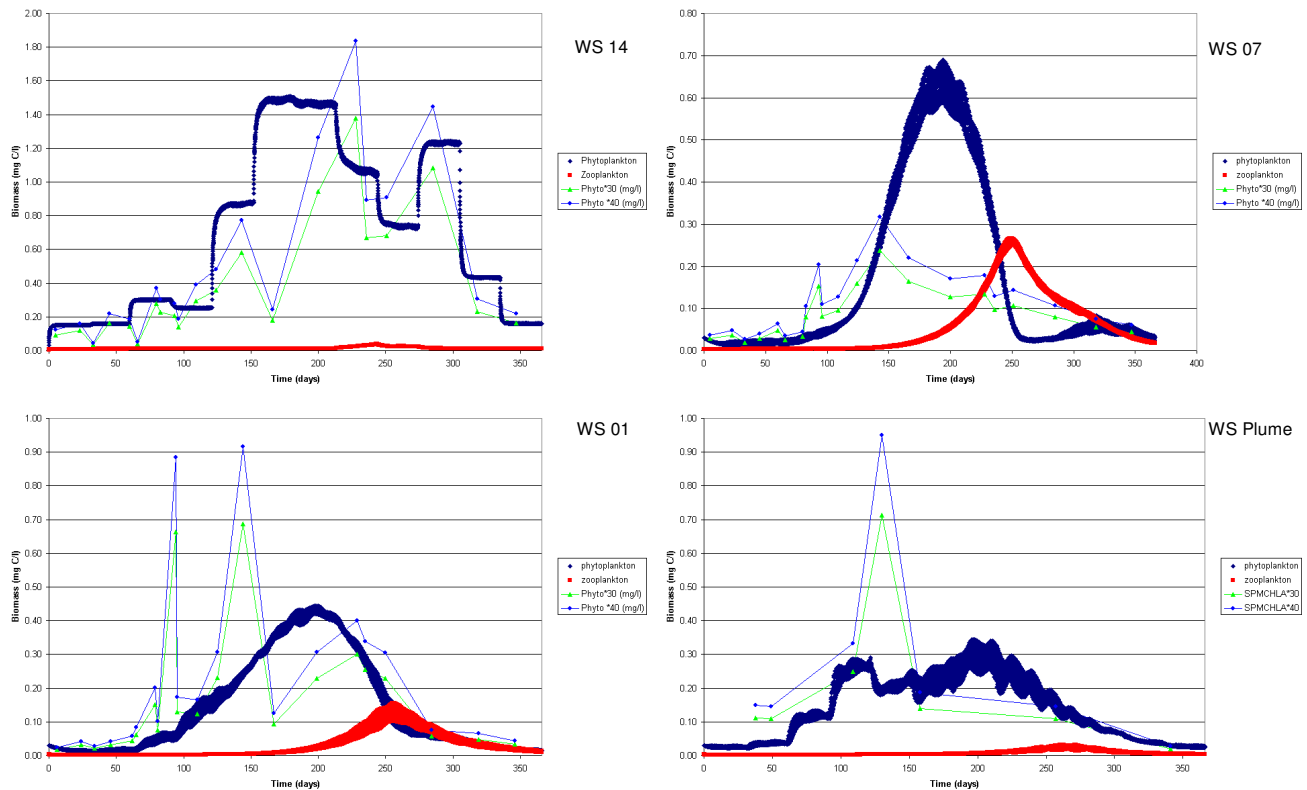


Figure 3.26: Predicted and observed phytoplankton and zooplankton biomass at different stations along the Scheldt Estuary.

Phytoplankton populations in the estuary represent a local phenomenon as indicated by the relatively short turn-over of phytoplankton populations compared with the large resident time of the Scheldt estuary. Salinity, irradiance and temperature have a major effect on species composition as shown by Muylaert *et al* (2000). Chl *a* levels in the Scheldt are generally higher in the freshwater region then decrease in the maximum turbidity zone followed by an increase further downstream as shown in Figure 3.27 (Goosen *et al* (1999). Muylaert and Sabbe (1999) and Lemaire *et al* (2002) found similar distributions whilst Van Spaendonk *et al*, 1993 found higher Chl *a* concentrations in the brackish part of the estuary compared with the marine part.

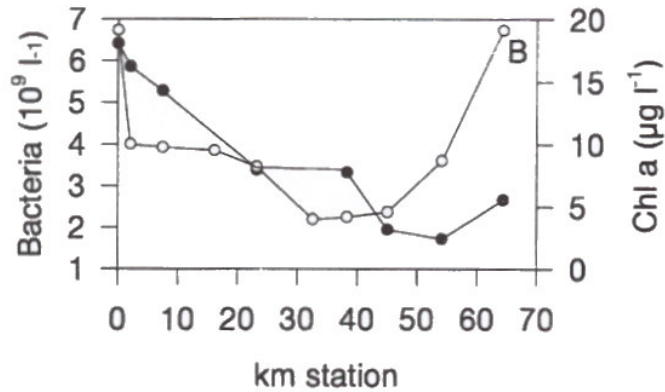


Figure 3.27: Concentrations of bacteria (filled circles) and chlorophyll *a* (open circles) in surface waters of the Scheldt from Temse in the upper estuary to Hansweert in the middle estuary (from Goosen *et al*, 1999).

The model predictions for phytoplankton (Figure 3.28) show a similar distribution to that described by Goosen *et al* (1999) with high values in the fresh water reaches which then decrease between 0-5 PSU and then increase somewhat downstream at higher salinities. In Figure 3.28, the top-down control from zooplankton can also be observed. After 200 days (July) the phytoplankton bloom is well develop throughout most of the estuary and zooplankton biomass is also increasing due to the abundance of food. By day 300 (October) phytoplankton biomass has reduced to pre-summer levels whist zooplankton populations are still well developed.

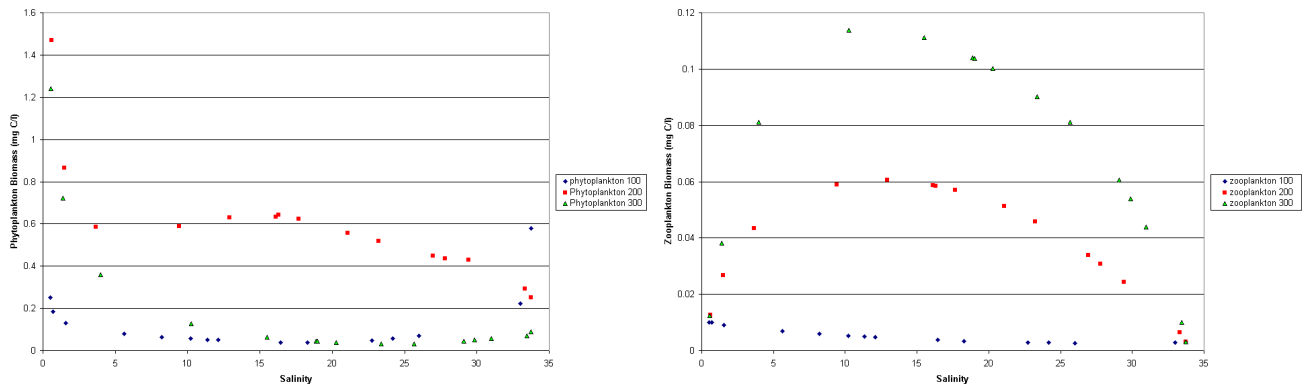


Figure 3.28: Phytoplankton and zooplankton biomass versus salinity after 100, 200 and 300 days (left and right respectively).

According to the OSPAR Commission (2003) values of over 9-10 µg Chl *a/l* are considered elevated and using the conversion factor applied in the model this would equate to values of 0.3-0.4 mg C/l. As previously described for oxygen levels the criteria described by the OSPAR commission were evaluated from the modelling results using 90th percentiles with a set of phytoplankton biomass categories as shown in Table 3.15. Results after 100, 200 and 300 days are shown in Figure 3.29 and it is apparent that elevated levels of phytoplankton are found in the upper reaches of the estuary throughout most of the year due in part to the high levels of phytoplankton imposed at the riverine boundary. Intermediate levels (group 2) phytoplankton biomass is found in the middle estuary in late spring and summer but decreases in extent in winter. The coastal bloom is not well represented in these graphs as the bloom does not last for more than the 90 percent of each of the 3 month time periods shown.

Table 3.15: Categories for phytoplankton biomass.

Category	Phytoplankton biomass ranges (mg C/l)
1	0.0-0.25
2	0.25-0.5
3	0.5-1.0

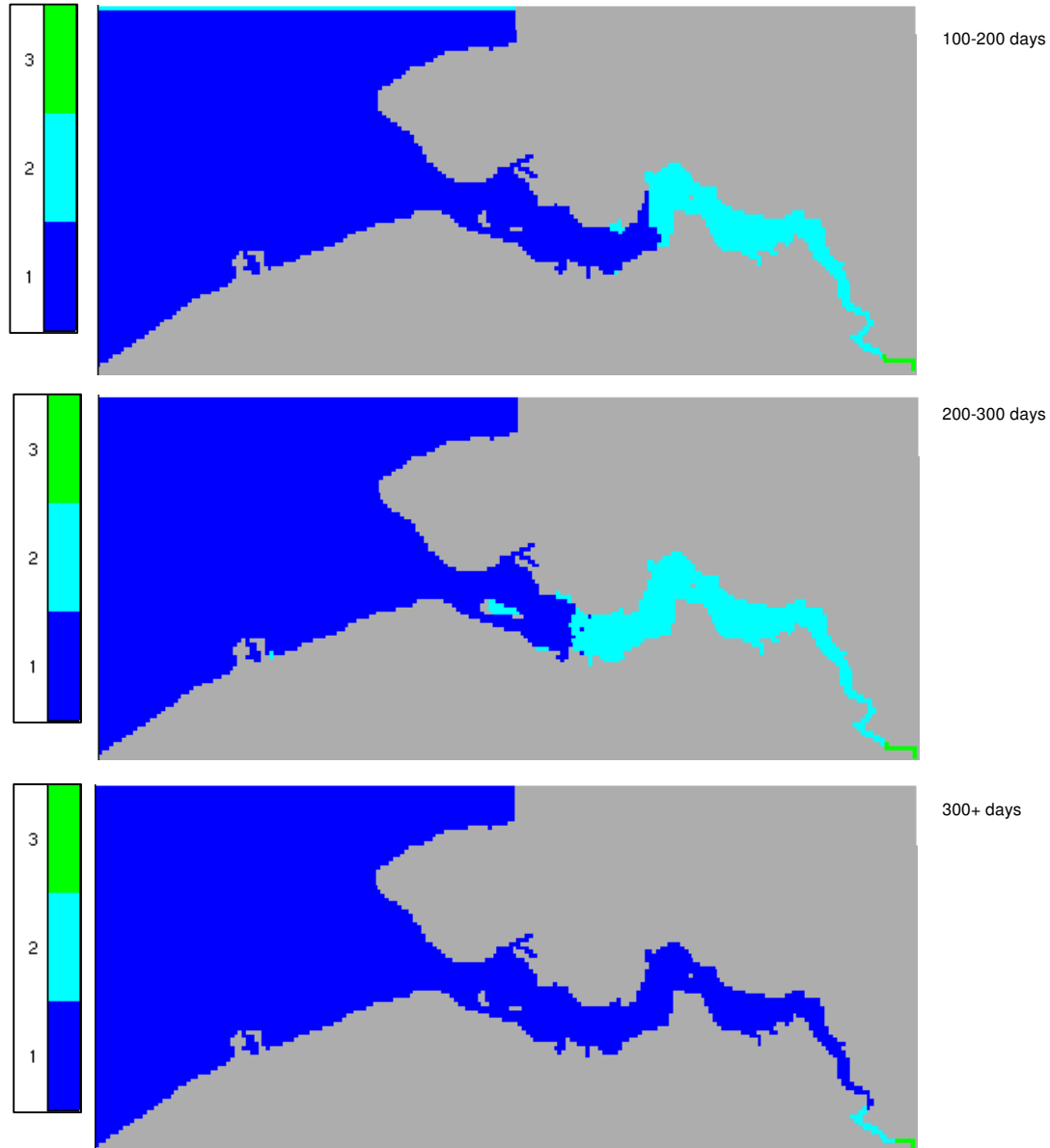


Figure 3.29: Categories of phytoplankton biomass in the Scheldt estuary over 3 time periods.

In order to analyse the coastal phytoplankton bloom monthly averaged values (from April, May and June) have been used with the categories described above (Figure 3.30). In Figure 3.30 the evolution and temporal succession of the two different blooms (estuarine and coastal) can be observed. During April the offshore/coastal bloom develops due to increased solar irradiance whilst the Scheldt estuary and plume has lower concentrations of phytoplankton. In May, only smaller isolated areas of the bloom remains in the North Sea near Zeebrugge and at the mouth of the estuary and by June the

estuarine bloom is well underway with increased phytoplankton biomass both in the estuary (especially the mid-upper estuary) and in the plume.

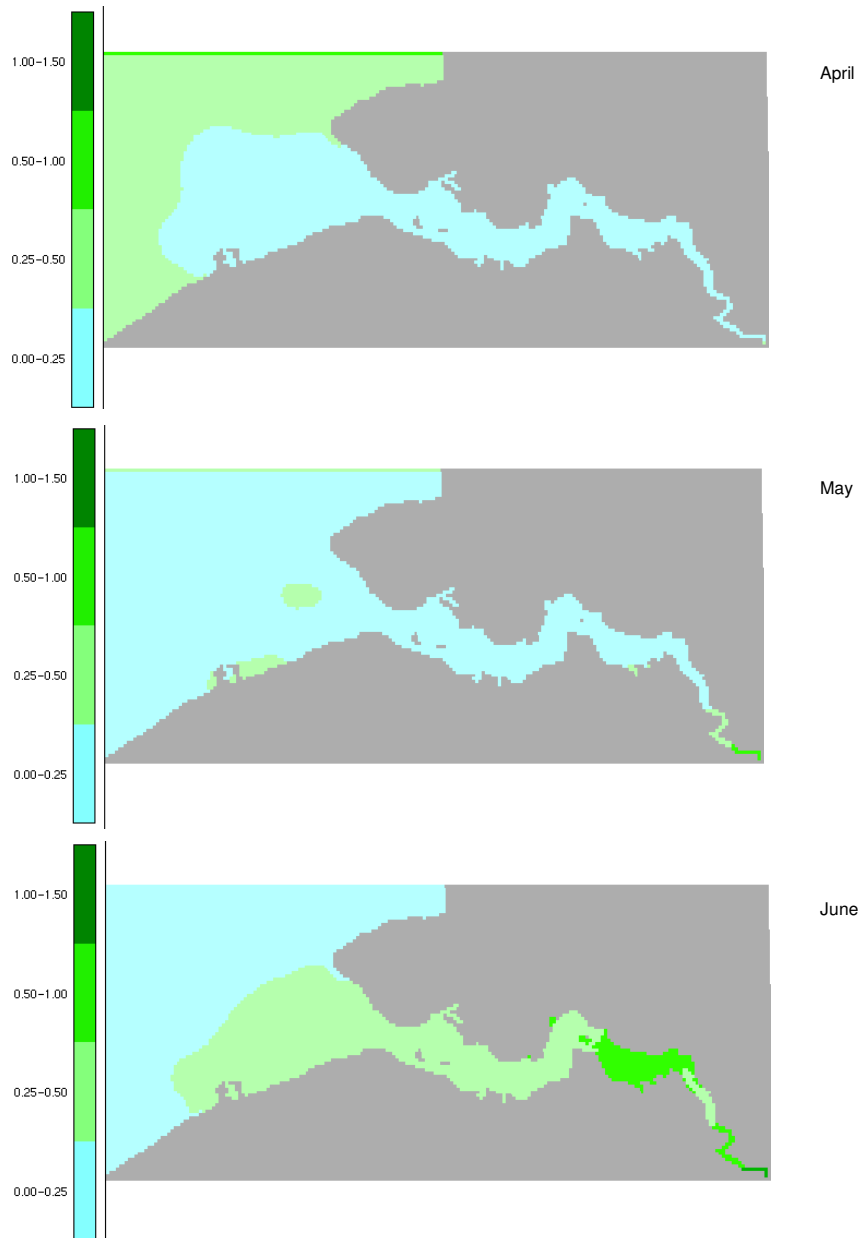


Figure 3.30: Categories of phytoplankton biomass in the Scheldt estuary in April, May and June.

In terms of zooplankton biomass, using the same methodology as defined above it can be shown that the model predicts and increase of zooplankton biomass in the centre of the estuary during summer (Figure 3.31). This bloom presumably plays a key role in controlling the development of the phytoplankton bloom as the light conditions improve over the summer. The categories defined for zooplankton biomass are summarised in Table 3.16.

Table 3.16: Categories for zooplankton biomass.

Category	Zooplankton biomass ranges (mg C/l)
1	0.0-0.125
2	0.125-0.25
3	0.25-0.5

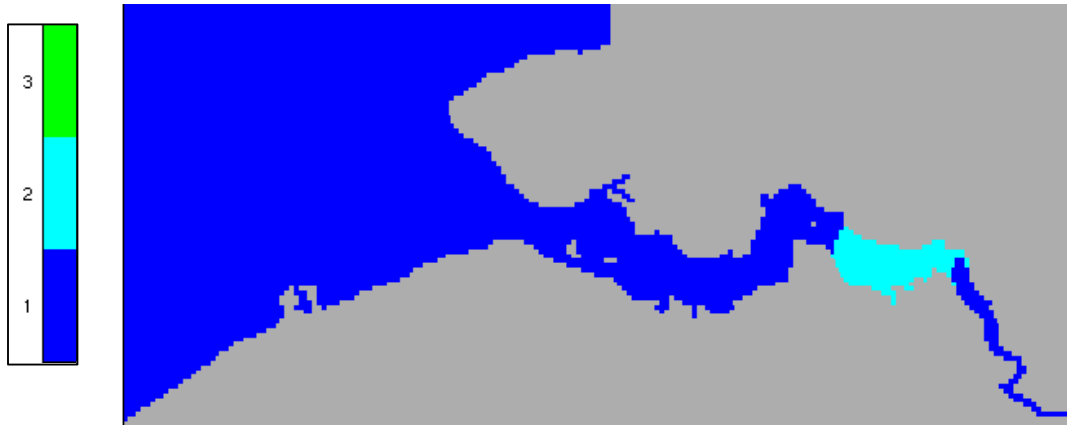


Figure 3.31: Categories of zooplankton biomass in the Scheldt estuary during the summer of 2000.

Validation of predicted zooplankton distribution and biomass has not been carried out in the current study due to lack of available data. As stated earlier in this report, when ecological modelling is carried out at higher trophic levels than phytoplankton validation is a very complicated task due to the lack of basic knowledge about food web relationships and fluxes.

4. DISCUSSION

The Scheldt estuary is a very dynamic and variable estuary in terms of river loadings and volume discharged (Struyf *et al*, in press) and nutrient reduction schemes have been implemented along the estuary and its tributaries due to the implementation of European directives and other international agreements and global environmental changes also contributes to this variation. Furthermore, this variation is also reflected in the level of variability in terms of the findings reported in the literature from different time periods in comparison with the current state of the Scheldt.

Generally speaking estuaries are able to reduce the amount of inorganic nutrients reaching the adjacent coastal waters. However, this appears to be only partly true for the Scheldt Estuary as whilst the system retains a proportion of the inorganic nitrogen, inorganic phosphorus reaches the mouth of the estuary with slightly elevated concentrations.

The MOHID ecological model with the parameterisation used as described in Appendix III seems to be able to reproduce the temporal and spatial variation of nutrients (as well as the hydrodynamic processes) occurring within the estuarine and coastal ecosystems with a reasonably high level of accuracy in comparison with the literature and observed values. However, higher values than expected for inorganic nitrogen species and an underestimation of oxygen concentrations were found. This may be due to the fact that whilst the modelling was carried out for the year 2000 the data used to reproduce the organic nutrient process in the model from Soetaert (pers. comm., unpublished data) and Zowlsman (1994) was collected prior to 2000 during a period in which the Scheldt improved its water quality. This may explain the slightly poorer water predictions in the estuary as a proportion of the dissolved oxygen in the estuary is used for the mineralisation process of these organic compounds. In addition, the mineralisation process would increase the amount of inorganic nitrogen compounds in the estuarine water, particularly ammonia and nitrite through nitrification, as nitrate seems not to be affected in a high degree by the process of nitrification.

In the Scheldt it is generally understood that nitrate concentrations increase during the growing season in the freshwater reaches due to nitrification from ammonia (Van Spaendonk *et al*, 1993) and denitrification (Kromkamp *et al*, 1995) and similar results were also found from the modelling although not examined in detail in the current study. Generally speaking the results of the modelling corroborate the observed data and recent findings in the literature and a number of conclusions may be drawn with regard to the nutrient status of the Scheldt namely:

- Nutrient limitation does not occur (Van Spaendonk, 1993)
- Eutrophic estuaries such as the Scheldt export most of the input of nitrogen and phosphate to offshore areas (Nowicki and Ovia, 1990 in Van Spaendonk, 1993)
- Primary production uptake and immobilisation of nitrogen and phosphorus does not affect significantly the distribution of these nutrients in the estuary (Billen *et al*, 1985)

The periodicity of the phytoplankton blooms occurring in the estuary appear to have been relatively well simulated by the MOHID model in comparison with the literature and observed values. The parameterisation used (Appendix III) fits the inner estuary better than the coastal area and in terms of relative magnitude the model tends to underestimate the first bloom occurring outside of the estuary, although the real magnitude is difficult to estimate due to the limitations of the conversion factor between carbon and chlorophyll *a*.

The results of the current study show that neither nitrogen nor phosphorus limit the primary production in the estuary and only ammonia seems to reach low limits in the estuary, as was concluded by Muylaert *et al* (2000) and Kromkamp *et al* (1995). Phytoplankton growth seems to be regulated by light and temperature whilst zooplankton tends to control the magnitude of the phytoplankton bloom. Furthermore, phytoplankton production seems to be locally produced despite the light limitation occurring in the upper reaches of the estuary, in concordance with the findings of Van Spaendonk *et al*, 1993.

One of the limitations of the ecological model is that only one phytoplankton group can be defined thus not being able to simulate the evolution of different communities adapted to different areas in the estuary continuum according to salinity, temperature, irradiance levels and residence times. However, this problem could be solved with the implementation of the module CE-QUAL-W2 which allows the definition of different groups of phytoplankton and is able to represent the succession of species along the salinity continuum. Modelling is an essential tool for the management a highly variable dynamic system such as the Scheldt estuary. However, it is crucial to utilise up to date and valid baseline data both in terms of validating and implementing any models and models parameters and boundary conditions need to be permanently updated utilising focused and robust field studies in order to be able to simulate the actual and future conditions in an area.

The MOHID model, as has been shown and validated in this report, seems to be able to simulate the hydrodynamics and ecological processes in the estuary and the surrounding coastal area with a high degree of accuracy. Almost all the empirical findings in the literature and the real observed data have been corroborated with the simulations. Furthermore, the majority of the data and software used during these modelling exercises is freely available for non-commercial purposes and the model can be run on any computer running under Microsoft Windows[®] 2000 and XP. The MOHID model also benefits from a user-friendly pre and post-processing interface which does not require a great deal of programming knowledge on the behalf of the end user.

4.1 Future Work

With the aim of obtaining more detailed results and better predictions a number of enhancements to the modelling could be made with further research as follows:

- Perform a deeper analysis of the data obtained during the modelling exercises, to gain a deeper understanding of the processes and its relative importance in the water quality obtained in the estuary.
- Adjust the loadings of organic nutrients in the Scheldt estuary with up to date information in order to increase predictive accuracy with regard to oxygen and inorganic nutrients levels.
- Implement the ecological model with bacteria and flagellates (currently under development), to obtain a better description of the mineralisation processes and gain detail in the heterotrophic processes.
- Further analysis of wind data for the Scheldt area in order to synthesise yearly wind measurements which avoids the need of real-time data for future predictions.
- Further sensitivity analysis required and longer term simulations carried out to assess long terms behaviour of the variables.

- Test different scenarios with regard to an increase in the river discharge as described by Struyf *et al* (in press) and a reduced suspended sediments scenario.
- Obtain and implement other minor sources of nutrients and organic matter discharges along the Scheldt catchment area from urban waste water treatment plants and channels that connect to the main estuarine body.
- Customise the model with the water quality model CE-QUAL-W2 (CE-QUAL-W2 model webpage: <http://www.cee.pdx.edu/~scott/w2/>). This model is implemented as a module in the MOHID model and some of the advantages are the possibility of modelling silicates, iron, different types of phytoplankton and a benthic water quality module.
- Model the rest of the estuary upstream Antwerp and the whole catchment area using the module MOHIDLAND (in development).
- Adaptation of the modelling grid to three dimensions in order to observe the limitation of light in the coastal area surrounding the estuarine mouth.
- Connect the Scheldt model with models developed for the Oosterschelde under the European project MaBene (Managing Benthic Ecosystems in relation to physical forcing and environmental constraints) (Project webpage: <http://www.nioo.knaw.nl/projects/mabene/>).
- Study the possibility of creating an operational model with automatic real-time data acquisition of atmospheric properties and river discharges.
- Couple model results with food web models such as AQUATOX (www.epa.gov/waterscience/models/aquatox) or Ecopath and Ecosim (www.ecopath.org) in order to predict other secondary eutrophication symptoms.
- Utilise other numerical techniques e.g. neural network models and recursive partitioning techniques to relate plankton communities, nutrient dynamics and other geochemical processes with higher trophic levels and directly with the symptoms of eutrophication in order to increase understanding of such processes and update and increase the current predictive capability of ecosystem models.
- Link outputs from ecosystem models such as MOHID with other models e.g. for benthic communities such as seagrass beds and infaunal communities. Currently developed models include BenOss (Cromeey *et al*, 1998) and DEPOMOD (Cromeey *et al*, 2002) linking organic input to benthic communities whilst a number of reference condition models are currently under development for the benthos (e.g. for implementation of the Water Framework Directive) and include models such as MARINPACS (Allen, 2004) and other modelling techniques to be applied as part of the MESH (Mapping European Seabed Habitats) project being led by JNCC.

4.2 Acknowledgements

For their invaluable assistance throughout this study: Developers of the MOHID model and staff at MARETEC (Marine and Environmental Technology Research Center) at the Instituto Superior Técnico (IST) University of Lisbon.

5. REFERENCES

- Abril, G., Nogueira, M., Etcheber, H., Cabeçadas, G., Lemaire, E. And Brogueira, M.J. (2002) Behaviour of organic carbon in nine contrasting European estuaries. *Estuarine, Coastal and Shelf Science*, **54**, 241-262
- Aquatox model webpage <http://www.epa.gov/waterscience/models/aquatox/> (Last accessed June 2004)
- Allen, J.H. (2004). The use of benthic predictive models on the data produced by the National Monitoring Plan. SNIFFER research report: MO(97)8/SR(02)38
- Arhonditsis, G.B. and Brett, M.T. (2004) Evaluation of the current state of mechanistic aquatic biogeochemical modelling. *Marine Ecology Progress Series*, **271**, 13-26
- Baeyens, W., van Eck, B., Lambert, C., Wollast, R. and Goeyens, L. (1998a). General description of the Scheldt estuary. *Hydrobiologia*, **366**, 1-14
- Baeyens, W., Elskens, M., van Ryssen, R. and Leermakers, M. (1998b). The impact of the Scheldt input on the trace metal distribution in the Belgian coastal area (results of 1981-1983 and 1995-1996). *Hydrobiologia*, **366**, 91-108
- Billen, G. (1975) Nitrification in the Scheldt estuary (Belgium and the Netherlands). *Estuarine and Coastal Marine Science*, **3**, 79-89
- Billen, G., Somville, M., de Becker, E. and Servais P. (1985) A nitrogen budget of the Scheldt hydrographical basin. *Netherlands Journal of Sea Research*, **19**, 223-230
- BMDC (Belgian Marine Data Centre) webpage <http://www.mumm.ac.be/datacentre/> (Last accessed June 2004)
- Bowie, G.L., Mills, W.B., Porcella, D.B., Cambell, C.L., Pagendorf, J.R., Rupp, G. L., Johnson, K.M., Chan, P.W., Gherini, S.A. and Chamberlin, C.E. (1985) *Rates, Constants and Kinetic Formulations in Surface Water Quality Modelling*. U.S. Environmental Protection Agency
- Braunschweig, F., Martins, F., Chambel, P. and Neves, R. (2003) A methodology to estimate renewal time scales in estuaries: the Tagus estuary case. *Ocean Dynamics*, **53**, 137-145
- Cabeçadas, G., Nogueira, M. and Brogueira, M. J. (1999) Nutrient dynamics and productivity in three European estuaries. *Marine Pollution Bulletin*, **38**, 1092-1096
- Cancino, L. and Neves, R. (1994) 3D-Numerical modelling of cohesive suspended sediment in the Western Scheldt estuary (The Netherlands). *Netherlands Journal of Aquatic Ecology*, **28**, 337-345
- Cancino, L. and Neves, R. (1999) Hydrodynamic and sediment suspension modelling in estuarine systems. Part II: Application to the Western Scheldt and Gironde estuaries. *Journal of Marine Systems*, **22**, 117-131
- CE-QUAL-W2 model webpage: <http://www.cee.pdx.edu/~scott/w2/> (Last accessed June 2004)

Council of the European Communities (2000), Directive 2000/60/EC of the European Parliament and of the Council of 23 October 2000 establishing a framework for Community action in the field of water policy. Official Journal of the European Communities, L327, 22 December 2000, pp. 1-73, Brussels.

Cromey, C.J., Black, K.D., Edwards, A. and Jack I.A. (1998). Modelling the Deposition and Biological Effects of Organic Carbon from Marine Sewage Discharges. *Estuarine Coastal and Shelf Science*, **47**, 295–308

Cromey, C. J., Nickell, T. D. & Black, K. D. (2002). DEPOMOD - Modelling the deposition and biological effects of waste solids from marine cage farms. *Aquaculture* 214, 211-239

De Bie, M.J.M., Starink, M., Boschker, H.T.S., Peene, J.J. and Laanbroek, H.J. (2002) Nitrification in the Schelde estuary: methodological aspects and pfactors influencing its activity. *FEMS Microbiology Ecology*, **42**, 99-107

De Jong, D.J. and de Jonge, V.N. (1995) Dynamics and distribution of microphytobenthic chlorophyll-a in the Western Scheldt estuary (SW Netherlands). *Hydrobiologia*, **311**, 21-30

De Smedt, F., Vuksanovic, V., Van Meerbeeck, S. and Reyns, D. (1998) A time-dependent flow model for heavy metals in the Scheldt estuary. *Hydrobiologia*, **366**, 143-155

Delhez E.J.M. and Carabin G. (2001) Integrated modelling of the Belgian coastal zone. *Estuarine, Coastal and Shelf Science*, **53**, 477-491

Elliott, M. & M.G. O' Reilly. 1991. The Variability and Prediction of Marine Benthic Community Parameters. pp. 231-238. In: M. Elliott & J.P. Ducrotroy (ed.) *Estuaries and Coasts: Spatial and Temporal Intercomparisons*, Olsen & Olsen, Fredensborg

EUROTROPH webpage: <http://www.ulg.ac.be/oceanbio/eurotroph/> (Last accessed June 2004)

Fettweis, M. Sas, M. and Monbaliu J. (1998) Seasonal, neap-spring and tidal variation of cohesive sediment concentration in the Scheldt estuary, Belgium. *Estuarine, Coastal and Shelf Science*, **47**, 21-36

Fokkink, R.J., Karssen, B., Wang, Z.B., van Kerckhoven, J.D.M. and Langerak, A. (1998) Morphological modelling of the Western Scheldt estuary. In: Dronkers, J. & Scheffers, M. (Eds.), *Physics of Estuaries and Coastal Seas*, proceedings of the 8th International Biennial Conference 1996, The Hague. Balkema, Rotterdam, 329-335

Francken, F., Wartel, S. and Parker, R. (2004) Factors influencing subaqueous dunes in the Scheldt estuary. *Geo-Marine Letters*, **24**, 14-21

Gasparini, S., Castel, J. and Irigoien, X. (1999) Impact of suspended particulate matter on egg production of the estuarine copepod, *Eurytemora affinis*. *Journal of Marine Systems*, **22**, 195-205

Gerringa, L.J.A., Hummel, H. and Moerdijk-Poortvliet T.C.W. (1998) Relations between free copper and salinity, dissolved and particulate organic carbon in the Oosterschelde ad Westerschelde, Netherlands. *Journal of Sea Research*, **40**, 193-203

Goosen, N.K., Kromkamp, J. Peene, J., Van Rijswijk, P. and Van Breugel, P. (1999) Bacterial and phytoplankton production in the maximum turbidity zone of three European estuaries: the Elbe, Westerschelde and Gironde. *Journal of Marine Systems*, **22**, 151-171

HMCZ (Hydro Meteo Centrum Zeeland) webpage, <http://www.hmcz.nl> (Last accessed June 2004)

Hellings, L., Dehairs, F., Tackx, M., Keppens, E. and Baeyens, W. (1999) Origin and fate of organic carbon in the freshwater part of the Scheldt estuary as traced by stable carbon isotope composition. *Biogeochemistry*, **47**, 167-186

ICBS-CIPE (Internationale Commissie voor de Bescherming van de Schelde- Commission Internationale pour la Protection de l'Escaut) webpage: <http://www.isc-cie.com> (Last accessed June 2004)

IOC, IHO, and BODC (2003), Centenary Edition of the GEBCO Digital Atlas. Published on CD-ROM on behalf of the Intergovernmental Oceanographic Commission and the International Hydrographic Organization as part of the General Bathymetric Chart of the Oceans; British Oceanographic Data Centre, Liverpool. Online: <http://www.ngdc.noaa.gov/mgg/gebco/gebco.html>

KNMI (Royal Netherlands Meteorological Institute) webpage <http://www.knmi.nl> (Last accessed June 2004)

Koelmans, A.A., van der Heijde, A., Knijff, L.M. and Aalderink, R.H. (2001) Integrated modelling of eutrophication and organic contaminant fate & effects in aquatic ecosystems. A review. *Water Research*, **35**, 3517-3536

Kromkamp, J., Peene, J., Van Rijswijk, P., Sandee, A. and Goosen N. (1995), Nutrients, light and primary production by phytoplankton and microphytobenthos in the eutrophic, turbid Westerschelde estuary (The Netherlands). *Hydrobiologia*, **311**, 9-19

Kromkamp, J., Peene, J. (1995) Possibility of net phytoplankton primary production in the turbid Schelde estuary (SW Netherlands). *Marine Ecology Progress Series*, **121**, 249-259

Krone, R.B. (1962) Flume studies of the transport of sediment in estuarial shoaling processes. Hydraulic Engineering Laboratory, University of California

Le Provost, C., Lyard, F., Molines, J.M., Genco, M.L. and Rabilloud F. (1998), A hydrodynamic ocean tide model improved by assimilating a satellite altimeter-derived data set, *Journal of Geophysical Research*, **103 (C3)**, 5513-5529

Lemaire, E., Abril, G., de Wit, R. and Etcheber, H. (2002) Distribution of phytoplankton pigments in nine European estuaries and implications for an estuarine typology. *Biogeochemistry*, **59**, 5-23

Lenhart, H. and Paetsch, J. (2001) Daily Nutrient Loads of the European Continental Rivers for the Years 1977 - 1998. Berichte aus dem Zentrum fuer Meeres- und Klimaforschung. Reihe B: *Ozeanographie*, 40. Database online: <ftp://ftp.ifm.uni-hamburg.de/pub/data/riverload/>

Luyten P.J., Jones J.E., Proctor R., Tabor A., Tett P. and Wild-Allen K., (1999) COHERENS – A Coupled Hydrodynamical-Ecological Model for Regional and Shelf Seas: User

Documentation. MUMM Report, Management Unit of the Mathematical Models of the North Sea, 914 pp.

MaBenE (Managing Benthic Ecosystems in relation to physical forcing and environmental constraints) webpage: <http://www.nioo.knaw.nl/projects/mabene/> (Last accessed June 2004)

Middelburg, J.J., Klaver, G., Nieuwenhuize, J. and Vlug, T. (1995) Carbon and nitrogen cycling in intertidal sediments near Doel, Scheldt estuary. *Hydrobiologia*, **311**, 57-69

Mulder, H.P.J. and Udink, C. (1991) Modelling of cohesive sediment transport. A case study: the Western Scheldt estuary. In: Edge, B.L. (Ed.), Proceedings of the 22nd International Conference on Coastal Engineering. American Society of Civil Engineers, New York, 3012-3023.

Muylert, K. and Sabbe, K. (1999) Spring phytoplankton assemblages in and around the maximum turbidity zone of the estuaries of the Elbe (Germany), the Schelde (Belgium/The Netherlands) and the Gironde (France). *Journal of Marine Systems*, **22**, 133-149.

Muylert, K., Sabbe, K. and Vyverman, W. (2000) Spatial and temporal dynamics of phytoplankton communities in a freshwater tidal estuary (Schelde, Belgium). *Estuarine, Coastal and Shelf Science*, **50**, 673-687

Neal, C., House, W.A., Whitton, B.A. and Leeks, G.J.L. (1998) Conclusions to special issue: water quality and biology of UK rivers entering the North Sea: the Land Ocean Interaction Study (LOIS) and associated work. *Science of the Total Environment*, **210/211**, 585-594.

OSPAR Commision (2000) OSPAR Action Plan 1998-2003. Update 2000. Available online <http://www.ospar.org> (last consulted Jun-2004)

OSPAR Commision (2003) OSPAR Integrated report 2003 on the eutrophication status of the OSPAR maritime area based upon the first application of the comprehensive procedure. Eutrophication series **189**, available online <http://www.ospar.org> (last consulted Jun-2004)

Partheniades, E. (1965) Erosion and deposition of cohesive soils. *Journal of Hydraulics Division of the American Society of Agricultural Engineers*, **91**, 105-139

Portela, L.I. and Neves, R. (1994) Numerical modelling of suspended sediment transport in tidal estuaries: A comparison between the Tagus (Portugal) and the Scheldt (Belgium-The Netherlands). *Netherlands Journal of Aquatic Ecology*, **28**, 329-335

Regnier, P., Wollast, R. and Steefel, C.I. (1997) Long-term fluxes of reactive species in macrotidal estuaries: Estimates from a fully transient, multicomponent reaction-transport model. *Marine Chemistry*, **58**, 127-145

Regnier, P., Moucher, A., Wollast, R. and Runday, F. (1998) A discussion of methods for estimating residual fluxes in strong tidal estuaries. *Continental Shelf Research*, **18**, 1543-1571

Regnier, P. and Steefel, C. I. (1999) A high resolution estimate of the inorganic nitrogen flux from the Scheldt estuary to the coastal North Sea during a nitrogen-limited algal bloom, spring 1995. *Geochimica et Cosmochimica Acta*, **63**, 1359-1374

Riera, P., Stal, L.J. and Nieuwenhuize, J. (2000) Heavy $\delta^{15}\text{N}$ in intertidal benthic algae and invertebrates in the Scheldt estuary (The Netherlands): Effect of river nitrogen inputs. *Estuarine, Coastal and Shelf Science*, **51**, 365-372

Savenije, H.H.G. (2001) A simple analytical expression to describe tidal damping or amplification. *Journal of Hydrology*, **243**, 205-215

Soetaert, K. and Herman, P.M.J. (1995a) Estimating estuarine residence times in the Westerschelde (The Netherlands) using a box model with fixed dispersion coefficients. *Hydrobiologia*, **311**, 215-224

Soetaert, K. and Herman, P.M.J. (1995b) Nitrogen dynamics in the Westerschelde estuary (SW Netherlands) estimated by means of the ecosystem model MOSES. *Hydrobiologia*, **311**, 225-246

Soetaert, K. and Herman, P.M.J. (1995c) Carbon flows in the Westerschelde estuary (The Netherlands) evaluated by means of an ecosystem model MOSES. *Hydrobiologia*, **311**, 247-266

Stewart, R. H., online. Introduction to Physical Oceanography (June 2003) Available from <http://oceanworld.tamu.edu/resources/ocng_textbook/contents.html>

Struyf, E., Van Damme, S. and Meire P. (In press) Possible effects of climate change on estuarine nutrient fluxes: a case study in the highly nutrified Schelde estuary (Belgium, The Netherlands). *Estuarine, Coastal and Shelf Science*.

Tappin, A. D. (2002) An examination of the fluxes of nitrogen and phosphorus in temperate and tropical estuaries: Current estimates and uncertainties. *Estuarine, Coastal and Shelf Science*, **55**, 885-901

Uncles, R.J., Stephens, J.A. and Smith, R.E. (2002) The dependence of estuarine turbidity on tidal intrusion length, tidal range and residence time. *Continental Shelf Research*, **22**, 1835-1856

Van der Spek, A.J.F. (1997) Tidal asymmetry and long-term evolution of Holocene tidal basins in The Netherlands: simulation of palaeo-tides in the Schelde estuary. *Marine Geology*, **141**, 71-90

Van Gils, J.A.G., Ouboter, M.R.L. and de Rooij, N.M. (1993) Modelling of water and sediment quality in the Scheldt estuary. *Netherlands Journal of Aquatic Ecology*, **27**, 257-265

Van Spaendonk, J.C.M., Kromkamp, J.C. and de Visscher, P.R.M. (1993) Primary production of phytoplankton in a turbid coastal plain estuary, the Westerschelde (The Netherlands). *Netherlands Journal of Sea Research*, **31**, 267-279

Wang, Z.B., Jeuken, M.C.J.L., Gerritsen, H., de Vriend, H.J. and Kornman, B.A. (2002) Morphology and asymmetry of the vertical tide in the Westerschelde estuary. *Continental Shelf Research*, **22**, 2599-2609

Wienke, S.M. and Cloern, J.E. (1987) The phytoplankton component of seston in San Francisco Bay. *Netherlands Journal of Sea Research*, **21**, 25-33

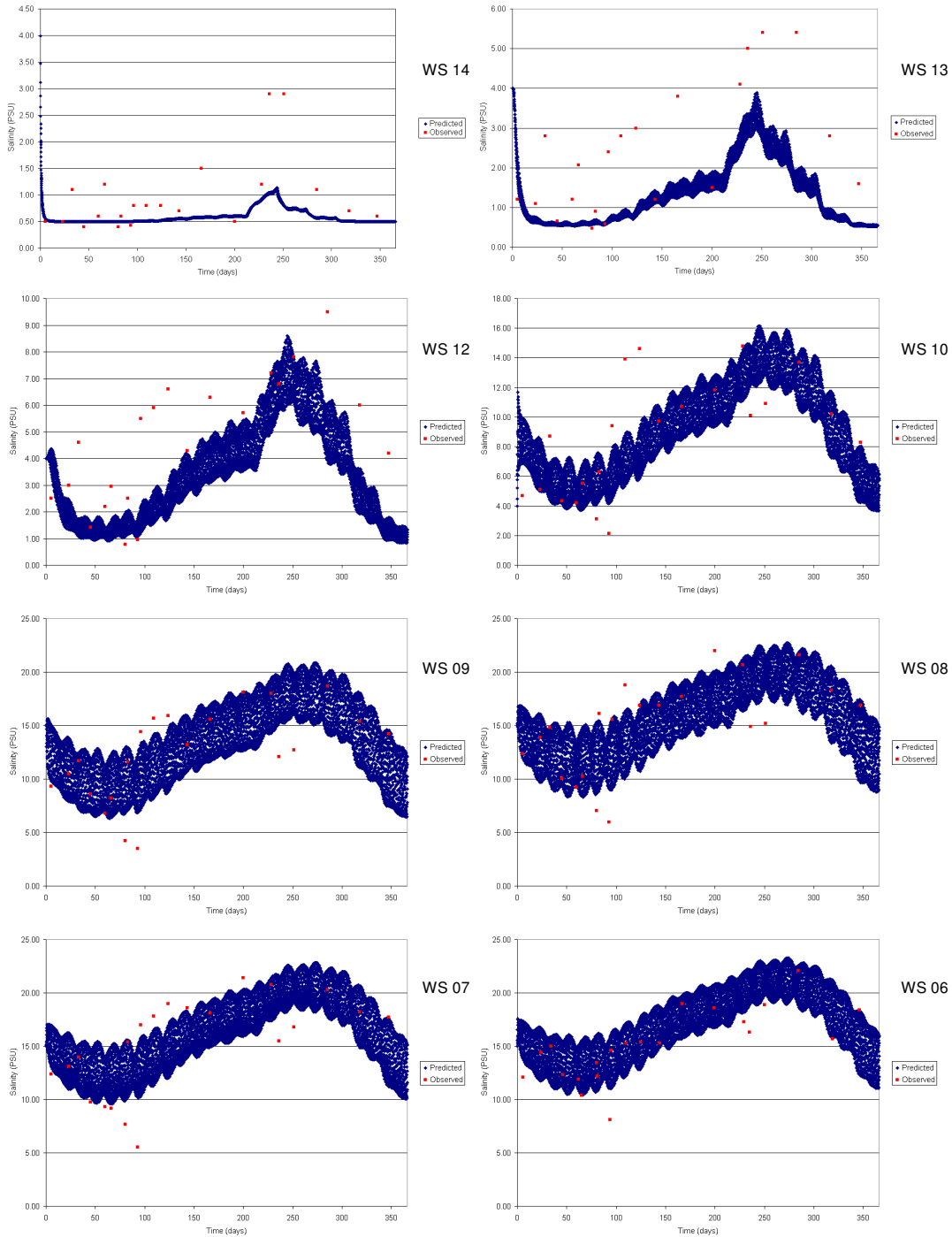
Winterwerp, J.C., Cornelisse, J.M. and Kuijper, C. (1991) A laboratory study on the behaviour of mud from the Western Scheldt under tidal conditions. Delft Hydraulics, The Netherlands, Rep. z161-37/HW/paper1.wm, 14 pp.

Zwolsman, J.J.G (1994) Seasonal variability and biogeochemistry of phosphorus in the Scheldt estuary, South-west Netherlands. *Estuarine, Coastal and Shelf Science*, **39**, 227-248

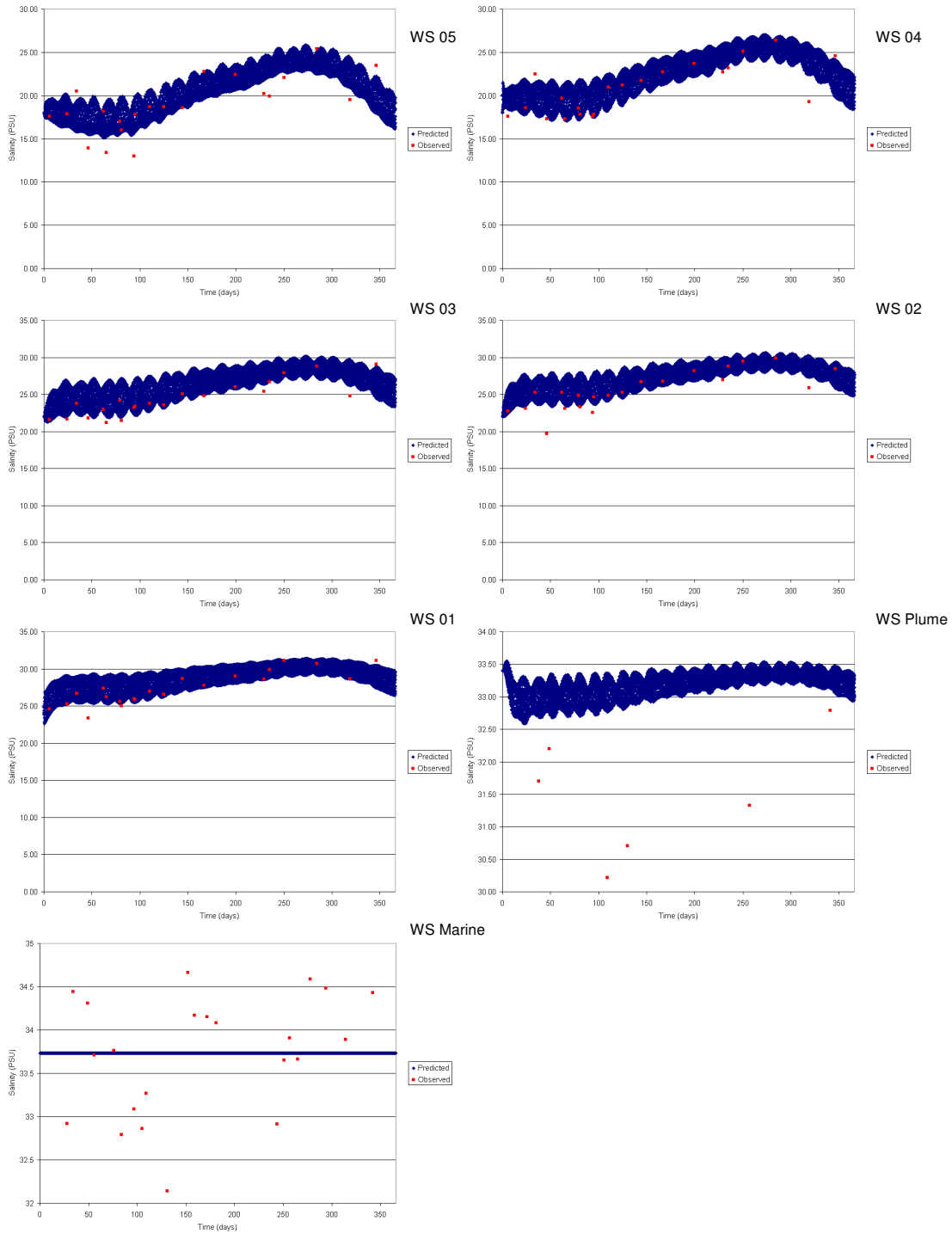
Zwolsman, J.J.G and Van Eck, G.T.M. (1999) Geochemistry of major elements and trace metals in suspended matter of the Scheldt estuary, southwest Netherlands. *Marine Chemistry*, **66**, 91-111

APPENDIX 1: PREDICTED AND OBSERVED PARAMETERS

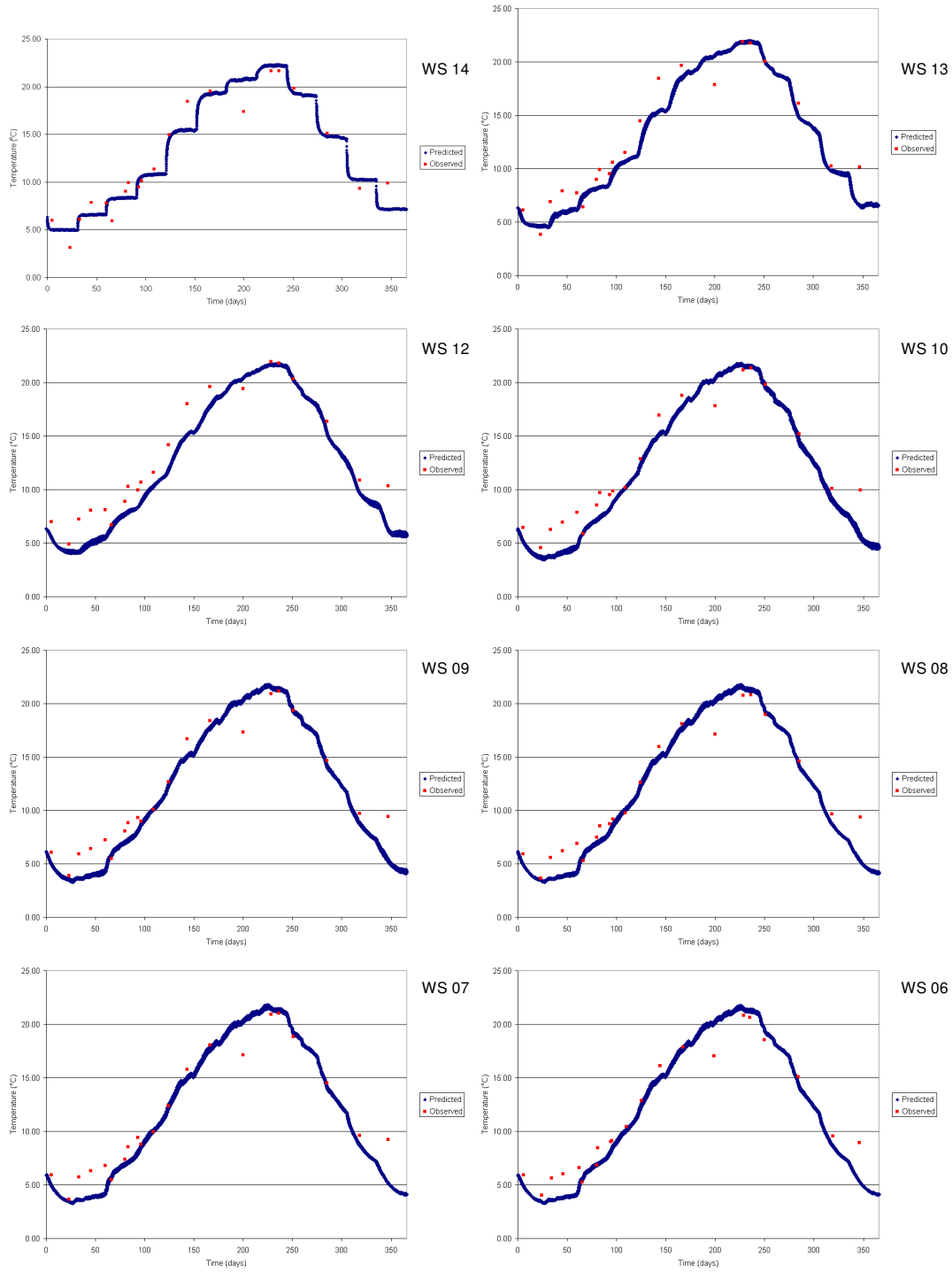
Salinity



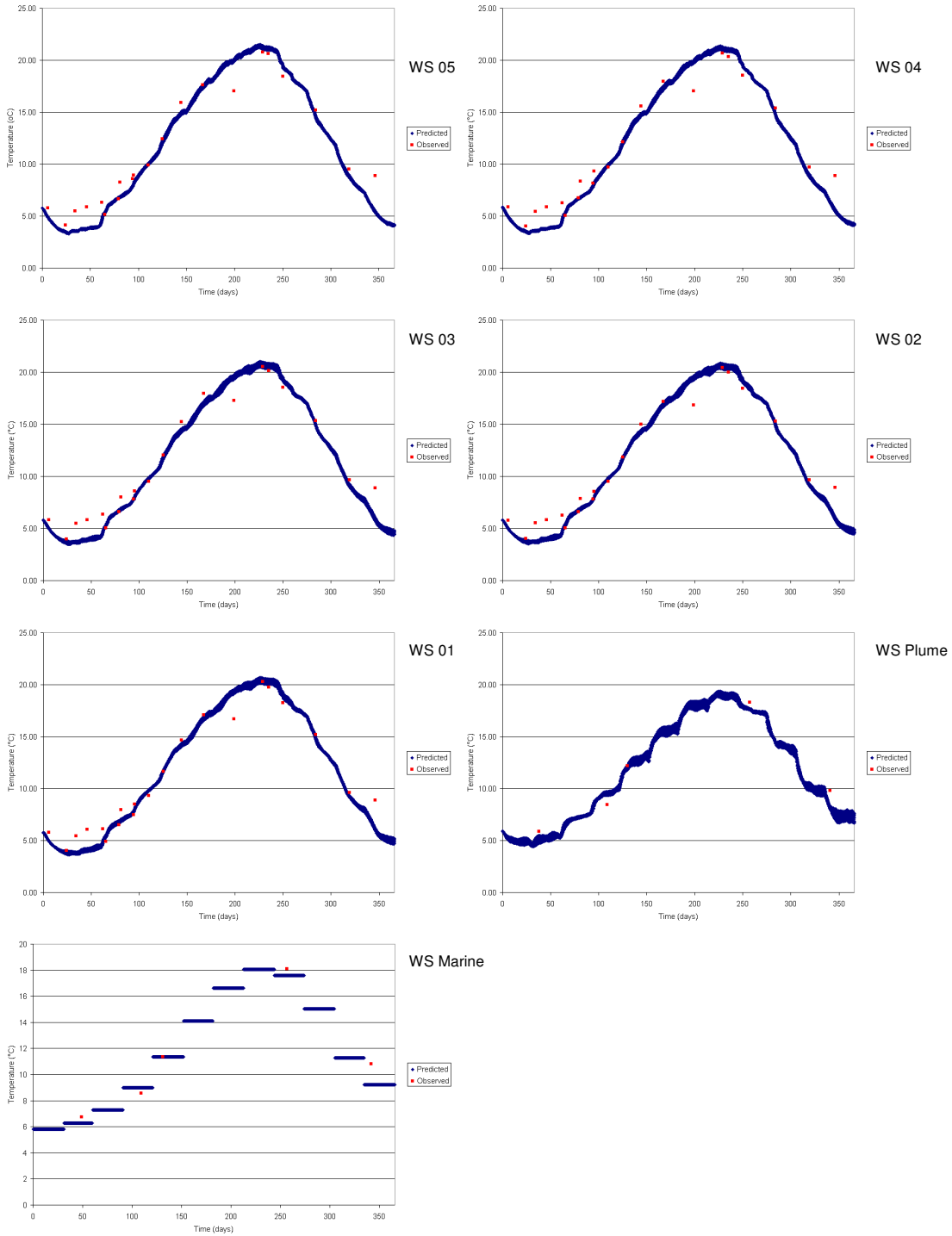
Salinity (cont..)



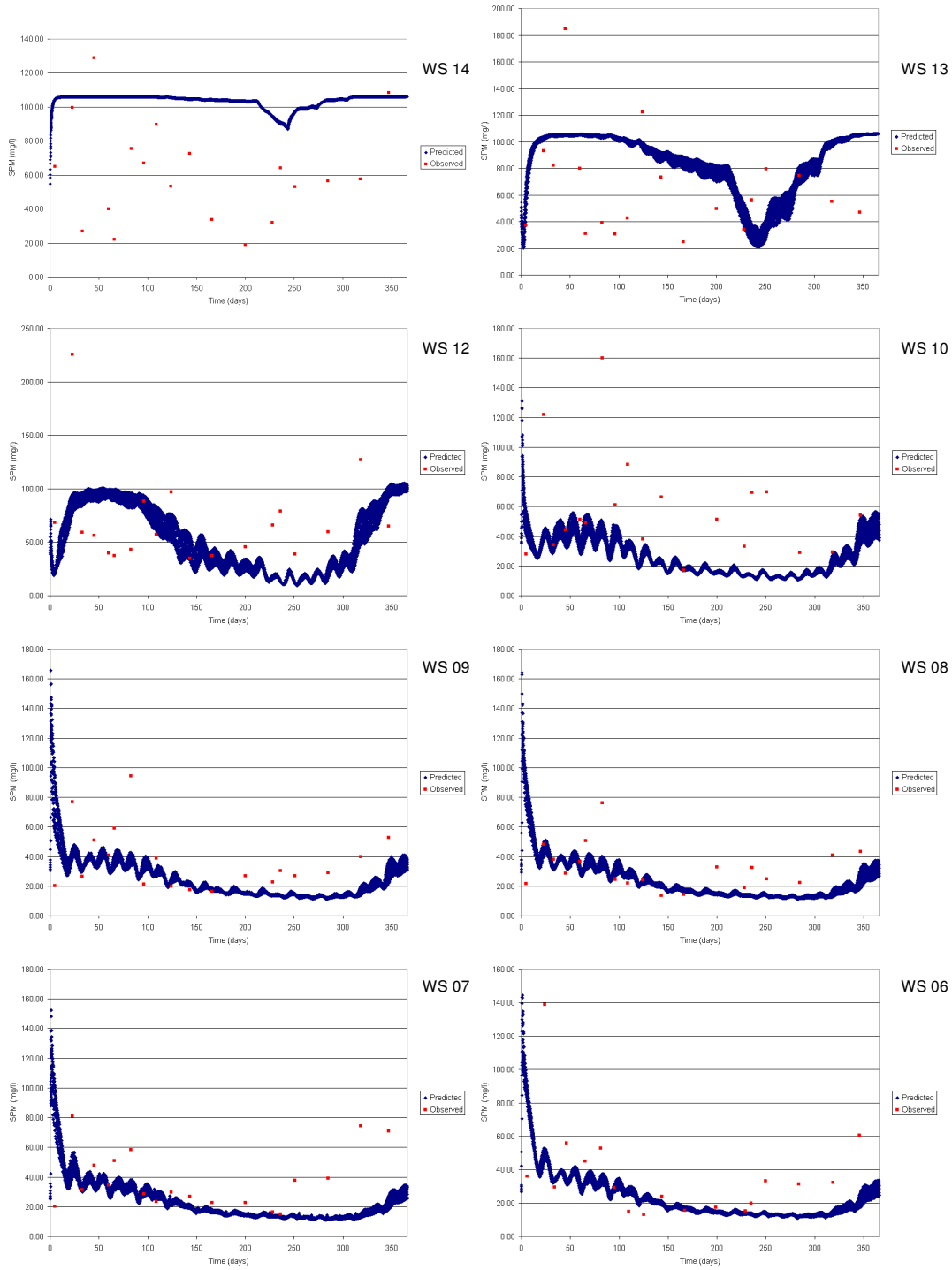
Temperature



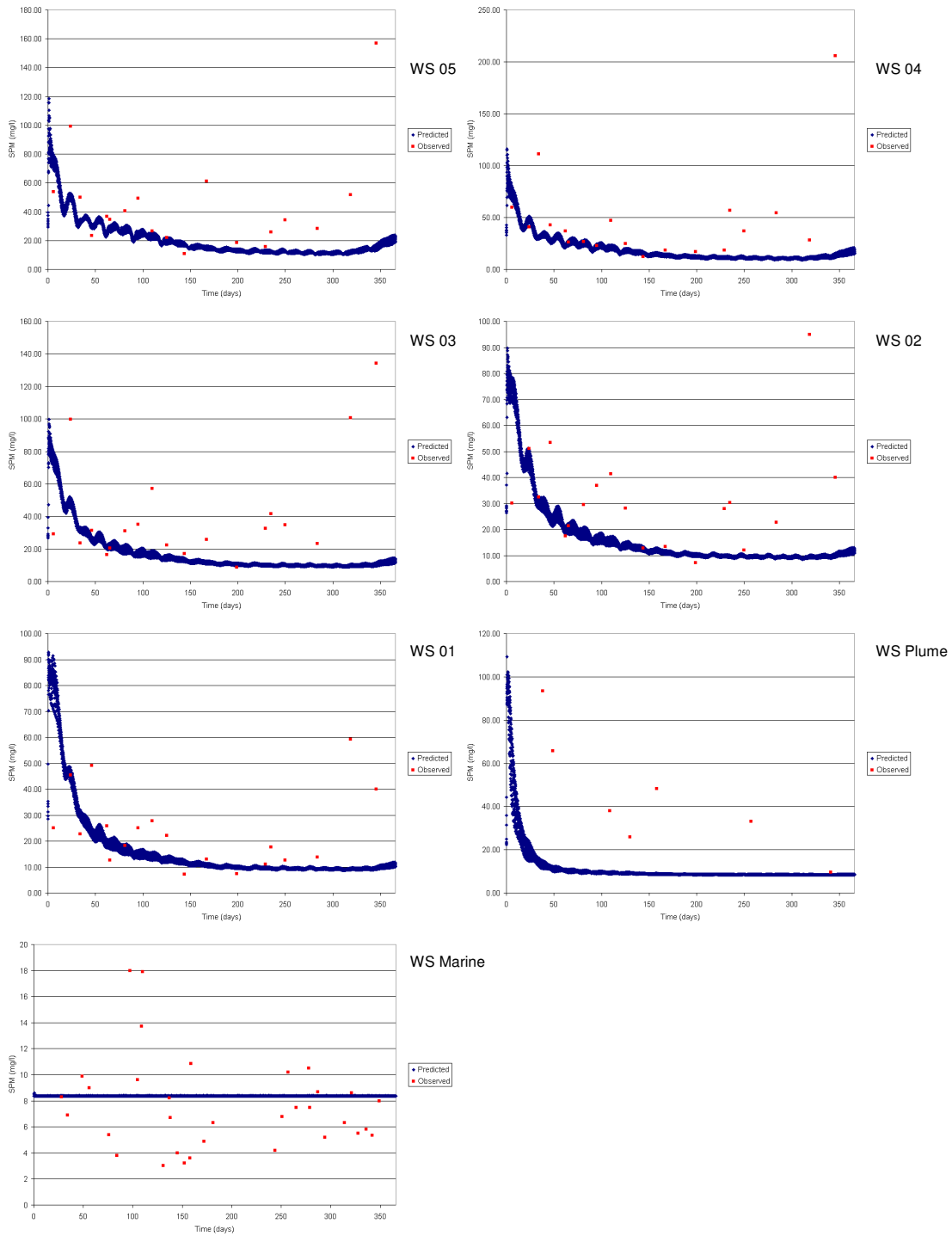
Temperature (cont..)



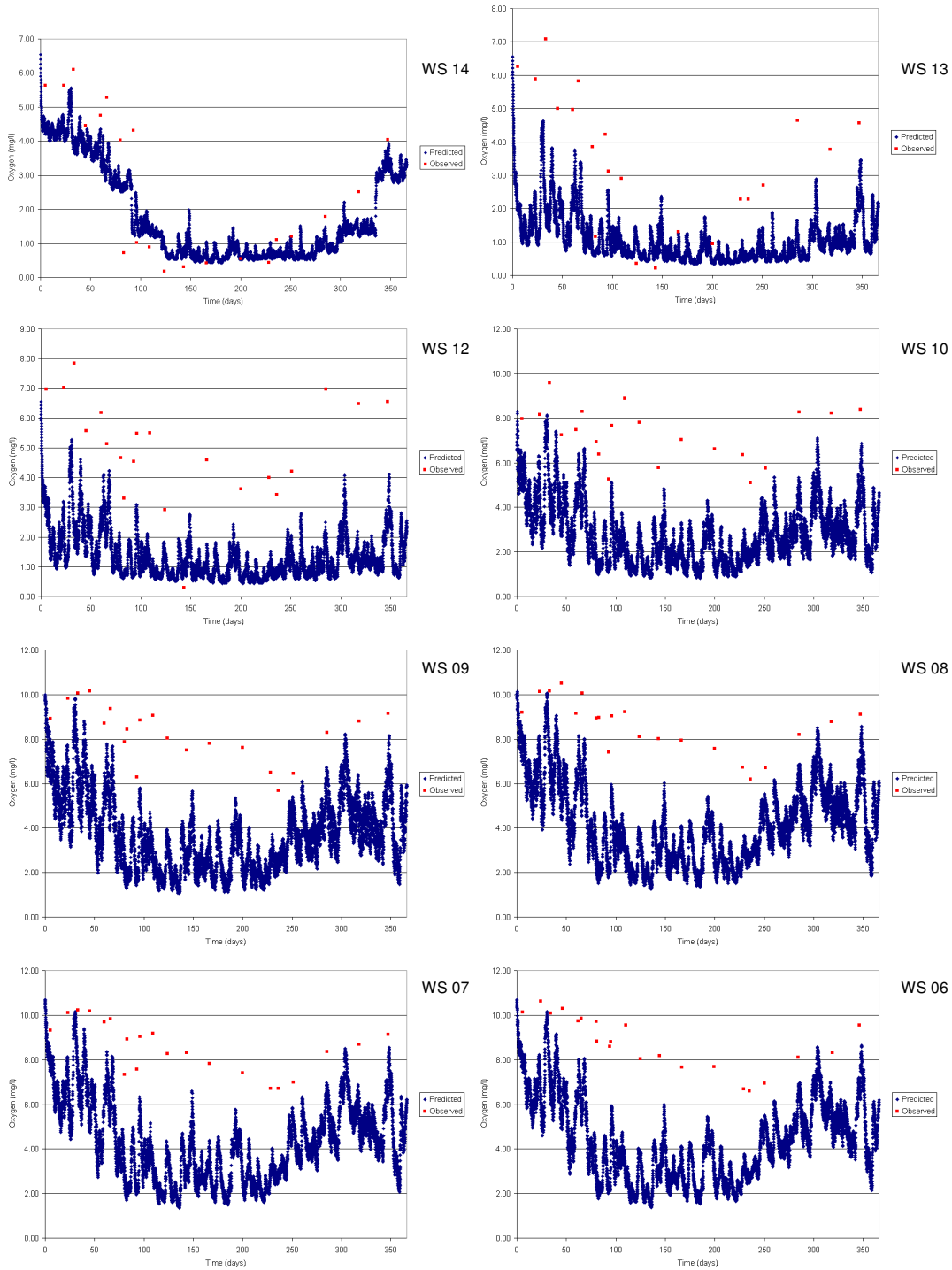
Suspended Particulate Matter



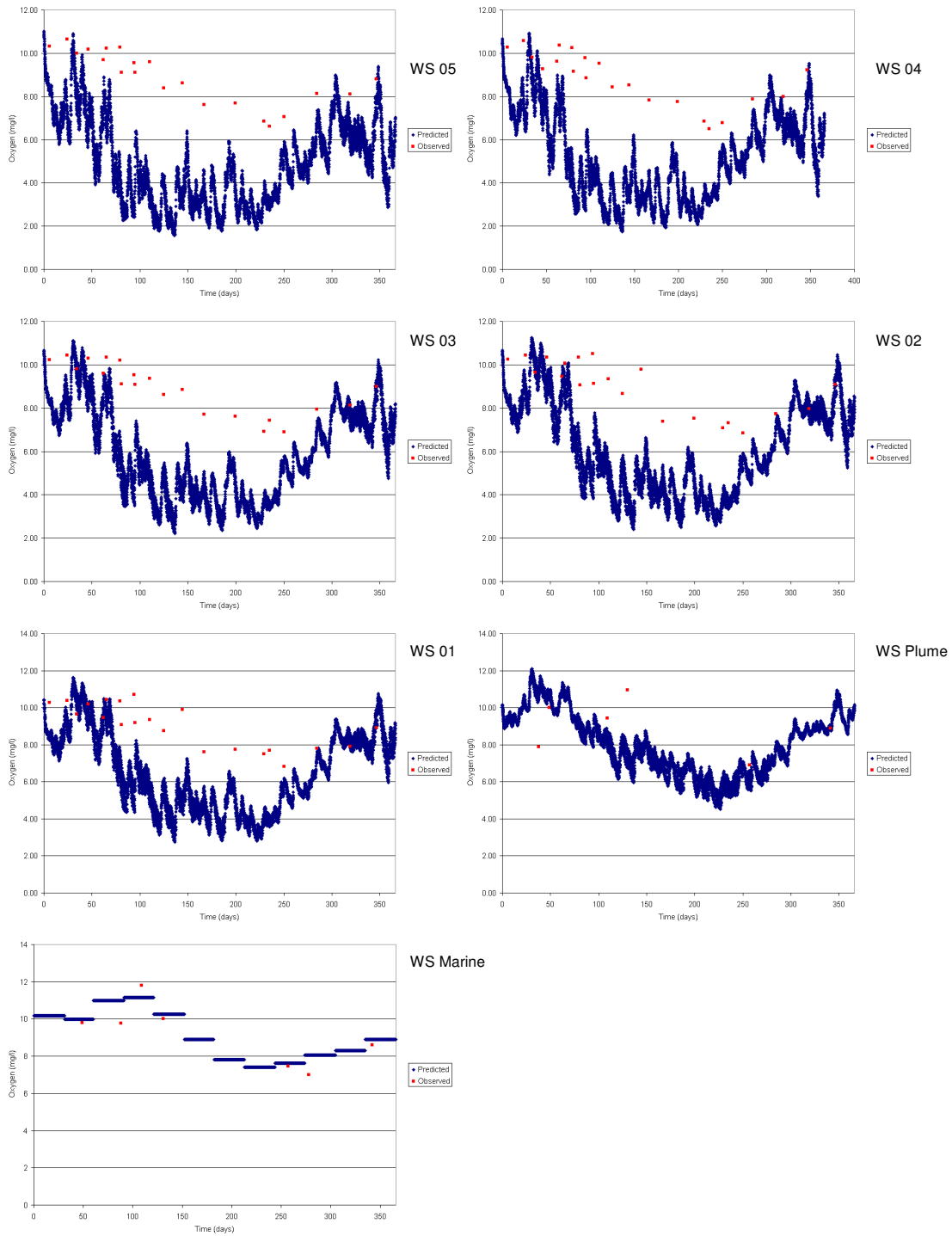
Suspended Particulate Matter (cont..)



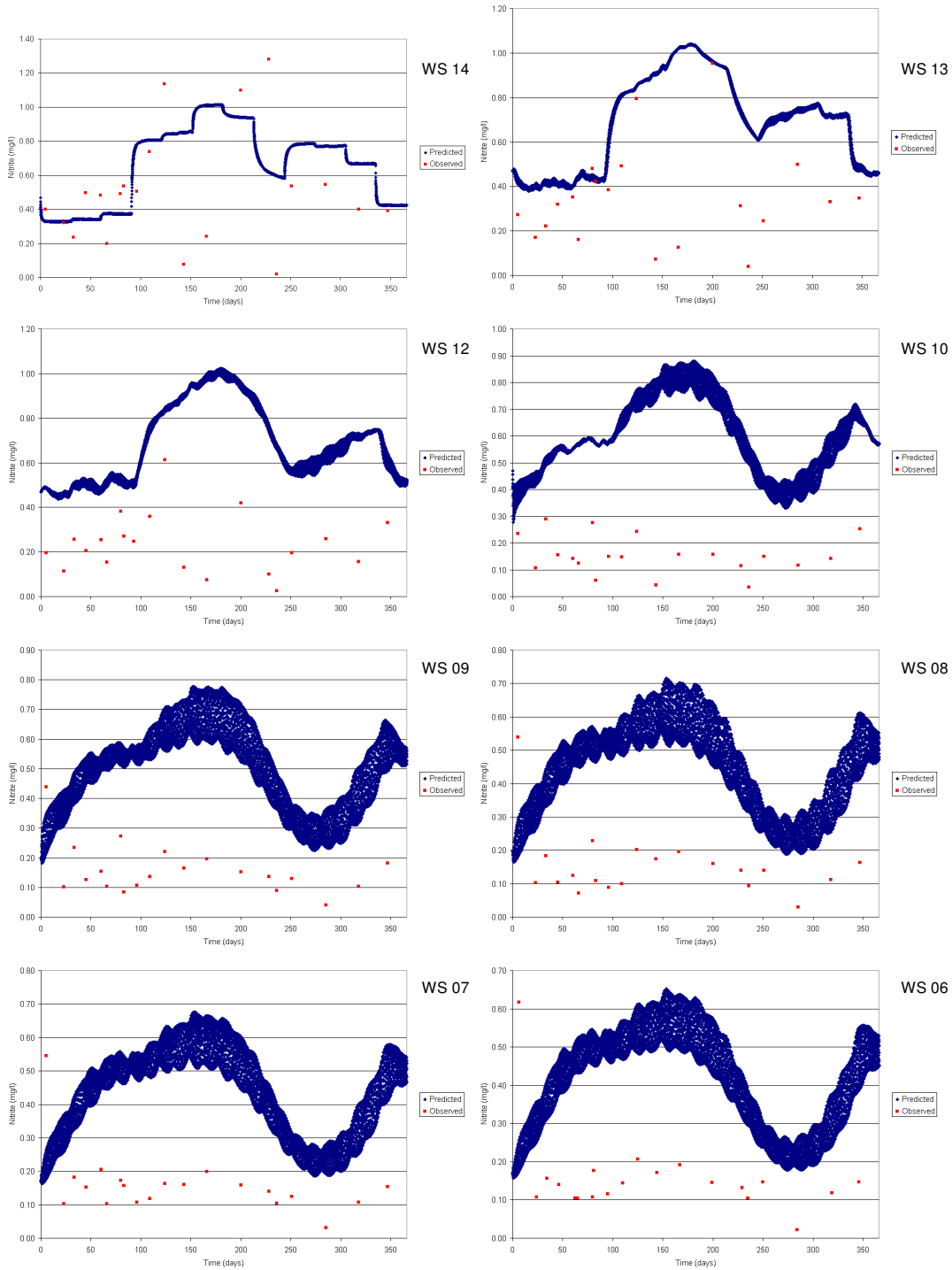
Oxygen



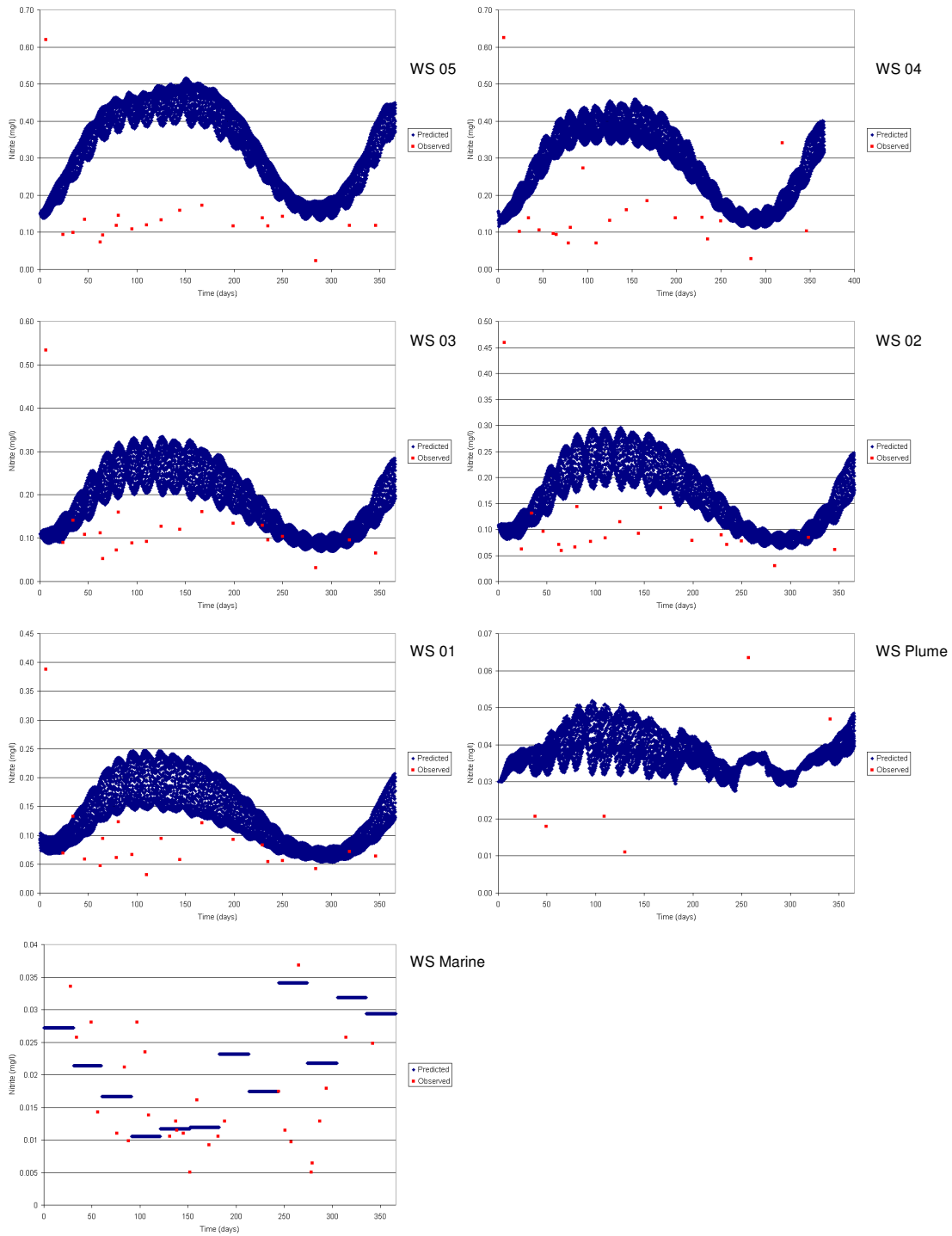
Oxygen (cont..)



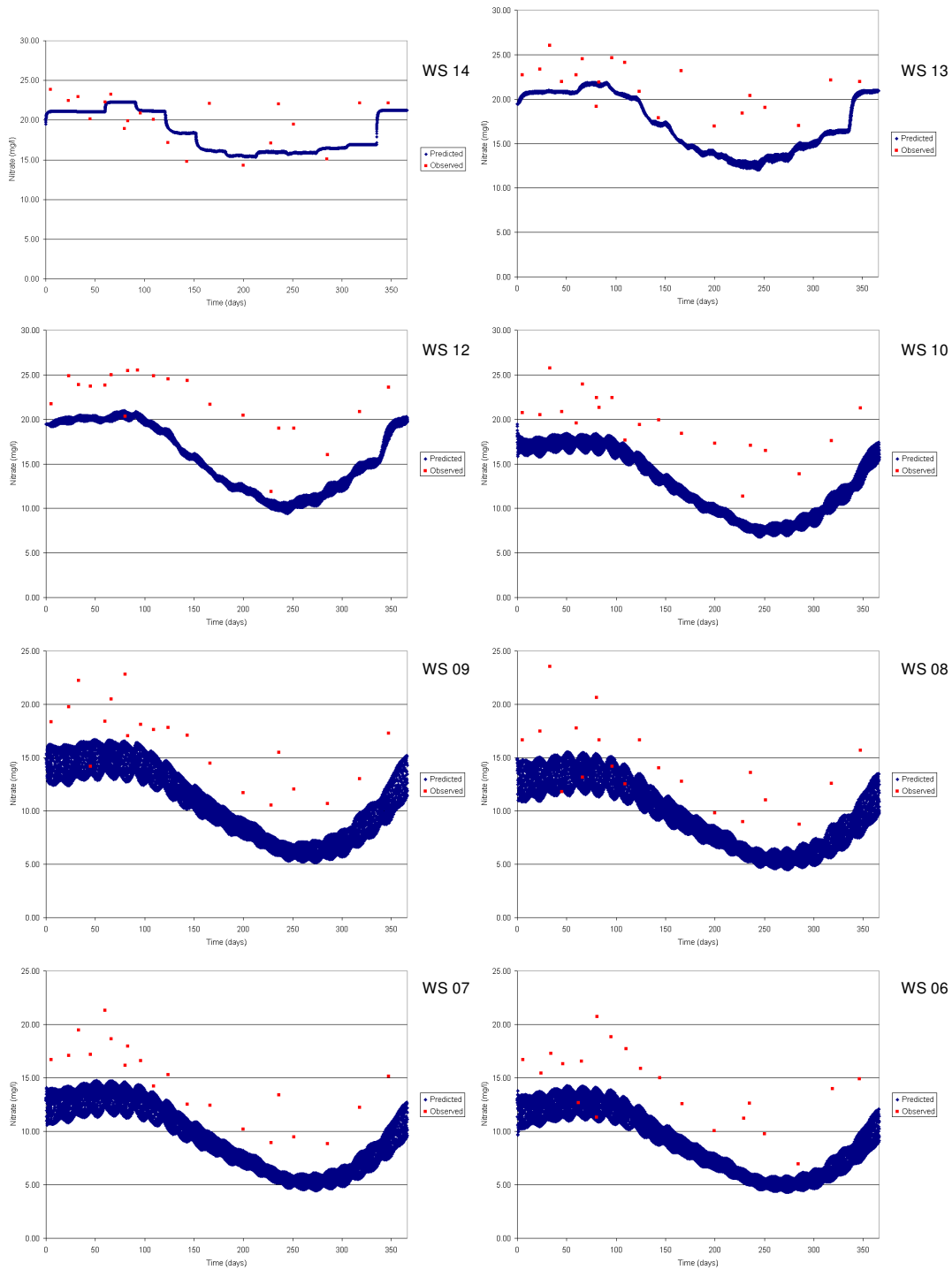
Nitrite



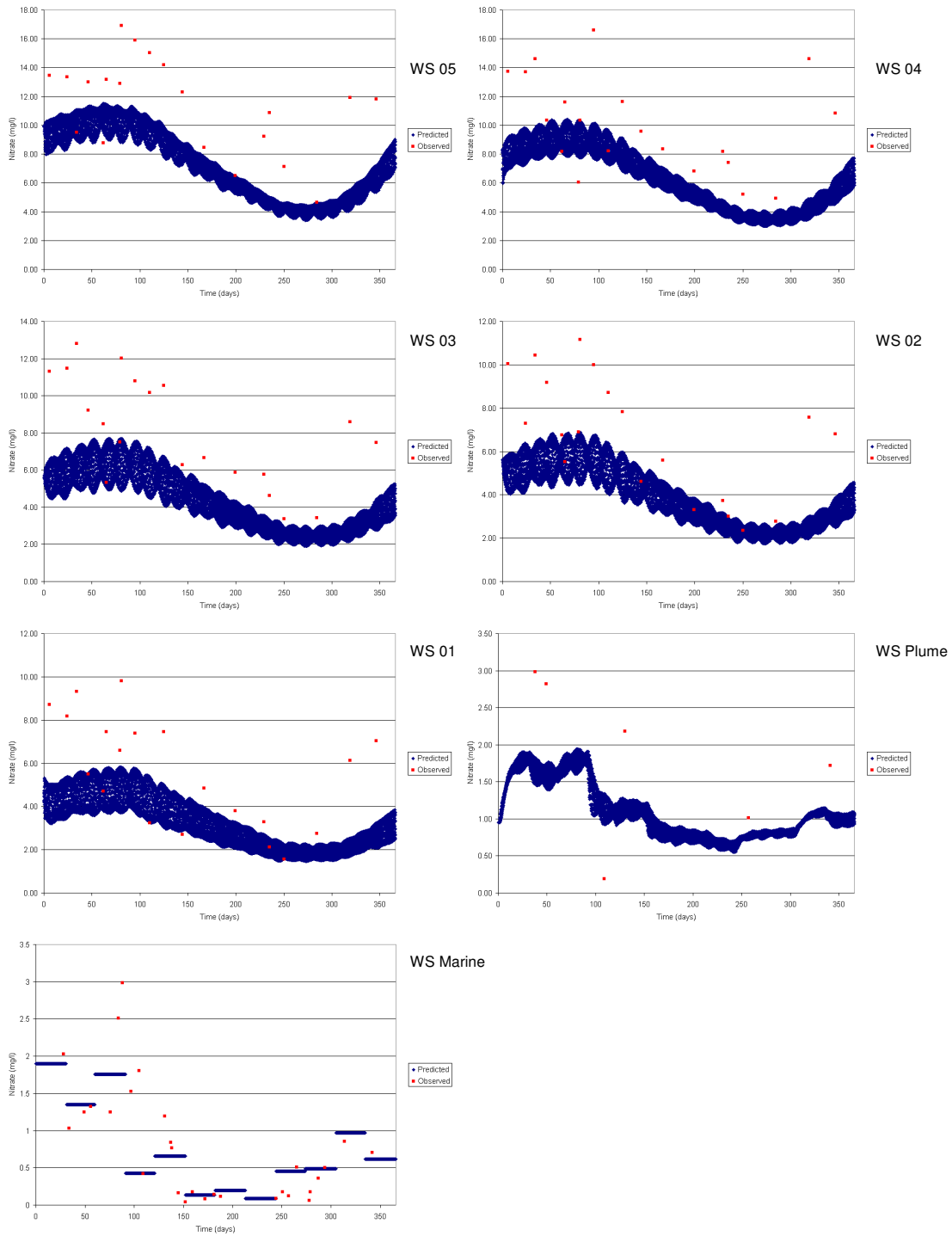
Nitrite (cont..)



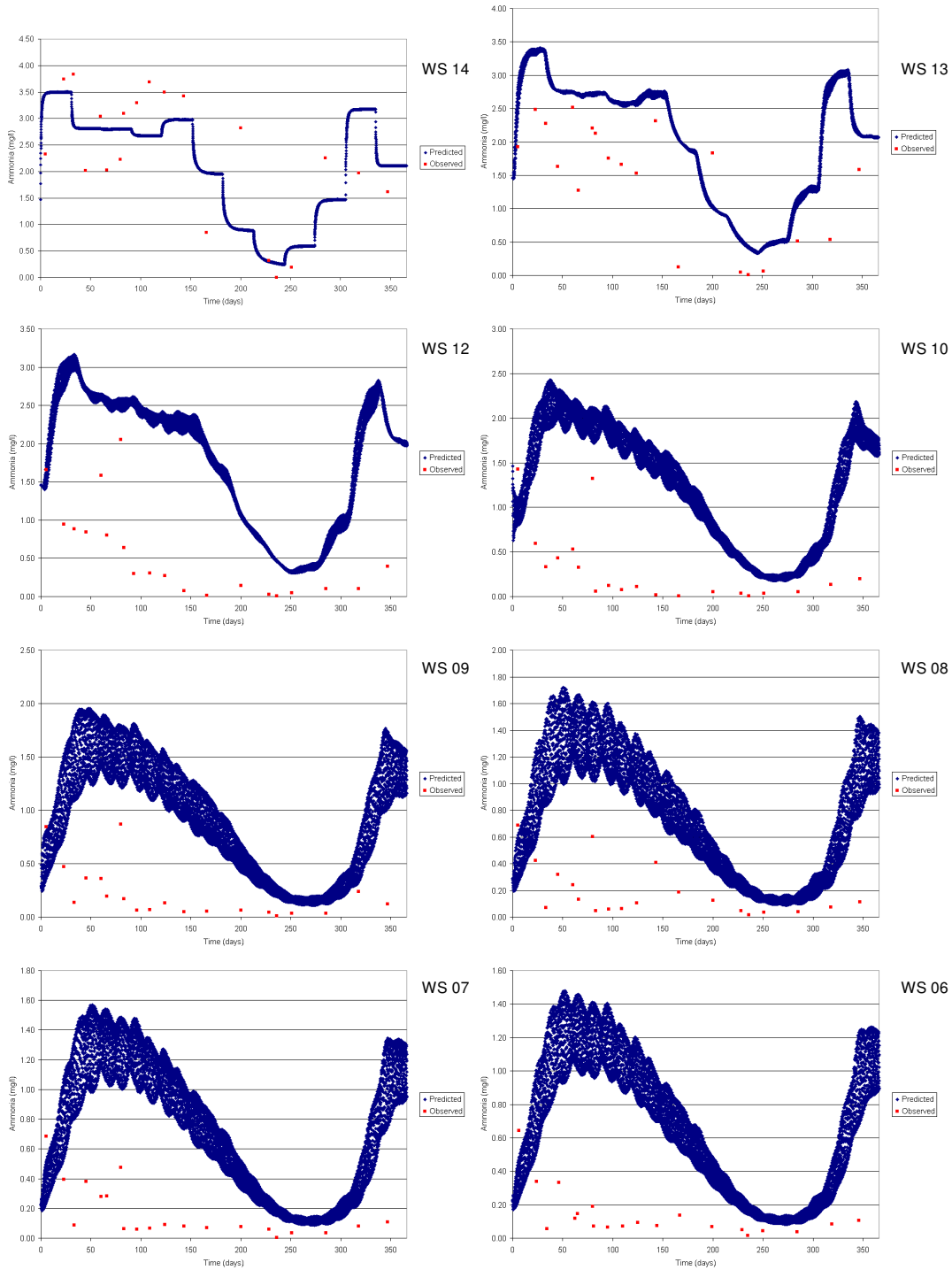
Nitrate



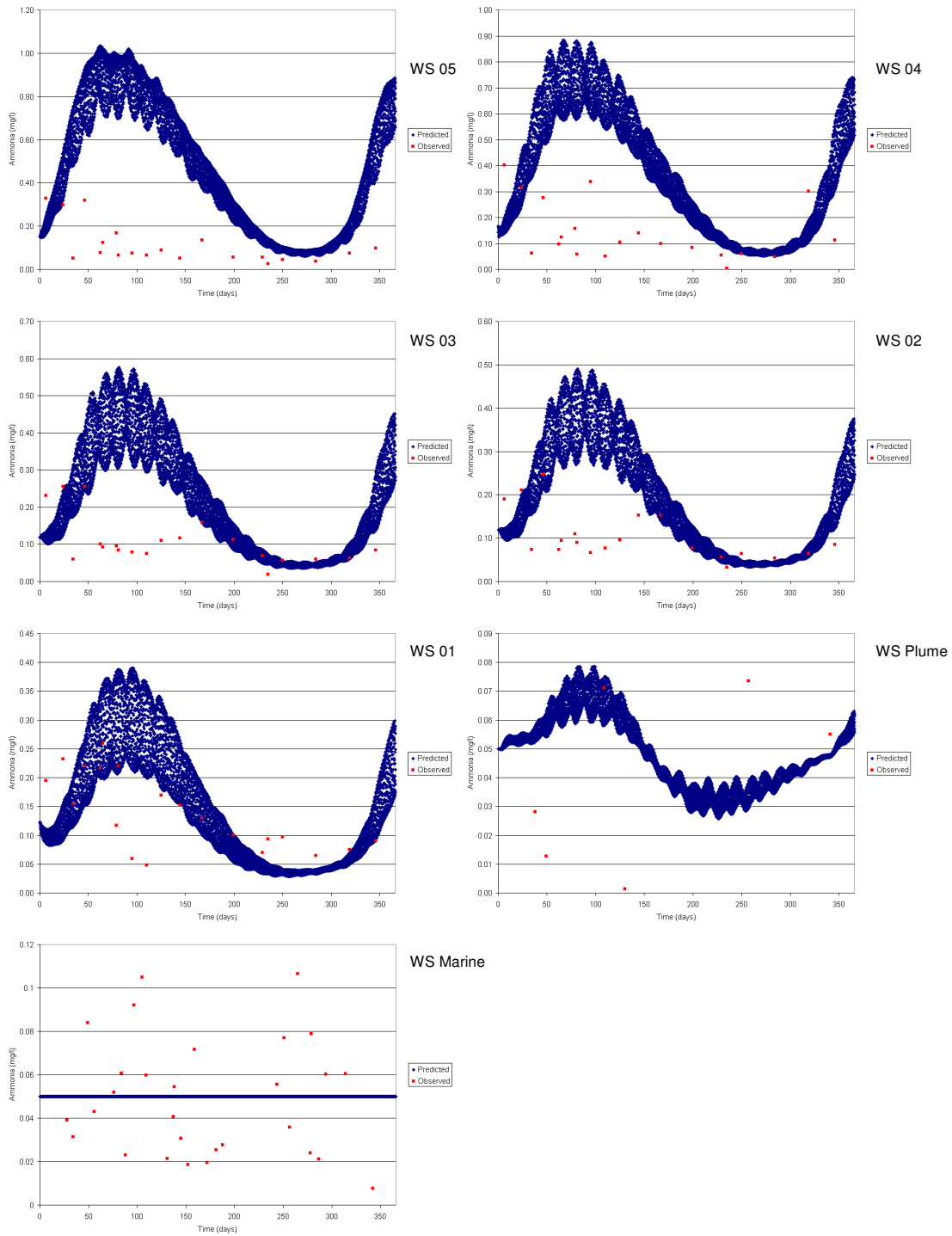
Nitrate (cont..)



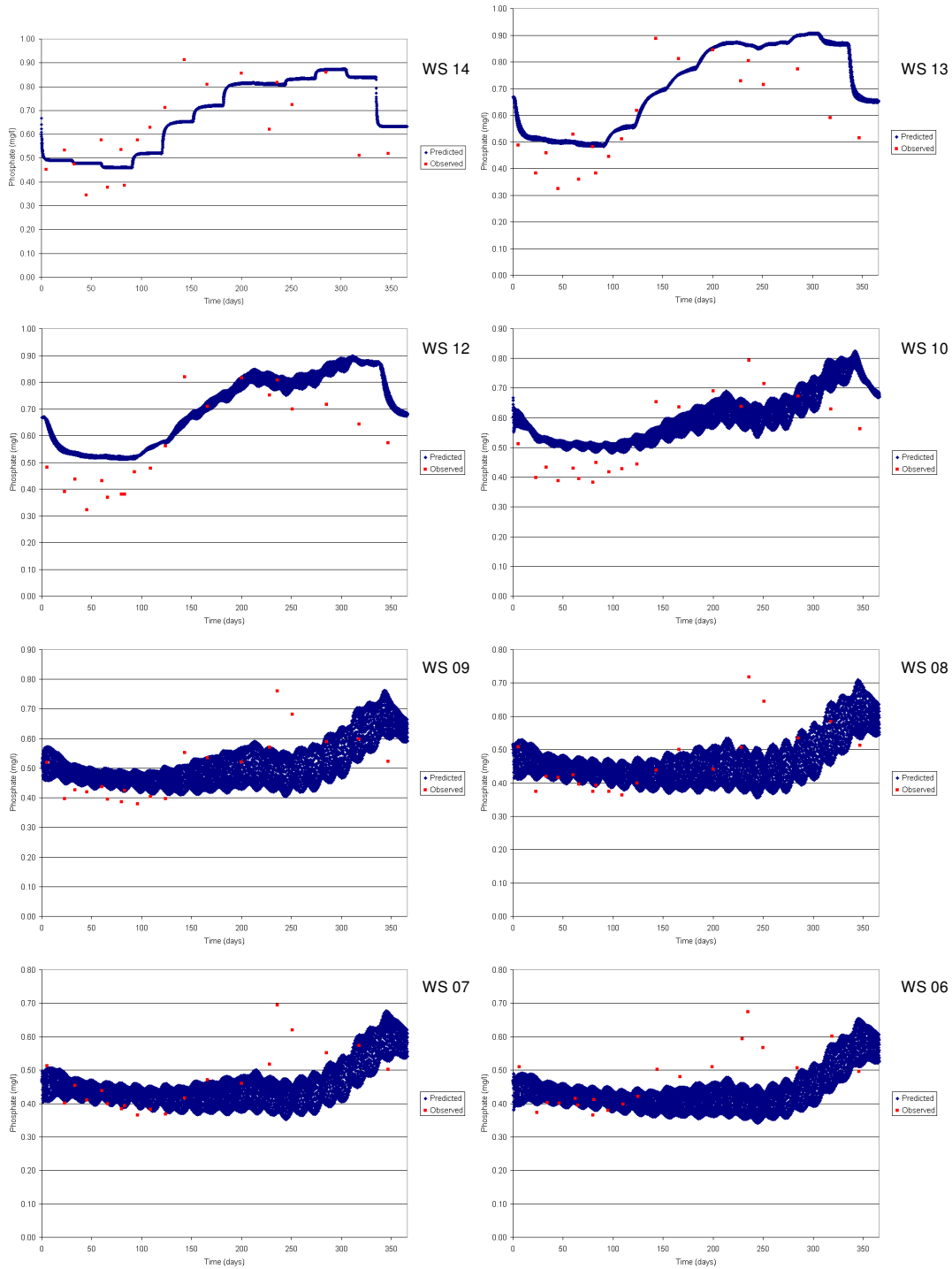
Ammonia



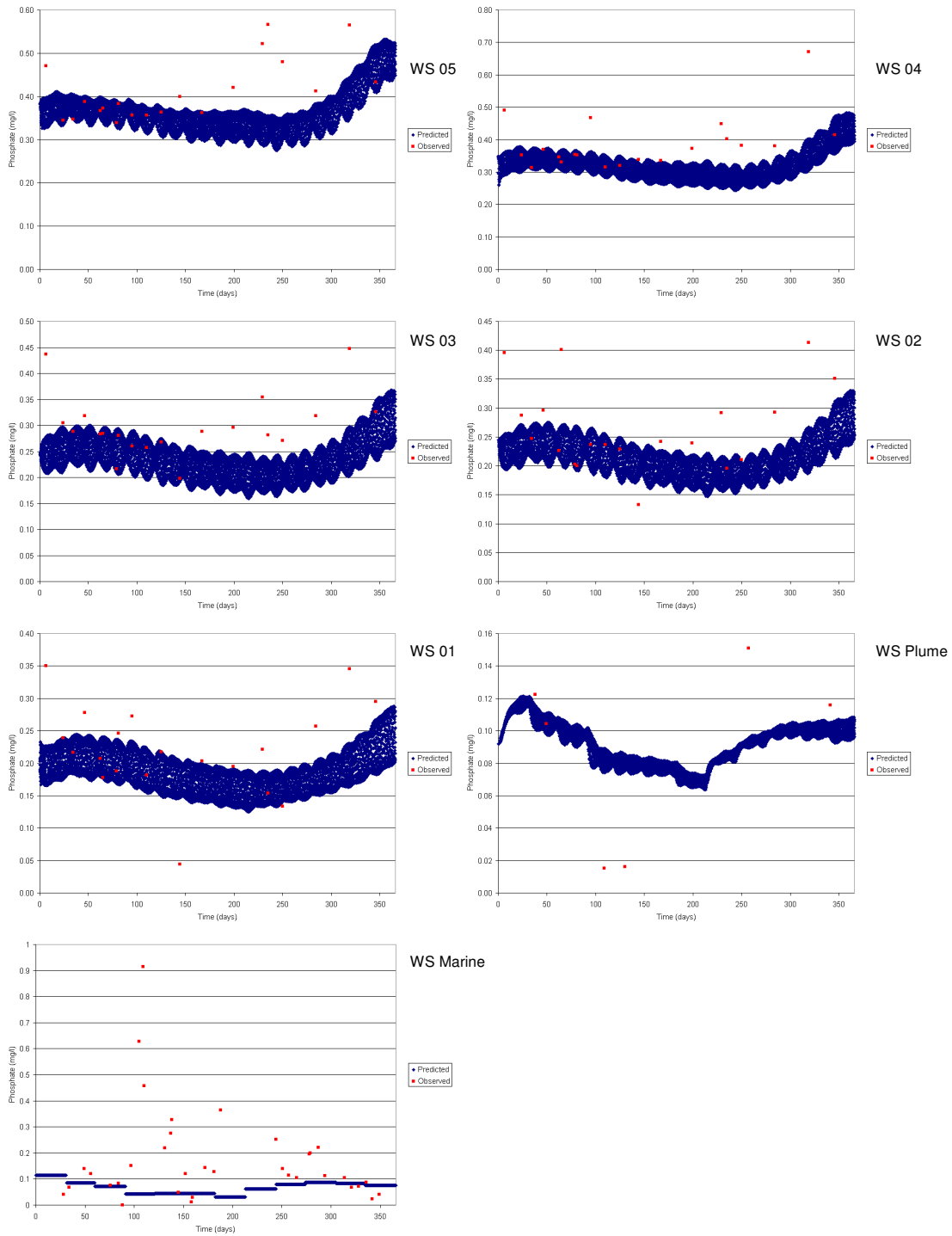
Ammonia (cont.)



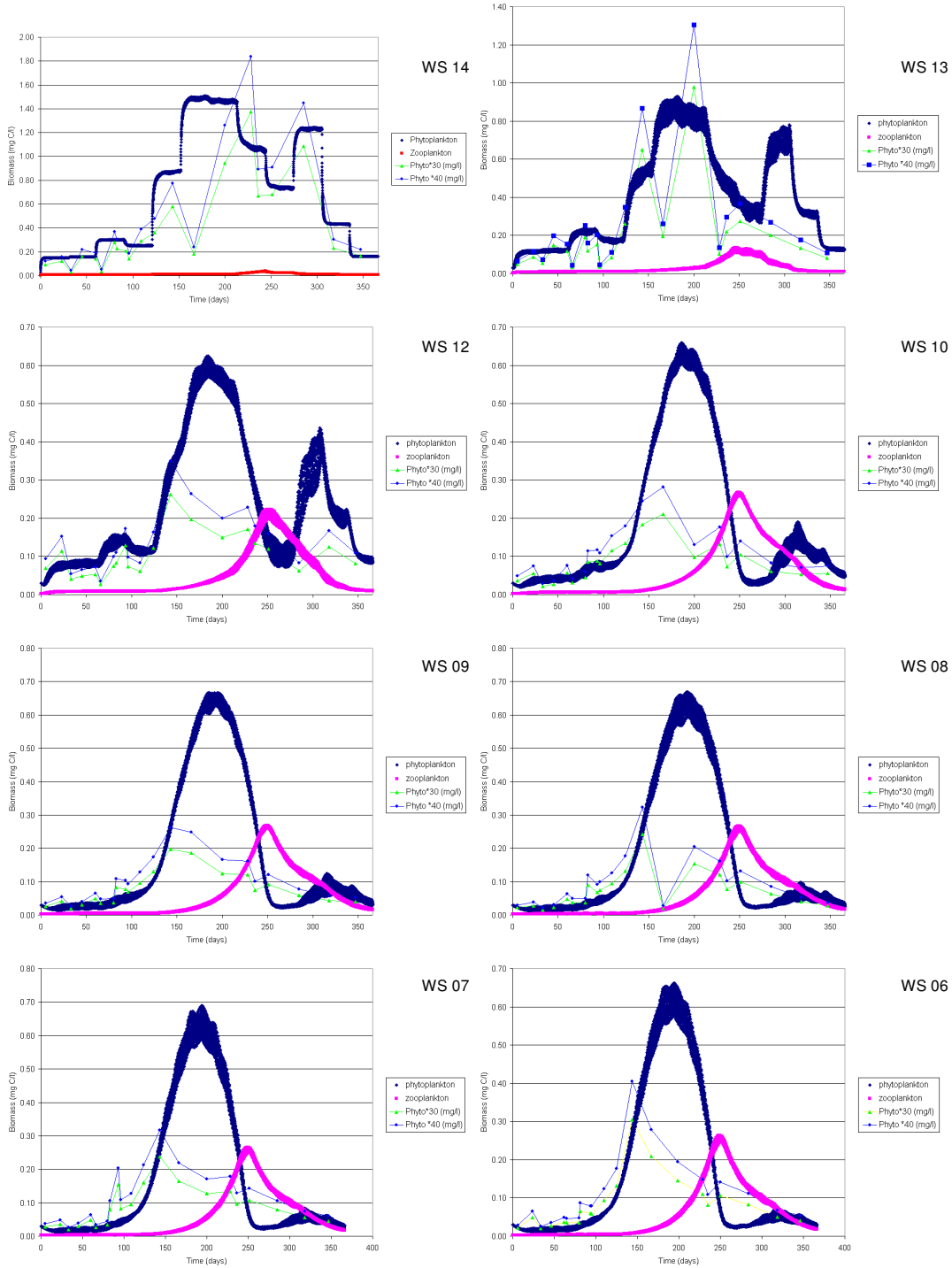
Phosphate



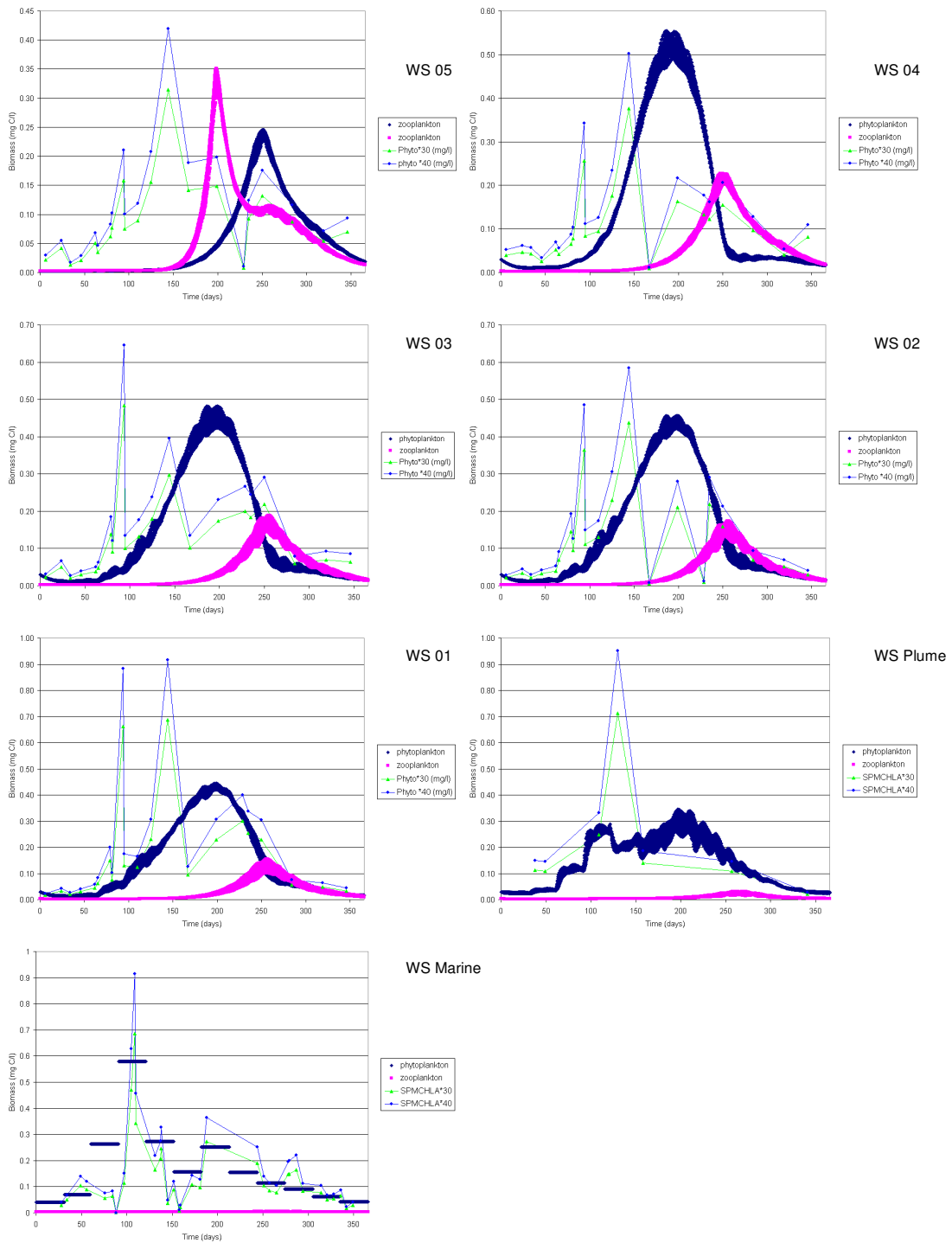
Phosphate (cont..)



Phytoplankton & Zooplankton



Phytoplankton & Zooplankton (cont..)

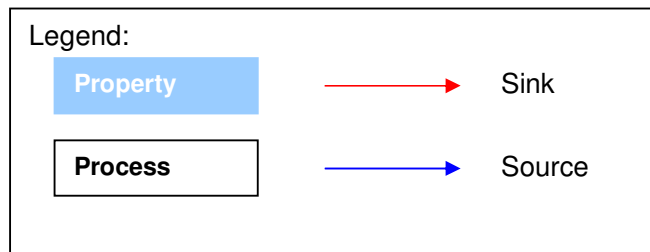


APPENDIX 2: ECOLOGICAL MODEL EQUATIONS

In this appendix, a summary of the ecological model formulations is presented, with the respective input keywords.

State Variables:

Variable	Definition	Unit
Φ_{phy}	Phytoplankton concentration	mgC.L ⁻¹
Φ_{zoo}	Zooplankton concentration	mgC.L ⁻¹
Φ_{NH4}	Ammonia concentration	mgN.L ⁻¹
Φ_{NO2}	Nitrite concentration	mgN.L ⁻¹
Φ_{NO3}	Nitrate concentration	mgN.L ⁻¹
Φ_{PON}	Particulate organic nitrogen concentration	mgN.L ⁻¹
Φ_{DONre}	Refractory dissolved nitrogen organic concentration	mgN.L ⁻¹
Φ_{DONnr}	Non-refractory dissolved nitrogen organic concentration	mgN.L ⁻¹
Φ_{IP}	Inorganic phosphorus (PO ₄ ³⁻) concentration	mgP.L ⁻¹
Φ_{POP}	Particulate organic phosphorus concentration	mgP.L ⁻¹
Φ_{DOPre}	Refractory dissolved phosphorus concentration	mgP.L ⁻¹
Φ_{DOPnr}	Non-refractory dissolved phosphorus concentration	mgP.L ⁻¹



Autotrophs

Phytoplankton

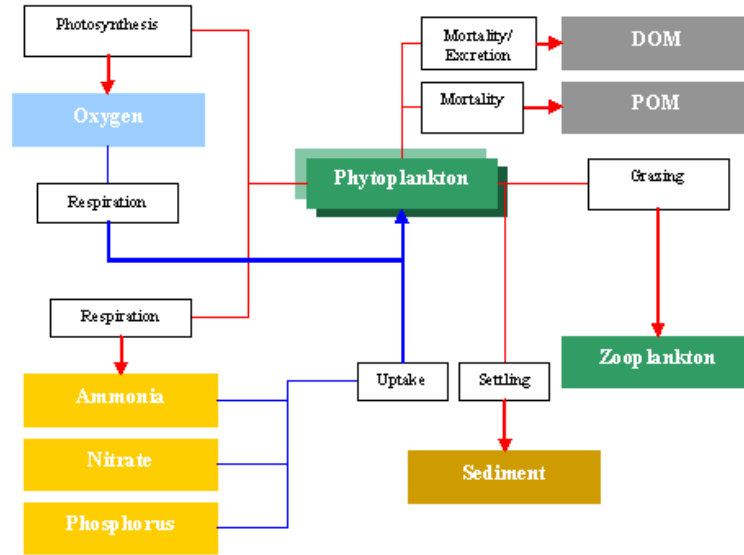


Figure A2.1– Internal flux of phytoplankton

$$\frac{\partial \Phi_{phy}}{\partial t} = (\mu_{phy} - r_{phy} - ex_{phy} - m_{phy}) \Phi_{phy} - G_{zoo}^{phy} \Phi_{zoo} \quad (0.1)$$

- μ_{phy} – phytoplankton gross growth rate [day⁻¹];
- r_{phy} – phytoplankton total respiration rate [day⁻¹];
- ex_{phy} – phytoplankton excretion rate [day⁻¹];
- m_{phy} – phytoplankton natural mortality rate (non-predatory) [day⁻¹];
- G_{zoo}^{phy} – zooplankton grazing rate on phytoplankton [day⁻¹];

$$\mu_{phy} = \mu_{max}^{phy}(T_{ref}) \cdot \Psi(T) \cdot \Psi(I) \cdot \text{Min}(\Psi(N), \Psi(P)) \quad (0.2)$$

- $\mu_{max}^{phy}(T_{ref})$ – maximum gross growth rate at the reference temperature
- $\Psi(T)$ – temperature limitation factor¹
- $\Psi(I)$ – light limitation factor
- $\Psi(N)$ – nitrogen limitation factor
- $\Psi(P)$ – phosphorus limitation factor

GROWMAXF

$$G_{zoo}^{phy} = \frac{\mu_{zoo}}{E} \quad (0.3)$$

μ_{zoo} – zooplankton gross growth rate [day⁻¹]

E – assimilation efficiency of the phytoplankton by the zooplankton [adim]

ASS_EFIC

Light Limiting Factor

$$\Psi(I) = \frac{e}{k \cdot z} \left(e^{-I_0 e^{-kz} / I_{opt}} - e^{-I_0 / I_{opt}} \right) \quad (0.4)$$

z – vertical position (cell vertical thickness)

I₀ – incident radiation [W/m²]

I_{opt} – optimum light intensity for phytoplankton photosynthesis [W/m²]

k – light extinction coefficient in the water column.

PHOTOIN

$$k = k_w + k_c \times Chla + k_s C_{ss} \quad (0.5)$$

$$Chla = \Phi_{phy} \frac{1}{60} \times 1000 \quad (0.6)$$

k_w – water light extinction coefficient [m⁻¹]

SW_KW

k_c – chlorophyll light extinction coefficient [m⁻¹]

SW_KC

k_s – solid suspended matter light extinction coefficient [m⁻¹]

SW_KS

Chla – chlorophyll a concentration [mgChla.m⁻³]

C_{ss} – solid suspended matter concentration (sum of SPM properties concentration)

Properties that can be SPM:

- Cohesive sediment
- Particulate organic nitrogen
- Particulate organic phosphorus
- Phytoplankton
- Zooplankton

Nutrients Limitation Factor

$$\Psi(N) = \frac{\Phi_{NH4} + \Phi_{NO3}}{K_N^X + \Phi_{NH4} + \Phi_{NO3}} \quad (0.7)$$

$$\Psi(P) = \frac{\Phi_{IP}}{K_P^X + \Phi_{IP}} \quad (0.8)$$

X ≡ Phytoplankton

K_N^X – nitrogen half-saturation constant [mgN.L⁻¹]

NSATCONS

K_P^X – phosphorus half-saturation constant [mgP.L⁻¹]

PSATCONS

Respiration

$$r_e^X = K_{re}^X e^{0.069T} \quad (0.9)$$

$$r_p^X = K_{rp}^X \mu_X \quad (0.10)$$

$$r_X = r_e^X + r_p^X \quad (0.11)$$

X ≡ Phytoplankton

r_X – total respiration rate [day⁻¹]

r_e^X – endogenous (or dark or basal) respiration rate [day⁻¹]

r_p^X – photorespiration respiration rate [day⁻¹]

K_{re}^X – endogenous respiration constant [day⁻¹]

FENDREPC

K_{rp}^X – fraction of actual photosynthesis which is oxidised by photorespiration [adim]

PHOTORES

Excretion

$$ex_x = K_e^x \cdot \mu_x \cdot (1 - \Psi(I)) \quad (0.12)$$

X ≡ Phytoplankton

K_e^x – excretion constant [adim]

EXCRCONS

Natural Mortality

$$m_x = m_{\max}^x(T_{ref}) \frac{\frac{\Phi_x}{\mu_x}}{K_m^x + \frac{\Phi_x}{\mu_x}} \quad (0.13)$$

$m_{\max}^x(T_{ref})$ – maximum mortality rate at the reference temperature [day^{-1}]

FMORTMAX

K_m^x – mortality half-saturation rate [Phytoplankton: $\text{mgC.L}^{-1}\text{day}^{-1}$]

FMORTCON

Zooplankton

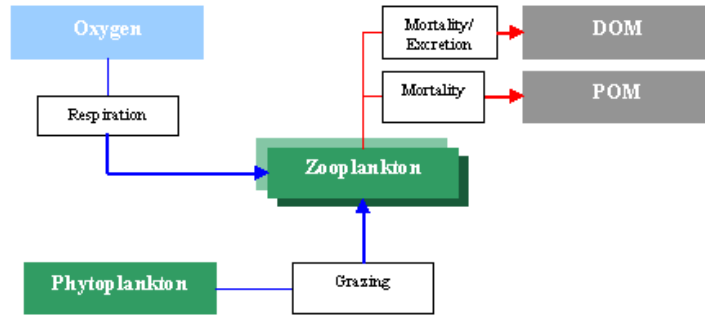


Figure A2.2 – Internal flux of Zooplankton

$$\frac{\partial \Phi_{zoo}}{\partial t} = (\mu_{zoo} - r_{zoo} - m_{zoo} - p_{zoo}) \Phi_{zoo} \quad (0.14)$$

μ_{zoo} – zooplankton gross growth rate [day⁻¹]

r_{zoo} – zooplankton respiration rate [day⁻¹]

m_{zoo} – zooplankton natural mortality rate [day⁻¹]

p_{zoo} – zooplankton predatory mortality rate [day⁻¹] (predation by higher trophic levels)

ZPREDMOR

$$\mu_{zoo} = \mu_{max}^{zoo}(T_{ref}) \Psi(T) \left(1 - e^{-\Lambda (\Phi_{phy} - \Phi_{phy}^{min})} \right) \quad (0.15)$$

$\mu_{max}^{zoo}(T_{ref})$ – zooplankton maximum gross growth rate at the reference temperature [d⁻¹]

$\Psi(T)$ – temperature limitation factor

Λ – Ivlev grazing constant [L.mgC⁻¹]

Φ_{phy} – phytoplankton concentration [mgC.L⁻¹]

Φ_{phy}^{min} – minimum phytoplankton concentration for the existence of grazing [mgC.L⁻¹]

GROWMAXZ

IVLEVCON

GRAZFITOMIN

$$r_{zoo} + m_{zoo} = d_{zoo}(T_{ref}) \cdot \Psi(T) \quad (0.16)$$

$d_{zoo}(T_{ref})$ – rate of consumption of carbon by respiration and non-predatory mortality at the reference temperature [1/day]

$\Psi(T)$ – temperature limitation factor

ZREFRESP

Nitrogen Cycle

Ammonia

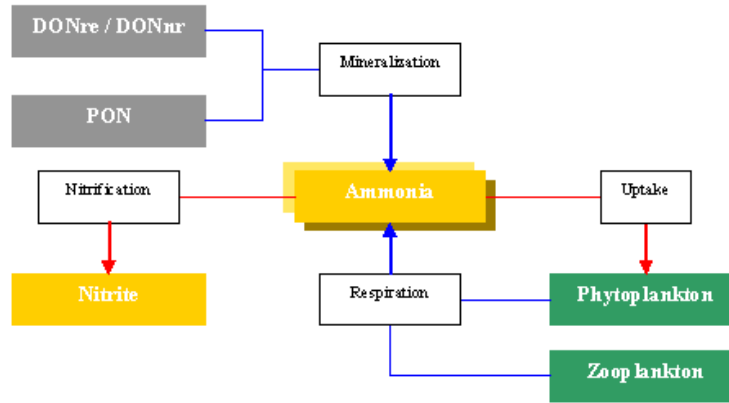


Figure A2.3 – Internal flux of Ammonia

$$\begin{aligned} \frac{\partial \Phi_{NH_4}}{\partial t} = & \underbrace{\left[f_{in/phy} (ex_{phy} + r_{phy}) \alpha_{N:C}^{phy} - \beta_{NH_4}^{phy} \mu_{phy} \alpha_{N:C}^{phy} \right]}_{\text{phytoplankton}} \Phi_{phy} + \quad (0.17) \\ & + \underbrace{\left[f_{in/zoo} (ex_{zoo} + p_{zoo}) \alpha_{N:C}^{zoo} \right]}_{\text{zooplankton}} \Phi_{zoo} + \underbrace{K_{min}^{DONre}}_{DONre} \Phi_{DONre} + \\ & + \underbrace{f_{orgP} K_{dec}^{PON}}_{PON} \Phi_{PON} + \underbrace{K_{min}^{DONnr}}_{DONnr} \Phi_{DONnr} - \underbrace{K_{nit}}_{\text{nitrification step 1}} \Phi_{NH_4} \end{aligned}$$

$\alpha_{N:C}^{phy}$ – phytoplankton N:C ratio (Redfield's ratio) [mgN.mgC⁻¹]

FRATIONC

$\alpha_{N:C}^{zoo}$ – zooplankton N:C ratio [mgN.mgC⁻¹]

ZRATIONC

$f_{in/phy}$ – soluble inorganic fraction of the phytoplankton excretions² [adim]

FSOLEXCR

$f_{in/zoo}$ – soluble inorganic fraction of the zooplankton excretions¹ [adim]

ZSOLEXCR

f_{orgP} – available PON for transformation into ammonia [adim]

PHDECOMP

h – deep layer height [m]

$\beta_{NH_4}^{phy}$ – phytoplankton ammonia preference factor [adim]

K_{dec}^{PON} – particulate organic nitrogen decomposition rate [day⁻¹]

K_{min}^{DONre} – refractory dissolved organic nitrogen mineralization rate [day⁻¹]

K_{nit} – nitrification rate [day⁻¹]

$$\beta_{N4}^X = \left(\frac{\Phi}{K_X + \Phi} \right) \left(\frac{\Phi}{K_X + \Phi} \right) + \left(\frac{\Phi}{K_X + \Phi} \right) \left(\frac{K_X}{K_X + \Phi} \right) \quad (0.18)$$

X = phytoplankton

$$K_{dec}^{PON} = K_{dec}^{PON}(T_{ref}) \cdot \theta_{dec}^{(T-T_{ref})} \quad (0.19)$$

$K_{dec}^{PON}(T_{ref})$ – PON reference decomposition rate [day^{-1}]

NOPREF

θ_{dec} – PON decomposition temperature coefficient [adim]

NOPCOEF

T_{ref} – reference temperature = 20°C

$$K_{min}^{DONre} = K_{min}^{DONre}(T_{ref}) \cdot \theta_{min}^{DONre(T-T_{ref})} \frac{\Phi_{phy}}{K_r^{phy} + \Phi_{phy}} \quad (0.20)$$

$K_{min}^{DONre}(T_{ref})$ – DONre mineralization rate at the reference temperature [day^{-1}]

NMINR

θ_{min}^{DONre} – DONre mineralization temperature coefficient [adim]

TMINR

K_r^{phy} – phytoplankton nutrient regeneration half-saturation constant [mgC.L^{-1}]

FREGSATC

T_{ref} – reference temperature = 20°C

$$K_{nit} = K_{nit}^{ref}(T_{ref}) \theta_{nit}^{(T-T_{ref})} \frac{\Phi_O}{K_{nit}^{sat} + \Phi_O} \quad (0.21)$$

$K_{nit}^{ref}(T_{ref})$ – nitrification rate at the reference temperature [day^{-1}]

NITRIFREF

θ_{nit} – nitrification temperature coefficient [adim]

TNITCOEF

K_{nit}^{sat} – nitrification half-saturation constant [$\text{mgO}_2.\text{L}^{-1}$]

NITSATCO

T_{ref} – reference temperature = 20°C

K_{min}^{DONnr} – non-refractory dissolved organic nitrogen mineralization rate [day^{-1}]

$$K_{min}^{DONnr} = K_{min}^{DONnr}(T_{ref}) \cdot \theta_{min}^{DONnr(T-T_{ref})} \frac{\Phi_{phy}}{K_r^{phy} + \Phi_{phy}} \quad (0.22)$$

$K_{min}^{DONnr}(T_{ref})$ – DONnr mineralization rate at the reference temperature [day^{-1}]

NMINENR

θ_{min}^{DONnr} – DONnr mineralization temperature coefficient [adim]

TMINNR

K_r^{phy} – phytoplankton nutrient regeneration half-saturation constant [mgC.L^{-1}]

FREGSATC

T_{ref} – reference temperature = 20°C

Nitrite

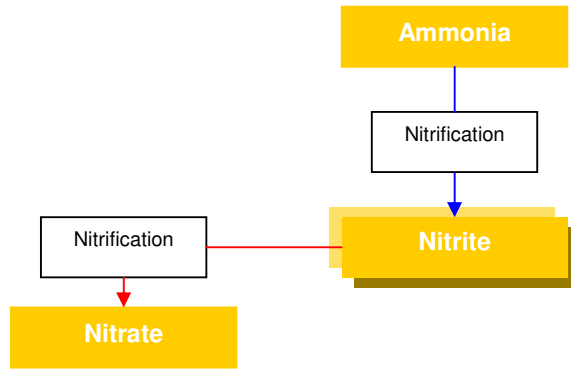


Figure A2.4 – Internal flux of Nitrite

$$\frac{\partial \Phi_{NO_2}}{\partial t} = K_{nit} \Phi_{NH_4} - K_{nit} \Phi_{NO_2} \quad (0.23)$$

Nitrate

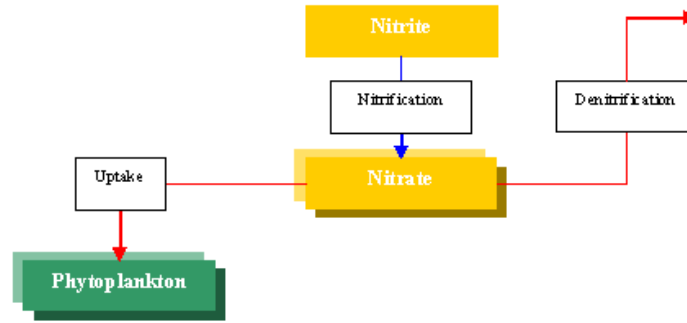


Figure A2.5 – Internal flux of Nitrate

$$\frac{\partial \Phi_{NO_3}}{\partial t} = - \underbrace{(1 - \beta_{NH_4}^{phy}) \alpha_{N:C}^{phy} \mu_{phy} \Phi_{phy}}_{phytoplankton} - \underbrace{(1 - \beta_{NH_4}^{MA}) \alpha_{N:C}^{MA} \mu_{MA} \frac{\Phi_{MA}}{h} \times 10^3}_{macroalgae} + K_{nit} \Phi_{NO_2} - K_{dnit} \Phi_{NO_3} \quad (0.24)$$

$$K_{dnit} = K_{dnit}^{ref} (T_{ref}) \theta_{dnit}^{(T-T_{ref})} \frac{K_{dnit}^{sat}}{K_{dnit}^{sat} + \Phi_O} \quad (0.25)$$

$K_{dnit}^{ref} (T_{ref})$ – denitrification rate at the reference temperature [day^{-1}]

DENITREF

θ_{dnit} – denitrification temperature coefficient

TDENCOEF

K_{dnit}^{sat} – denitrification half-saturation constant [$\text{mgO}_2 \cdot \text{L}^{-1}$]

DENSATCO

T_{ref} – reference temperature = 20°C

Particulate Organic Nitrogen

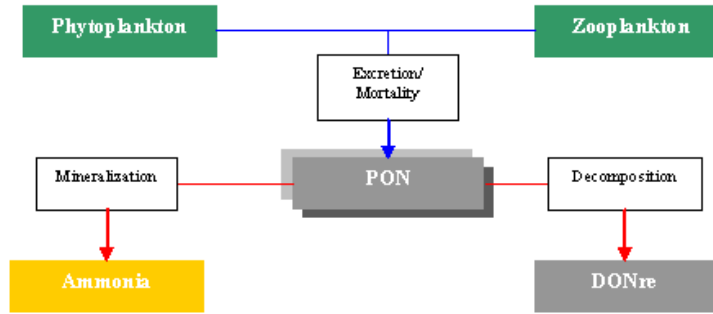


Figure A2.6 – Internal flux of Particulate Organic Nitrogen

$$\begin{aligned}
 \frac{\partial \Phi_{PON}}{\partial t} = & \underbrace{\left[(1 - f_{in/phy})(1 - f_{orgD/phy})(ex_{phy} + r_{phy}) + m_{phy} \right]}_{\text{phytoplankton}} \alpha_{N:C}^{phy} \Phi_{phy} - & (0.26) \\
 & - \underbrace{\left[(1 - f_{in/zoo})(1 - f_{orgD/zoo})(r_{zoo} + p_{zoo}) + m_{zoo} \right]}_{\text{zooplankton}} \alpha_{N:C}^{zoo} \Phi_{zoo} + (\delta_{phy}^N + \varphi_N) \Phi_{zoo} - \\
 & - \underbrace{(1 - f_{orgP}) K_{dec}^{PON}}_{\text{DONre}} \Phi_{PON} - \underbrace{f_{orgP} K_{dec}^{PON}}_{\text{ammonia}} \Phi_{PON}
 \end{aligned}$$

$f_{in/phy}$ – soluble inorganic fraction of the phytoplankton excretions

FSOLEXCR

$f_{orgD/phy}$ – dissolved organic fraction of the phytoplankton organic excretions

FDISSDON

$f_{in/zoo}$ – soluble inorganic fraction of the zooplankton excretions

ZSOLEXCR

$f_{orgD/zoo}$ – dissolved organic fraction of the zooplankton organic excretions

ZDISSDON

φ_N – non-assimilated phytoplankton (LostChainNitrogen)

$$\varphi_N = \mu_{zoo} (\alpha_{N:C}^{phy} - \alpha_{N:C}^{zoo}) \quad (0.27)$$

δ_{phy}^N – stoichiometric food web losses (LostPhytoGrazNitrogen)

$$\delta_{phy}^N = (1 - E) \frac{\mu_{zoo}}{E} \alpha_{N:C}^{zoo} + \varphi_N \quad (0.28)$$

Non-Refractory Dissolved Organic Nitrogen

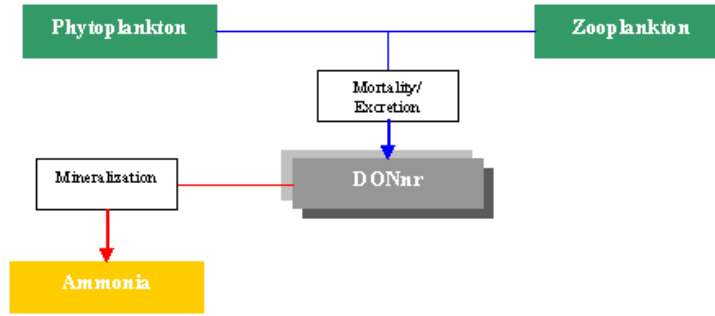


Figure A2.7 – Internal flux of Non-Refractory Dissolved Organic Nitrogen

$$\frac{\partial \Phi_{DONnr}}{\partial t} = \underbrace{(1 - f_{inlphy}) f_{orgDlphy} (ex_{phy} + r_{phy}) \alpha_{N:C}^{phy} \Phi_{phy}}_{phytoplankton} + \underbrace{(1 - f_{inlzoo}) f_{orgDlzoo} (ex_{zoo} + p_{zoo}) \alpha_{N:C}^{zoo} \Phi_{zoo}}_{zooplankton} - \underbrace{K_{min}^{DONnr} \Phi_{DONnr}}_{ammonia} \quad (0.29)$$

Refractory Dissolved Organic Nitrogen

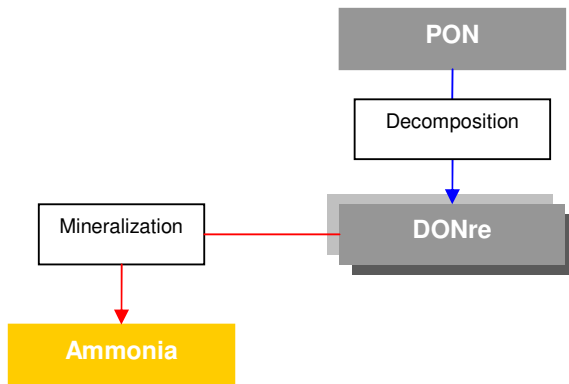


Figure A2.8 – Internal flux of Refractory Dissolved Organic Nitrogen

$$\frac{\partial \Phi_{DONre}}{\partial t} = \underbrace{(1 - f_{orgP}) K_{dec}^{PON} \Phi_{PON}}_{PON} - \underbrace{K_{min}^{DONre} \Phi_{DONre}}_{ammonia} \quad (0.30)$$

Phosphorous Cycle

Inorganic Phosphorus

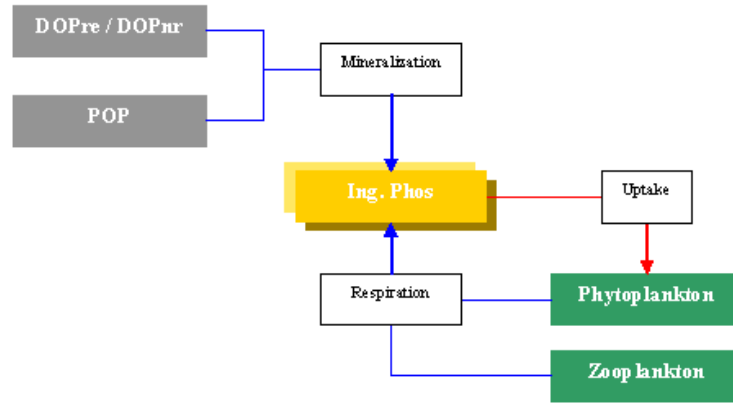


Figure A2.9 – Internal flux of Inorganic Phosphorus

$$\begin{aligned} \frac{\partial \Phi_{IP}}{\partial t} = & -\underbrace{\mu_{phy} \alpha_{P:C}^{phy} \Phi_{phy}}_{\text{phytoplankton}} + & (0.31) \\ & + \underbrace{\left[f_{in/zoo} (e_{x_{zoo}} + p_{zoo}) \alpha_{P:C}^{zoo} \right] \Phi_{zoo}}_{\text{mesozooplankton}} \\ & + \underbrace{K_{min}^{DOPre} \Phi_{DOPre}}_{DOPre} + \underbrace{f_{orgP} K_{dec}^{POP} \Phi_{POP}}_{POP} + \underbrace{K_{min}^{DOPnr} \Phi_{DOPnr}}_{DOPnr} \end{aligned}$$

$\alpha_{P:C}^{phy}$ – phytoplankton P:C ratio (Redfield's ratio) [mgP.mgC⁻¹]

FRATIOPC

$\alpha_{P:C}^{zoo}$ – zooplankton P:C ratio [mgP.mgC⁻¹]

ZRATIOPC

K_{dec}^{POP} – particulate organic phosphorus decomposition rate [day⁻¹]

$K_{min}^{DOPre}(T_{ref})$ – DOPre mineralization rate [day⁻¹]

$K_{min}^{DOPnr}(T_{ref})$ – DOPnr mineralization rate [day⁻¹]

$$K_{dec}^{POP} = K_{dec}^{POP}(T_{ref}) \cdot \theta_{dec}^{(T-T_{ref})} \quad (0.32)$$

$K_{dec}^{POP}(T_{ref})$ – POP reference decomposition rate [day⁻¹]

PPARTMIN

θ_{dec} – POP decomposition temperature coefficient [adim]

TPPARTMINCOEF

T_{ref} – reference temperature = 20°C

$$K_{min}^{DOPre} = K_{min}^{DOPre}(T_{ref}) \cdot \theta_{min}^{DOPre(T-T_{ref})} \frac{\Phi_{phy}}{K_r^{phy} + \Phi_{phy}} \quad (0.33)$$

$K_{\min}^{DOPre}(T_{ref})$ – DOPre mineralization rate at the reference temperature **PMINR**

[day⁻¹]

θ_{\min}^{DOPre} – DOPre mineralization temperature coefficient [adim] **PMINRCOEF**

K_r^{phy} – phytoplankton nutrient regeneration half-saturation constant **FREGSATC**

[mgC.L⁻¹]

T_{ref} – reference temperature = 20°C

$$K_{\min}^{DOPnr} = K_{\min}^{DOPnr}(T_{ref}) \cdot \theta_{\min}^{DOPnr}(T - T_{ref}) \frac{\Phi_{phy}}{K_r^{phy} + \Phi_{phy}} \quad (0.34)$$

$K_{\min}^{DOPnr}(T_{ref})$ – DOPnr mineralization rate at the reference temperature **PMINNR**

[day⁻¹]

θ_{\min}^{DOPnr} – DOPnr mineralization temperature coefficient [adim] **PMINNRCOEF**

T_{ref} – reference temperature = 20°C

Particulate Organic Phosphorus

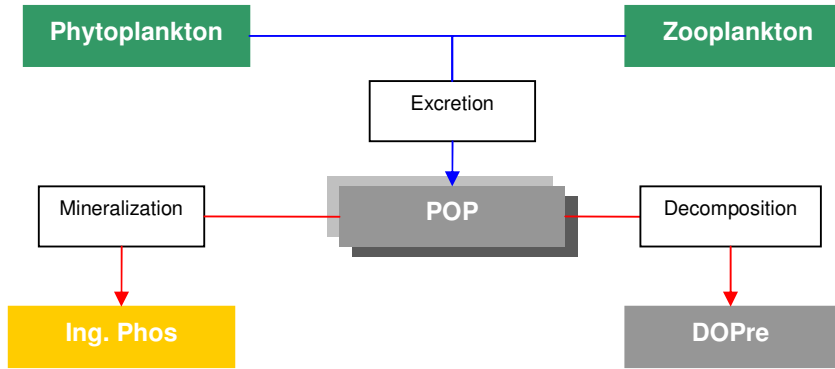


Figure A2.10 – Internal flux of Particulate Organic Phosphorus

$$\begin{aligned}
 \frac{\partial \Phi_{POP}}{\partial t} = & \underbrace{\left[(1 - f_{inl/phy})(1 - f_{orgDl/phy})(ex_{phy} + r_{phy}) + m_{phy} \right]}_{phytoplankton} \alpha_{P:C}^{phy} \Phi_{phy} - & (0.35) \\
 & + \underbrace{\left[(1 - f_{inl/zoo})(1 - f_{orgDl/zoo})(r_{zoo} + p_{zoo}) + m_{zoo} \right]}_{zooplankton} \alpha_{P:C}^{zoo} \Phi_{zoo} + (\delta_{phy}^P + \varphi_P) \Phi_{zoo} - \\
 & - \underbrace{(1 - f_{orgP}) K_{dec}^{POP}}_{DOPre} \Phi_{POP} - \underbrace{f_{orgP} K_{dec}^{POP}}_{IP} \Phi_{POP}
 \end{aligned}$$

φ_P – non-assimilated phytoplankton (LostChainPhosphorus)

$$\varphi_P = \mu_{zoo} (\alpha_{P:C}^{phy} - \alpha_{P:C}^{zoo}) \quad (0.36)$$

δ_{phy}^P – stoichiometric food web losses (LostPhytoGrazPhosphorus)

$$\delta_{phy}^P = (1 - E) \frac{\mu_{zoo}}{E} \alpha_{P:C}^{zoo} + \varphi_P \quad (0.37)$$

Non-Refractory Dissolved Organic Phosphorus

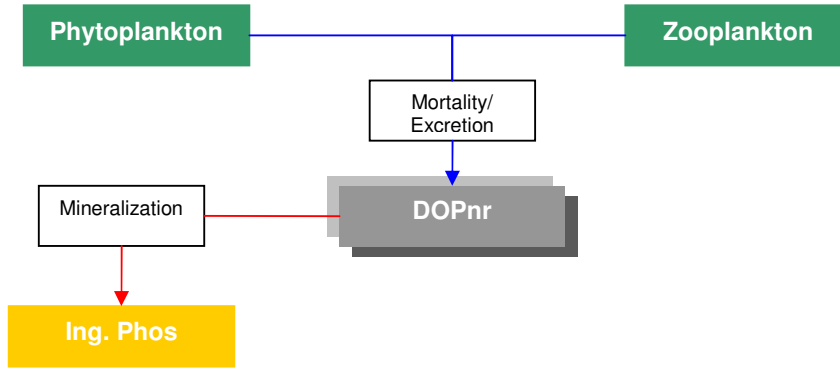


Figure A2.11 – Internal flux of Non-Refractory Dissolved Organic Phosphorus

$$\frac{\partial \Phi_{DOPnr}}{\partial t} = \underbrace{(1 - f_{in/phy}) f_{orgD/phy} (ex_{phy} + r_{phy}) \alpha_{P:C}^{phy} \Phi_{phy}}_{phytoplankton} - \underbrace{(1 - f_{in/zoo}) f_{orgD/zoo} (r_{zoo} + p_{zoo}) \alpha_{P:C}^{zoo} \Phi_{zoo}}_{zooplankton} + \underbrace{K_{min}^{DOPnr} \Phi_{DOPnr}}_{IP} \quad (0.38)$$

Refractory Dissolved Organic Phosphorus

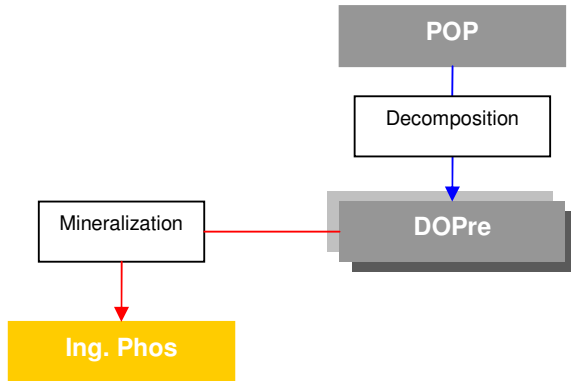


Figure A2.12– Internal flux of Refractory Dissolved Organic Phosphorus

$$\frac{\partial \Phi_{DOPre}}{\partial t} = \underbrace{(1 - f_{orgP}) K_{dec}^{POP} \Phi_{POP}}_{POP} - \underbrace{K_{min}^{DOPre} \Phi_{DOPre}}_{IP} \quad (0.39)$$

Oxygen Cycle

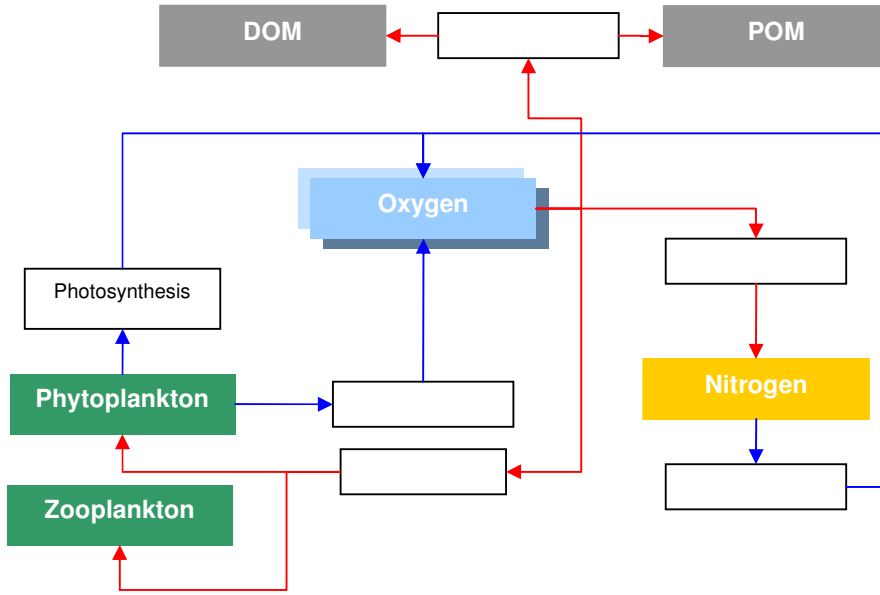


Figure A2.13 - Internal Flux of Oxygen

$$\frac{\partial \Phi_O}{\partial t} = \left\{ \underbrace{\mu_{phy} \alpha_{O:C}^{photo}}_{\text{photosynthesis}} + \underbrace{(1 - \beta_{NH4}^{phy}) \mu_{phy} \alpha_{O:N}^{NO3} \alpha_{N:C}^{phy}}_{\text{nitrate uptake}} + \underbrace{\mu_{phy} \alpha_{O:P}^{IP} \alpha_{P:C}^{phy}}_{\text{IP uptake}} - \underbrace{r_{phy} \alpha_{O:C}^{photo}}_{\text{respiration}} \right\} \Phi_{phy} + \quad (0.40)$$

$$+ \underbrace{(r_{zoo} + m_{zoo}) \alpha_{O:C}^{zoo} \Phi_{zoo}}_{\text{zooplankton}} - \underbrace{K_{nit}^O \Phi_{NH4}}_{\text{nitrification}} + \underbrace{K_{dnit}^O \Phi_{NO3}}_{\text{denitrification}} -$$

$$- \underbrace{K_{dec}^{PON} \alpha_{min O:N} \Phi_{PON} - K_{min}^{DONre} \alpha_{min O:N} \Phi_{DONre} + K_{min}^{DONnr} \alpha_{min O:N} \Phi_{DONnr}}_{\text{organic nitrogen}} -$$

$$- \underbrace{K_{dec}^{POP} \alpha_{min O:P} \Phi_{POP} - K_{min}^{DOPre} \alpha_{min O:P} \Phi_{DOPre} - K_{min}^{DOPnr} \alpha_{min O:P}^1 \Phi_{DOPnr}}_{\text{organic nitrogen}}$$

$\alpha_{O:C}^{photo}$ – photosynthesis oxygen/carbon ratio (2O/1C) = 32/12 g/g

$\alpha_{O:C}^{plankton}$ – plankton oxygen/carbon ratio (2O/1C) = 2.6 g/g

$\alpha_{O:C}^{zoo}$ – zooplankton respiration oxygen/carbon ratio (2O/1C) = 32/12 g/g

$\alpha_{O:N}^{NO3}$ – nitrate oxygen/nitrogen ratio (3O/1N) = 48/14 g/g (secondary oxygen production due to nitrate uptake)

$\alpha_{O:P}^{IP}$ – orthophosphate oxygen/phosphorus ratio (4O/1P) = 64/31 g/g (secondary oxygen production due to inorganic phosphorus uptake)

PHOTOSOC

PLANK_OC_RATIO

ZOCRATIO

NITONRAT

PHOSOPRAT

$$K_{nit}^O = K_{nit} \alpha_{O:N}^{nit} \Phi_o \quad (0.41)$$

$\alpha_{O:N}^{nit}$ – oxygen consumption due to nitrification ($\text{NH}_4^+ + 2\text{O}_2 \rightarrow \text{NO}_3^- + \text{H}_2\text{O} + 2\text{H}^+$) (4O/1N)
 [mgO/mgN] = 64/14 g/g

$$K_{dnit}^O = K_{dnit} \alpha_{O:N}^{dnit} \frac{5}{4} \quad (0.42)$$

$\alpha_{O:N}^{dnit}$ – during denitrification the organic material is decomposed, we need to convert Oxygen mass to Nitrogen mass = 32/14 mgO2/mgN

$$\alpha_{min\ O:N} = \frac{1}{\alpha_{N:C}^{phy}} \times \alpha_{O:C}^{CO_2} \times \frac{\Phi_o}{0.5 + \Phi_o} \quad (0.43)$$

$\alpha_{min\ O:N}$ – Mineralization oxygen/ nitrogen ratio

$$\alpha_{min\ O:P} = \frac{1}{\alpha_{P:C}^{phy}} \times \alpha_{O:C}^{CO_2} \times \frac{\Phi_o}{0.5 + \Phi_o} \quad (0.44)$$

$\alpha_{min\ O:P}$ – Mineralization oxygen/ phosphorus ratio

$\alpha_{min\ O:P}^1$ – Mineralization oxygen/ phosphorus ratio = Oxygen consumed during organic phosphorous mineralization

OPMINRATIO

$\alpha_{O:C}^{CO_2}$ – oxygen/carbon rate in CO_2 = 32/12 mgO/mgC

Temperature Effect

$$\Psi(T) = K_A(T) \cdot K_B(T) \quad (0.45)$$

$$K_A(T) = \frac{K_1 e^{\gamma_1(T-T_{\min})}}{1 + K_1 [e^{\gamma_1(T-T_{\min})} - 1]} \quad (0.46)$$

$$\gamma_1 = \frac{1}{(T_{\min}^{opt} - T_{\min})} \text{Ln} \left[\frac{K_2(1 - K_1)}{K_1(1 - K_2)} \right] \quad (0.47)$$

$$K_B(T) = \frac{K_4 e^{\gamma_2(T_{\max} - T)}}{1 + K_4 [e^{\gamma_2(T_{\max} - T)} - 1]} \quad (0.48)$$

$$\gamma_2 = \frac{1}{(T_{\max} - T_{\max}^{opt})} \text{Ln} \left[\frac{K_3(1 - K_4)}{K_4(1 - K_3)} \right] \quad (0.49)$$

T_{\min}^{opt} – minimum temperature for the optimal growth interval (°C)

**TOPTFMIN;
TOPTZMIN**

T_{\max}^{opt} – maximum temperature for the optimal growth interval (°C)

**TOPTFMAX;
TOPTZMAX**

T_{\min} – minimum tolerable temperature (°C)

TFMIN; TZMIN

T_{\max} – maximum tolerable temperature (°C)

TFMAX; TZMAX

K1, K2, K3, K4 – constants to control temperature response curve shape

TFCONST_i; TZCONST_i

Excretion Fractions

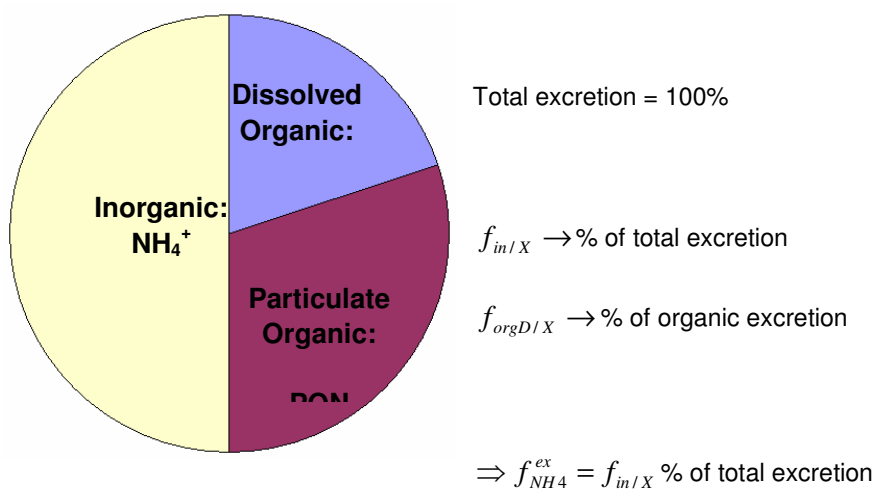


Figure A2.14 – Excretion Fractions (not at scale)

APPENDIX 3: PARAMETERS LIST

Reference temperature = 20°C

Nitrogen

Keyword	Variable	Description	Units	Default
DENITREF	$K_{dnt}^{ref}(T_{ref})$	denitrification rate at the reference temperature	day ⁻¹	0.07*
DENSATCO	K_{dnt}^{sat}	denitrification half-saturation constant	mgO ₂ .L ⁻¹	0.1
NITRREF	$K_{nit}^{ref}(T_{ref})$	nitrification rate at the reference temperature	day ⁻¹	0.06
NITSATCO	K_{nit}^{sat}	nitrification half-saturation constant	mgO ₂ .L ⁻¹	6.0
NMINENR	$K_{min}^{DONnr}(T_{ref})$	DONnr mineralization rate at the reference temperature	day ⁻¹	0.1
NMINR	$K_{min}^{DONre}(T_{ref})$	DONre mineralization rate at the reference temperature	day ⁻¹	0
NOPCOEF	θ_{dec}	PON decomposition temperature coefficient	adim	1.02
NOPREF	$K_{dec}^{PON}(T_{ref})$	PON reference decomposition rate	day ⁻¹	0.01
NSATCONS	K_N^{Phy}	nitrogen half-saturation constant	mgN.L ⁻¹	0.014
PHDECOMP	f_{orgP}	available PON for transformation into ammonia	adim	0.5
TDENCOEF	θ_{dnt}	denitrification temperature coefficient	aim	1.046
TMINNR	θ_{min}^{DONnr}	DONnr mineralization temperature coefficient	adim	1.02
TMINR	θ_{min}^{DONre}	DONre mineralization temperature coefficient	adim	1.02
TNITCOEF	θ_{nit}	nitrification temperature coefficient	adim	1.08

* Van Gils, Ouboter & Rooij (1993)

Phosphorus

Keyword	Variable	Description	Units	Default
PMINNR	$K_{\min}^{DOPnr}(T_{rej})$	DOPnr mineralization rate at the reference temperature	day ⁻¹	0.22
PMINR	θ_{\min}^{DOPnr}	DOPnr mineralization temperature coefficient	adim	1.064
PMINR	$K_{\min}^{DOPre}(T_{rej})$	DOPre mineralization rate at the reference temperature	day ⁻¹	0.0
PMINTCOEF	θ_{\min}^{DOPre}	DOPre mineralization temperature coefficient	adim	1.064
PPARTMIN	$K_{dec}^{POP}(T_{ref})$	POP reference decomposition rate	day ⁻¹	0.03
PSATCONS	K_p^{Phy}	phosphorus half-saturation constant	mgP.L ⁻¹	0.005
TPPARTMINCOEF	θ_{dec}	POP decomposition temperature coefficient	adim	1.08

Oxygen

Keyword	Variable	Description	Units	Default
NITONRAT	$\alpha_{O:N}^{NO3}$	nitrate oxygen/nitrogen ratio (3O/1N) = 48/14 g/g (secondary oxygen production due to nitrate uptake)	adim	3.429
ONMINRATIO		Mineralization oxygen/ nitrogen ratio	adim	2.286
OPMINRATIO	$\alpha_{\min O:P}^1$	Mineralization oxygen/ phosphorus ratio	adim	127.27
PHOSOPRAT	$\alpha_{O:P}^{IP}$	orthophosphate oxygen/phosphorus ratio (4O/1P) = 64/31 g/g (secondary oxygen production due to inorganic phosphorus uptake)	adim	2.064
PHOTOSOC	$\alpha_{O:C}^{photo}$	photosynthesis oxygen/carbon ratio (2O/1C) = 32/12 g/g	adim	2.66
PLANK_OC_RAT	$\alpha_{O:C}^{plankton}$	plankton oxygen/carbon ratio (2O/1C) = 32/12 g/g	adim	2.66
ZOCRATIO	$\alpha_{O:C}^{zoo}$	zooplankton respiration oxygen/carbon ratio (2O/1C) = 32/12 g/g	adim	2.66

Phytoplankton

Keyword	Variable	Description	Units	Default
EXCRCONS	K_e^{Phy}	excretion constant	adim	0.08
FDISSDON	$f_{orgDI\ phy}$	dissolved organic fraction of the phytoplankton organic excretions	adim	0.4
FENDREPC	K_{re}^{Phy}	endogenous respiration constant	day ⁻¹	0.0175
FMORTCON	K_m^{Phy}	phytoplankton mortality half-saturation rate	mgC.L ⁻¹ .day ⁻¹	0.3
FMORTMAX	$m_{max}^X(T_{ref})$	maximum mortality rate at the reference temperature	day ⁻¹	0.03
FRATIONC	$\alpha_{N:C}^{phy}$	phytoplankton N:C ratio (Redfield's ratio)	mgN.mgC ⁻¹	0.091**
FRATIOPC	$\alpha_{P:C}^{phy}$	phytoplankton P:C ratio (Redfield's ratio)	mgP.mgC ⁻¹	0.017**
FREGSATC	K_r^{phy}	phytoplankton nutrient regeneration half-saturation constant	mgC.L ⁻¹	1.0
FSOLEXCR	$f_{inI\ phy}$	soluble inorganic fraction of the phytoplankton excretions	adim	0.25
GROWMAXF	$\mu_{max}^{phy}(T_{ref})$	maximum gross growth rate at the reference temperature	day ⁻¹	2.2
PHOTOIN	I_{opt}	optimum light intensity for phytoplankton photosynthesis	W/m ²	100.0
PHOTORES	K_{rp}^{Phy}	fraction of actual photosynthesis which is oxidised by photorespiration	adim	0.018
TFCONST1	K_1	constant to control temperature response curve shape	adim	0.05
TFCONST2	K_2	constant to control temperature response curve shape	adim	0.98
TFCONST3	K_3	constant to control temperature response curve shape	adim	0.98
TFCONST4	K_4	constant to control temperature response curve shape	adim	0.02
TFMAX	T_{max}	maximum tolerable temperature	°C	37.0
TFMIN	T_{min}	minimum tolerable temperature	°C	4.0
TOPTFMAX	T_{max}^{opt}	maximum temperature for the optimal growth interval	°C	26.5
TOPTFMIN	T_{min}^{opt}	minimum temperature for the optimal growth interval	°C	25.0

** Zwolsman (1994)

Zooplankton

Keyword	Variable	Description	Units	Default
ASS_EFIC	E	assimilation efficiency of the phytoplankton by the zooplankton	Adim	0.6
GRAZFITOMIN	Φ_{phy}^{min}	threshold standing stock of phytoplankton below which grazing cease	mgC.L ⁻¹	0.0045
GROWMAXZ	$\mu_{max}^{zoo}(T_{ref})$	zooplankton maximum gross growth rate at the reference temperature	day ⁻¹	0.1
IVLEVCON	Λ	Ivlev grazing constant	L.mgC ⁻¹	13
TOPTZMAX	T_{max}^{opt}	maximum temperature for the optimal growth interval	°C	25.1
TOPTZMIN	T_{min}^{opt}	minimum temperature for the optimal growth interval	°C	24.8
TZCONST1	K ₁	constant to control temperature response curve shape	Adim	0.05
TZCONST2	K ₂	constant to control temperature response curve shape	Adim	0.98
TZCONST3	K ₃	constant to control temperature response curve shape	Adim	0.98
TZCONST4	K ₄	constant to control temperature response curve shape	Adim	0.02
TZMAX	T_{max}	maximum tolerable temperature	°C	35.0
TZMIN	T_{min}	minimum tolerable temperature	°C	5.0
ZDISSDON	$f_{orgDIzoo}$	dissolved organic fraction of the zooplankton organic excretions	Adim	0.25
ZPREDMOR	p_{zoo}	zooplankton predatory mortality rate [1/day] (predation by higher trophic levels)	day ⁻¹	0.01
ZRATIONC	$\alpha_{N:C}^{zoo}$	Zooplankton N:C ratio	mgN.mgC ⁻¹	0.13
ZRATIOPC	$\alpha_{P:C}^{zoo}$	zooplankton P:C ratio	mgP.mgC ⁻¹	0.024
ZREFRESP	$d_{zoo}(T_{ref})$	rate of consumption of carbon by respiration and non-predatory mortality at the reference temperature	day ⁻¹	0.036
ZSOLEXCR	f_{inIzoo}	soluble inorganic fraction of the zooplankton excretions	Adim	0.25